Theoretical Chemistry of the Heaviest Elements

Valeria Pershina

Abstract Theoretical chemical research in the area of the heaviest elements is extremely important. It deals with predictions of properties of exotic species and their behavior in sophisticated and expensive experiments with single atoms and permits the interpretation of experimental results. Spectacular developments in the relativistic quantum theory and computational algorithms have allowed for accurate calculations of electronic structures of the heaviest elements and their compounds. Due to the experimental restrictions in this area, the theoretical studies are often the only source of useful chemical information. The works on relativistic calculations and predictions of chemical properties of elements with $Z \geq 104$ are overviewed. Preference is given to those related to the experimental research. The increasingly important role of relativistic effects in this part of the Periodic Table is demonstrated.

1 Introduction

The main aim of chemical research in the area of the heaviest elements is to assign a new element its proper place in the Periodic Table. Conceptually, it is the atomic number, Z, and electronic configuration of an element that define its position there. Since the latter cannot be measured for the very heavy elements, information on its chemical behavior is often used for this purpose. Unfortunately, with increasing nuclear charge cross-sections and production rates drop so rapidly that such

An erratum to this chapter is available at 10.1007/978-3-642-37466-1_10

V. Pershina (✉)
GSI Helmholtzzentrum für Schwerionenforschung, Darmstadt, Germany
e-mail: V.Pershina@gsi.de

M. Schädel and D. Shaughnessy (eds.), *The Chemistry of Superheavy Elements*,
DOI: 10.1007/978-3-642-37466-1_3,

chemical information can be accessed only for elements with a half-life of the order of at least few seconds and longer (see "Synthesis of Superheavy Elements"). In this case, some fast chemistry techniques are used (see "Experimental Techniques"). They are based on the principle of chromatographic separations either in the gas phase exploiting differences in volatility of elements or their compounds, or in the aqueous phase by solvent extraction or ion-exchange separations using differences in the complex formation. Chemistry of elements 104 (Rf) through 108 (Hs), and of elements 112 (Cn) and 114 (flerovium, Fl) has been successfully studied using these techniques (see "Liquid-Phase Chemistry of Superheavy Elements" and "Gas-Phase Chemistry of Superheavy Elements").

Due to very short half-lives, chemical information obtained from these experiments is limited to the knowledge of only few properties. It mostly answers the question about whether a new element behaves similarly to their lighter congeners in a chemical group, or whether some deviations from the trends occur due to very strong relativistic effects on their valence electron shells. Knowledge of many other important properties such as, e.g., chemical composition, stability, geometrical configuration, ionization potential (IP), electron affinity (EA), etc., cannot be measured at all. Thus, for the heaviest elements, theoretical studies become extremely important and are often the only source of useful chemical information. They are also invaluable in predicting and/or interpreting the outcome of sophisticated and expensive experiments with single atoms. Moreover, it is only the theory that can reveal how relativistic effects influence chemical properties: only a comparison of the observed behavior with that predicted on the basis of relativistic *versus.* non-relativistic calculations does allow assessing the importance and magnitude of relativistic effects.

Theoretical chemical research on the heaviest elements is not less challenging than the experimental one. It should be based on the most accurate relativistic electronic structure calculations in order to reliably predict properties and experimental behavior of the new elements and their compounds. It also needs development of special approaches that bridge calculations with quantities that cannot be so easily predicted from calculations. Due to recent spectacular developments in the relativistic quantum theory, computational algorithms and techniques, very accurate calculations of properties of the transactinide elements and their compounds are now possible, which allow for reliable predictions of their experimental behavior. These theoretical works are overviewed here. Special attention is paid to the predictive power of the theoretical studies for the chemical experiments. The role of relativistic effects is discussed in detail.

Early reviews on predictions of transactinide element properties based on relativistic atomic calculations and extrapolations are those of [1–5]. More recent reviews on the theoretical chemistry of the heaviest elements covering also investigations of molecular, complex, and solid-state properties are those of [6–14]. Chemical and physical properties of the heaviest elements including theoretical aspects are also discussed in [15].

2 Architecture of the Periodic Table

When Seaborg in 1944 introduced his 'actinide' concept [16], the theory played an important role in his decision to place newly discovered elements in a second series where the filling of the 5f-shell takes place, similarly to the 'lanthanide' series where the filling of the 4f-shell takes place. Thus, the filled-shell concept was in accord with the newly found periodicity in chemical properties and resulted in the discovery of the heavy actinides up to No at that time [17]. Since then, the theory advanced to such an extent that the Periodic Table (Fig. 1) is now predicted with sufficient accuracy up to very high Z numbers. That was possible due to the development of very accurate relativistic quantum chemical methods and programs, which could reliably calculate electronic configurations of heavy element atoms and ions. Ground states of the superheavy elements up to $Z = 172$ were predicted in the late 1960s and early 1970s by Mann [18], Fricke, Waber, Greiner [19, 20], Desclaux [21], and later by Nefedov [22] using the Dirac–Fock (DF) and Dirac–Fock-Slater (DFS) methods. The results up to 1975 are summarized in [1, 2] (see also references therein). More accurate multiconfiguration Dirac–Fock (MCDF) [23–31] and Dirac-Coulomb-Breit (DCB) coupled cluster (CC) calculations (see [32, 33] and references therein) performed later basically confirmed those earlier predictions and furnished more accurate values of the electronic energy states.

According to results of these calculations, in the first nine transactinide elements, Rf through Cn, filling of the 6d shell takes place. Followed by them are 7p elements 113 through 118, with element 118 falling into the group of noble

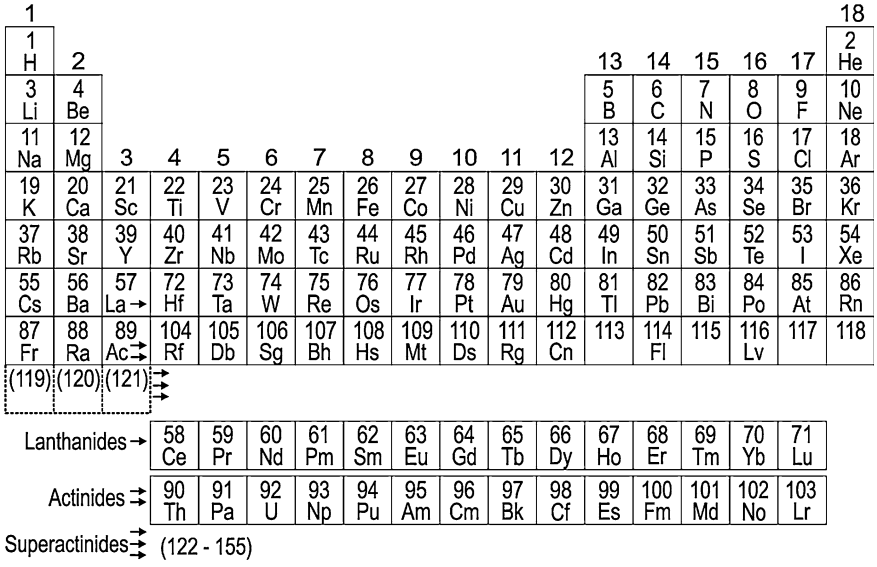

Fig. 1 Modern Periodic Table of the Elements

gases. In elements 119 and 120, the filling of the 8s shell takes place so that these elements will obviously be homologs of alkali and alkali-earth elements in group 1 and 2, respectively. Element 121 has a relativistically stabilized 8p electron in its ground state electron configuration [34], in contrast to the prediction based on a simple extrapolation in the group. In the next element, Z = 122, a 7d electron is added to the ground state, so that it is $8s^2 7d8p$ in contrast to the $7s^2 6d^2$ state of Th [35]. This is the last element where accurate DCB CC calculations exist.

For heavier elements, calculations start to disagree on the ground states (Table 1). The situation there becomes more complicated: 7d, 6f, and 5g levels, and furthermore 9s, $9p_{1/2}$ and $8p_{3/2}$ levels are located energetically so close to each other that clear structures of the pure p, d, f, and g blocks are not distinguishable anymore. The usual classification on the basis of a simple electronic configuration and placement of the elements in this part of the Periodic Table become problematic. Thus, e.g., according to [1, 2], the Periodic Table has a very long 8th period starting from Z = 119 and counting 46 elements, so that the last element of this period is 164, while elements 167 through 172 are $8p_{3/2}$ ones (due to the very large SO effects on the 8p AOs) belonging to the 9th period. The 5g shell is being filled in elements 125 through 144. Elements 165 and 166 are then 9s ones belonging to group 1 and 2, respectively.

Seaborg and Keller have designed another table [3–5], even though they used the same DF calculations of Fricke et al. [1, 2]. In their table, elements of the 8th period are those from Z = 119 through 168, including those from Z = 122 through 153, called superactinides. In difference to the results of [1, 2], the 8p elements are those from Z = 163 to 168, and the 9s elements are those with Z = 169 and 170. Such an arrangement of the elements is, however, not reflecting the filling of the AOs obtained in the original DF calculations, so that the Periodic Table of [1, 2] is more appropriate.

In a recent work based on MCDF (with average level, AL, energy functional) calculations of highly charged states of some elements of the 8th period it was, however, suggested that elements of the 5g series are those from Z = 121 to Z = 138 [31]. Elements 139 and 140 are assigned then to group 13 and 14, respectively, denoting that they are $8p_{1/2}$ elements, while those from Z = 141 to 155 are 6f elements. The 8th period finishes then at element 172. Thus, the Periodic Table of Pyykkö [31] looks quite different to that of Fricke and Waber [1, 2]. One should, however, note that ionized states cannot give information about ground

Table 1 Ground states of elements 121–124 (Z = 120 core +), 140 and 143 (Z = 120 core + $8p_{1/2}^2$ +) and of some of their ions

Method	121	122	123	124…	140	143	Ref.
DCB FSCC	8p	7d8p	–	–	–	–	[34,35]
MCDF/OL	–	–	–	–	$5g^{15}8p^4 6f$	–	[36]
MCDF/AL	8p	7d8p	$6f^2 8p$	$6f^2 8p^2$	$5g^{14}6f^3 7d8p^2$	$5g^{17}6f^2 7d^2$	[30]
MCDF/AL	8p	$8s^2$ (2+)	$6f^1$ (4+)	$6f^1$ (5+)	$5g^{16}8p^2$ (2+)	$5g^{18}7d^3$	[31]
DF	8p	7d8p	6f7d8p	$6f^3 8p$	$5g^{14}6f^3 7d8p^2$	$5f^{17}6f^2 7d^2$	[1, 2]

states of the elements, so that those assignments are rather tentative. An attempt to define ground states of the heaviest elements on the example of Z = 140 using the latest version of the MCDF method (with the optimal level, OL, energy functional) failed [36]. The author arrived to a conclusion that such calculations are presently restricted due to the computer limitations. It was also stated that at the present level of the MCDF theory, the Periodic Table ends at Z = 173, i.e., when the energy of the 1s electron goes below $-2mc^2$. A detail discussion about the end of the Periodic Table depending on the approximation is given in [36].

Thus, at the modern level of the relativistic electronic structure theory, the problem of defining ground states of elements heavier than 122 remains. Very accurate correlated calculations of the ground states with inclusion of the quantum electrodynamic (QED) effects at the self-consistent field (SCF) level are needed in order to reliably predict the future shape of the Periodic Table. At the time of writing, an accepted version of the Table is that of Fig. 1, with the superactinides comprising elements Z = 122 through 155 as suggested in [1, 2].

The structure of the modern Periodic Table cannot be understood without knowing the influence of relativistic effects on electronic valence shells. This is considered in the following section.

3 Relativistic and QED Effects for the Heaviest Elements

With increasing Z of heavy elements causing a stronger attraction to the core, an electron is moving faster, so that its mass increase is

$$m = m_0 / \left[1 - (v/c)^2\right]^{1/2}, \tag{1}$$

where m_0 is the rest mass, v is the velocity of the electron, and c is the speed of light. The Bohr model for a hydrogen-like species gives the following expressions for the velocity, energy, and orbital radius of an electron

$$v = (2\pi e^2/nh)Z, \tag{2}$$

$$E = -(2\pi^2 e^4/n^2 h^2)mZ^2, \tag{3}$$

$$r = Ze^2/mv^2, \tag{4}$$

where n is the principal quantum number, e is the charge of the electron, and h is Planck's constant. With increasing Z along the Periodic Table, the m/m_0 ratio becomes larger. For H it is 1.000027. From the 6th period onwards, this ratio exceeds by 10%, so that relativistic effects cannot be neglected anymore. For example, for Fl, $m/m_0 = 1.79$ and it is 1.95 for element 118. (See also [37] for other examples). The contraction (Eq. 4) and stabilization (Eq. 3) of the hydrogen-

like s and $p_{1/2}$ electrons is a direct relativistic effect and it was shown to originate from the inner K and L shell regions [38]. This effect was found to be also large for the valence region due to the direct action of the relativistic perturbation operator on the inner part of the valence density [39]. Figure 2 shows, e.g., a relativistic contraction of the 7s AO of element 105, Db, $\Delta_R\langle r\rangle_{ns} = \langle r\rangle_{nr} - \langle r\rangle_{rel}/\langle r\rangle_{nr} = 21\%$. Figure 3 shows a relativistic contraction of 25% and stabilization of 5.8 eV of the 7s AO of Cn.

The relativistic contraction and stabilization of the ns AO reach their maximum in the 7th period at Cn [8] (Fig. 4). The shift of the maximum to Cn in the 7th period in contrast to Au in the 6th period is because in Rg and Cn, the ground state electronic configurations are d^9s^2 and $d^{10}s^2$, respectively, while the corresponding electronic configurations in the 6th period are Au($d^{10}s^1$) and Hg($d^{10}s^2$).

The second (indirect) relativistic effect is the destabilization and expansion of outer d and f orbitals: The relativistic contraction of the s and $p_{1/2}$ shells results in a more efficient screening of the nuclear charge, so that the outer orbitals, which never come close to the core, become more expanded and energetically destabilized. (The expansion and destabilization of the (n–1)d AOs with Z are shown in Fig. 3 for group-12 elements, as an example). While the direct relativistic effect originates in the immediate vicinity of the nucleus, the indirect relativistic effect is influenced by the outer core orbitals. It should be realized that though contracted s and $p_{1/2}$ core (innermore) orbitals cause indirect destabilization of the outer orbitals, relativistically expanded d and f AOs cause the indirect stabilization of the valence s and p-AOs. That partially explains the very large relativistic stabilization of the 6s and 7s AOs in Au and Cn, respectively. Since d shells (it is also valid for the f shells) become fully populated at the end of the nd series, a maximum of the indirect stabilization of the valence s and p AOs will occur there [39].

The third relativistic effect is the well-known spin–orbit (SO) splitting of levels with $l > 0$ (p, d, f, etc.) into $j = l \pm ½$. It also originates from the inner shell region in the vicinity of nucleus. The SO splitting for the same l decreases with increasing number of subshells, i.e., it is much stronger for inner (core) shells than

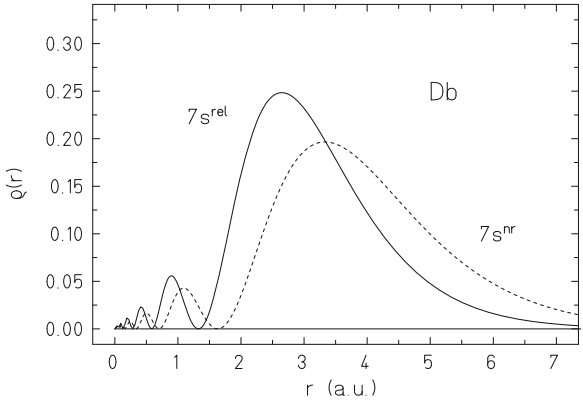

Fig. 2 Relativistic (*solid line*) and non-relativistic (*dashed line*) radial distribution of the 7s valence electrons in Db. From [11]

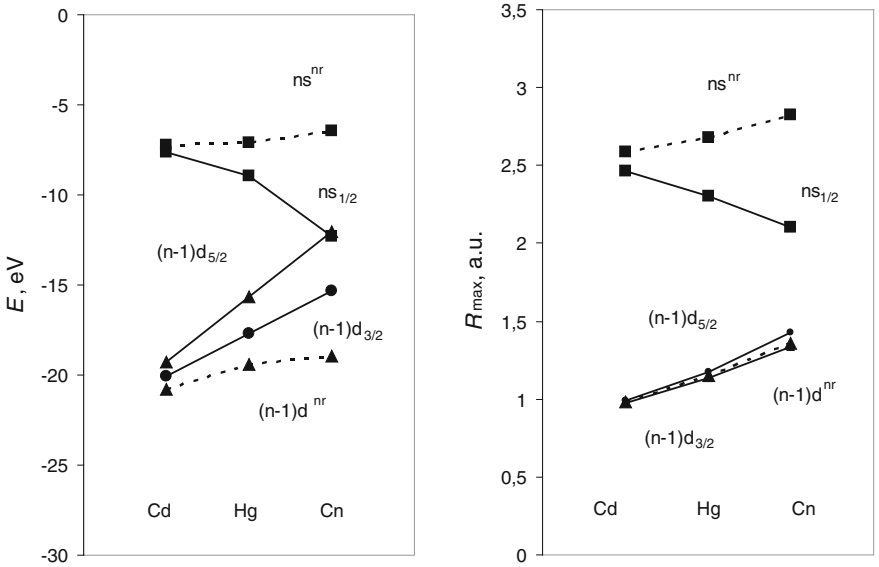

Fig. 3 Relativistic (*solid line*) and nonrelativistic (*dashed line*) energies, E, and the maximum of the radial charge distribution, R_{max}, of the valence ns and (n–1)d AOs of group-12 elements. The data are from [21]. Reprinted with permission from V. Pershina, Radiochim. Acta **99**, 459 (2011). Copyright 2011 Oldenbourg Wissenschaftsverlag GmbH

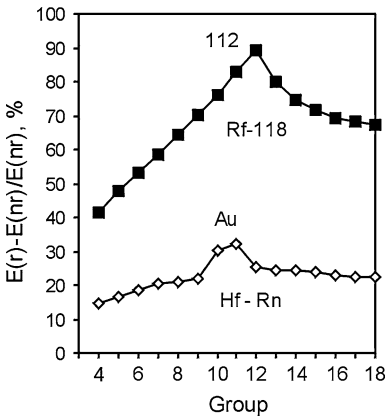

Fig. 4 The relativistic stabilization of the 6s and 7s orbitals in the 6th and 7th rows of the Periodic Table. Re-drawn from [8]. The DF data are from [21]

for outer shells. The SO splitting decreases with increasing l for the same principal quantum number, i.e., the $np_{1/2}$-$np_{3/2}$ splitting is larger than the $nd_{3/2}$-$nd_{5/2}$ and both are larger than the $nf_{5/2}$-$nf_{7/2}$. It is explained by the orbital densities in the vicinity of the nucleus decreasing with increasing l. In transactinide compounds SO coupling becomes similar, or even larger, in size compared to typical bond energies.

All the three effects change approximately as Z^2 for the valence shells down a column of the Periodic Table. It was suggested that relativistic effects depend even on higher powers of Z, especially for the heaviest elements [40]. Dependence of relativistic effects on electronic configuration in the neutral atoms of d- and f-block elements is discussed in [41].

The relativistic destabilization and SO splitting of the 6d AOs increase along the 6d series. Together with the stabilization of the 7s AOs, this results in an inversion of the 7s and $6d_{5/2}$ energy levels in Cn, so that its first ionized electron is $6d_{5/2}$ and not 7s as in Hg (Fig. 3). (The inversion of the 7s and $6d_{5/2}$ levels in the 7th period starts already at Hs). Figure 3 also shows that trends in the relativistic and non-relativistic energies and R_{max} of the ns AOs (the same is valid for the $np_{1/2}$ AOs) are opposite with increasing Z in the groups, which results in the opposite trends in relativistic and nonrelativistic properties defined by those AOs.

In the 7p series, the stabilization of the $7s^2$ is so large that it becomes practically an inert pair. The SO splitting of the 7p AOs increases along the series reaching 11.8 eV at element 118 (Fig. 5).

In the 8p and 9p elements, the SO interaction is so large, that their series split into the $p_{1/2}$ and $p_{3/2}$ ones [1, 2], so that the structure of the Periodic Table has no more clear blocks. For the heavier elements, relativistic effects on their valence orbitals are even more pronounced and could lead to properties that are very different to those of the lighter homologs. Without relativistic effects the properties would, however, also be very different due to the loosely bound valence s and p electrons.

Breit effects (accounting for magnetostatic interaction and retardation effects to the order of $1/c^2$) on energies of valence orbitals and IP are usually small, e.g., 0.02 eV for element 121, but can be as large as 0.1 eV for transition energies

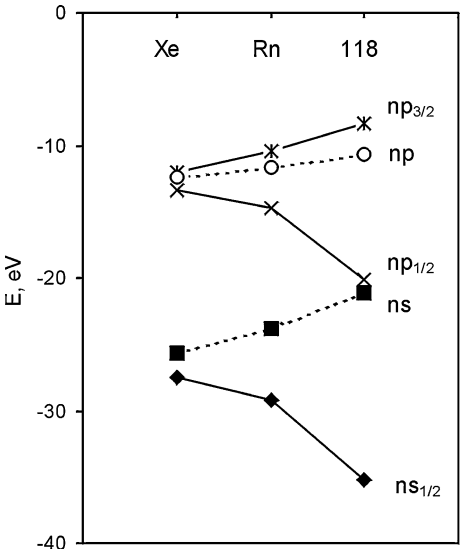

Fig. 5 Relativistic stabilization of the ns and $np_{1/2}$ orbitals and the spin–orbit splitting of the np orbitals for the noble gases Xe, Rn and element 118. The Dirac–Fock atomic energies are from [21] and the Hartree–Fock (nonrelativistic) values are from [8]

between the states including f orbitals [34]. They can also reach few % for the fine-structure level splitting in the 7p elements and are of the order of correlation effects there.

QED effects are known to be very important for inner shells [42, 43] in accurate calculations of X-ray spectra (see [44, 45] for the heaviest elements). For highly charged few electron atoms they were found to approach the Breit correction to the electron–electron interaction. Similar effects were also found for valence ns electrons [46]. A comparison of the valence ns Lamb shift (the vacuum polarization and self-energy) with the ns AO energy and the relativistic, Breit, and nuclear volume contributions to it for coinage metals at the DF level is shown in Fig. 6. The result for the valence ns electron is a destabilization, while for (n–1)d electron is an indirect stabilization. In the middle range (Z = 30–80) both the valence-shell Breit and the Lamb-shift terms behave similarly to the kinetic relativistic effects scaling as Z^2. For the highest Z values the increase is faster.

The nuclear volume effects grow even faster with Z. Consequently, for the superheavy elements, its contribution to the orbital energy should be the second important one after the relativistic contribution. QED corrections for the valence shells in heavy many-electron atoms of elements Rg through Fl, and 118 through 120 calculated using a perturbation theory are given in [47]. Thus, e.g., QED on the DCB IP of element 120 is −0.013 eV, while it is 0.023 eV for Cn. For element 118, QED effects on the binding energy of the 8s electron cause a 9% reduction

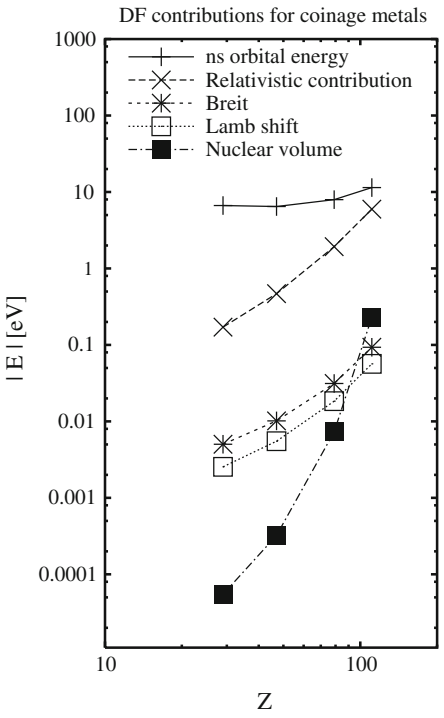

Fig. 6 Comparison of the valence ns Lamb shift with the orbital energy and the relativistic, Breit, and nuclear volume contributions to it for coinage metals. Reproduced with permission from P. Pyykkö, M. Tokman, L.N. Labzowsky, Phys. Rev. A **57**, R689 (1998). Copyright 1998 American Physical Society

(0.006 eV) of EA [48]. Thus, the QED effects are not negligible: they are of the order of 1–2% of the kinetic relativistic effects, which means that the existing studies of relativistic effects are up to 99% [46] (or 101% [36]) correct.

4 Relativistic Quantum Chemical Methods for Atoms and Molecules

4.1 Dirac Equation

Presently the highest level of theory for many-body methods for molecules is the DCB Hamiltonian

$$h_{\mathrm{DCB}} = \sum_i h_D(i) + \sum_{i<j} \left(1/r_{ij} + B_{ij}\right), \tag{5}$$

where the one-electron Dirac operator is

$$h_D(i) = c\vec{\alpha}_i\vec{p}_i + c^2(\beta_i - 1) + V^n(i) \tag{6}$$

Here, $\vec{\alpha}$ and β are the four-dimentional Dirac matrices, and V^n is the nuclear attraction operator. The Breit term in the low photon frequency limit is

$$B_{ij} = -\frac{1}{2}\left[(\vec{\alpha}_i\vec{\alpha}_j)r_{ij}^{-1} + (\vec{\alpha}_i\vec{r}_{ij})(\vec{\alpha}_j\vec{r}_{ij})r_{ij}^{-3}\right]. \tag{7}$$

The operators of the Dirac Eq. (5) are 4×4 matrix operators, and the corresponding wave function is therefore a four-component ($4c$) vector (spinor). The V^n includes the effect of the finite nuclear size, while some finer effect, like QED, can be added to the h_{DCB} perturbatively, although the self-energy QED term is more difficult to treat [36, 47, 48]. The DCB Hamiltonian in this form contains all effects through the second order in α, the fine-structure constant.

Since the relativistic many-body Hamiltonian cannot be expressed in a closed potential form, which means it is unbound, projection one- and two-electron operators are used to solve this problem. The operator projects onto the space spanned by the positive-energy spectrum of the Dirac–Fock-Coulomb (DFC) operator. In this form, the "no-pair" Hamiltonian is restricted then to contributions from the positive-energy spectrum and puts Coulomb and Breit interactions on the same footing in the SCF calculation [49].

Since the Dirac equation is written for one electron, the real problem of methods for a many-electron system is an accurate treatment of the instantaneous electron–electron interaction, called electron correlation. The latter is of the order of magnitude of relativistic effects and contributes to a larger extent to bonding energy and other properties. The DCB Hamiltonian (Eq. 5) accounts for these effects in the first order via the $V_{ij} = 1/r_{ij}$ term. Some higher order of magnitude

correlation effects are taking into account by the configuration interaction (CI), many-body perturbation (MBPT), including the Møller-Plesset (MP) theory, or, presently, at the highest level of theory, coupled cluster with single-double and perturbative triple, CCSD(T), excitations, or Fock-space CC (FSCC) techniques.

4.2 Atomic Codes

The most straightforward way to solve the Dirac many-electron Eq. 5 is that without an approximation. The DCB CC method [32, 33] is based on such a solution and is presently the most powerful method used for atomic calculations.

In the CC approach, correlation effects are taken into account by action of the excitation operator

$$S = \sum_{m \geq 0} \sum_{n \geq 0} \left(\sum_{l \geq m+n} S_l^{(m,n)} \right) \tag{8}$$

defined in the Fock-space CC approach with respect to a closed-shell reference determinant. In addition to the traditional decomposition into terms with different total number of excited electrons (l), S is partitioned according to the number of valence particles (m) or holes (n). Presently, the method is, however, limited to one or two (single-double excitations, CCSD, e.g. $(m,n) \leq 2$) particle valence sectors of the Fock space, i.e., it can treat the states which can be reached from a closed shell by adding or removing no more than two electrons.

Further developments are under way to remove this limitation [32, 33]. Thus, the high-sectors FSCC code is under development, which will allow for treating systems with up to 6 valence electrons/holes in an open shell. Relativistic Hilbert space CC (HSCC) method is also worked on, which could be used for systems with more than a couple of electrons/holes in the active valence shell. The mixed sector (MS) CC method will be a generalization of the previous two (FSCC and HSCC) and will combine their advantages. A further improvement is the introduction of the intermediate Hamiltonian (IH). It is a generalization of the effective Hamiltonian (EH) method and serves as a core of most multi-root multireference approaches. The standard multireference FSCC and HSCC methods (described above) are used in the effective Hamiltonian framework. The most problematic technical problem of the EH method is poor (or no) convergence of iterations due to presence of so-called intruder states. Recently many groups developed different forms of "intruders –free" intermediate Hamiltonian formulations of FSCC and HSCC. These formulations substantially extend the scope and applicability of the multi-root multireference CC methods. The XIH (extrapolated intermediate Hamiltonian) method is a specific (very efficient) form of IH developed by the Eliav-Kaldor group [32, 33].

The DCB FSCC method is very accurate, with an average error of 0.1 eV for excitation energies, since it takes into account most of dynamic correlation effects

omitted in the MCDF method and a core polarization. The DC FSCC and CCSD(T) methods incorporated in the DIRAC program package [50] have a slightly lower accuracy than the DCB FSCC one [32, 33]. Both the DCB and DC FSCC/CCSD(T) methods were applied to the heaviest elements up to Z = 122 (see [32, 33] and references therein, as well as various examples below). Due to the mentioned limitation of the methods, they can, however, presently not handle the elements of the midst of the d, f, or g-series.

In the relativistic *ab initio* DC(B) calculations, in contrast to non-relativistic ones, large basis sets are needed to describe accurately the inner shell region where relativistic perturbation operators are dominant. The condition of the kinetic balance relating the large and small components of the 4*c* wave function should be observed. Kinetically balanced Gaussian type wave functions with a Gaussian distribution for the nuclear potential are presently best suited. The practical basis sets for the heaviest elements are the universal ones [51], those of Visscher [52], Faegri [53, 54], and Dyall [54, 55]. The prolapse-free relativistic Gaussian basis sets for elements up to Z = 119 suitable for 4*c* molecular calculations are those of [56].

A practical instrument for many-electron open shell system is still the MCDF method. There are several modifications of it implemented into computational codes of Desclaux [57], developed further by Indelicato [36], of Grant [58] and Fröse-Fisher [59]. Based on the CI technique, the MCDF method accounts for most of the correlation effects while retaining a relatively small number of configurations. It can treat a large number of open shell configurations and can be applied to elements with any number of valence electrons. It omits, however, dynamic correlation, since excitations of the type $(nj) \rightarrow (n'j)$ cannot be handled, and some core polarization, which makes it less accurate than the DC(B) CC methods. An average error for IP of heavy elements is about 1 eV. Calculations for many heaviest and superheavy elements were performed with the use of the AL version [23–31], as well as with a more accurate OL one [36].

QED are presently included perturbatively on top of the self-consistent-field (SCF) calculations [36, 47, 48].

Atomic calculations for the heaviest elements were also performed using other approaches while studying molecular properties (see Sect. 5). Thus, e.g., electronic states of Fl were calculated using the relativistic complete active space MCSCF (CASMCSCF) CI method [60].

Earlier, chemical properties of the transactinides were predicted using single-configuration DF and DS calculations using approximations of Eqs. 5, 6 and numerical techniques [1, 2, 18–21]. The obtained energy terms were then corrected by the difference with experiment for the lighter homologs to reach the required accuracy. Elements up to Z = 172 were treated with the use of these methods. (Element 184 was also considered, as an example of an even heavier element). Overall, results of the modern *ab initio* correlated atomic calculations agree rather well with the (corrected) DF and DS ones from the early studies.

4.3 Molecular Methods

Methods used for relativistic calculations of the heaviest element systems are, in principle, the same used for any other relativistic system, provided basis sets for the heaviest elements are available. They are described in several issues, with those of [61–63] particularly recommended.

4.3.1 Wavefunction Based (*ab initio*) Methods

4 component (4c) methods. Molecular fully relativistic methods use the same DFC or DC(B) Hamiltonians (Eqs. 5, 6) as the atomic ones. Based on them molecular LCAO codes including correlation effects are at the stage of further development [64, 65]. The problems of electron correlation and proper basis sets make the use of these *ab initio* DF methods limited for molecular applications. Presently, correlation effects are taken into account by the CI, MBPT and CCSD(T) techniques. The basis sets and problems connected with their use are the same as for atomic ab *initio* calculations [51–55].

In these methods, calculations of two-electron integrals require large disk space and computational time. They are, therefore, still too computer time intensive and not sufficiently economical to be applied to the heaviest elements in a routine manner, especially to complex systems studied experimentally. Mostly small molecules, like hydrides or fluorides were studied with their use. The main aim of those works was investigation of the influence of relativistic and correlation effects on properties of model systems. One of successful implementations of this group of methods is a part of the DIRAC program package [50].

2 component (2c) methods. Due to the practical limitations of the 4*c* methods, 2*c* ones are very popular in molecular calculations. In this approximation, the "positronic" and electronic solutions of the Dirac-Hartree–Fock (DHF) method are decoupled [66, 67]. This reduces the number of matrix elements in the Hamiltonian to interactions solely among electrons (positive-energy states) and nuclei and, therefore, saves valuable computer time. Perhaps, the most applied method of decoupling the large and small components of the wave function is the Douglas-Kroll-Hess (DKH) approximation [68].

4.3.2 Relativistic Pseudo-Hamiltonians

An efficient way to solve a many-electron problem is to apply the pseudopotential (PP) approximation. Pseudopotential calculations are less accurate than all-electron, "but they simulate the results of the latter often surprisingly well, for substantially smaller expenses" [69]. The methods are widely used in electronic structure theory for chemically interesting compounds of all elements of the Periodic Table including the heaviest. There are several excellent reviews on this type of methods (see, e.g., [70, 71]).

According to this approximation, frozen inner shells are omitted and replaced in the one-electron part of the Hamiltonian by an additional term, the so-called pseudopotential (V^{PP})

$$H_V = -\frac{1}{2}\sum_{i}^{n_V}\nabla_i^2 + \sum_{i<j}^{n_V}\frac{1}{r_{ij}} + \sum_{i}^{n_V}\sum_{a}^{N_C}\left[V_a^{PP}(r_{ai}) - \frac{Q_a}{r_{ai}}\right] + \sum_{a<b}^{N_C}\frac{Q_a Q_b}{r_{ab}}, \qquad (9)$$

with n_V valence electrons and N_c cores (nuclei). The indices *a, b* run over all cores (nuclei), *i, j* over all valences electrons, Q_a is the charge of core *a*. As a result, the number of basis functions is drastically reduced and, hence the number of two-electron integrals. The additional one-electron pseudopotential integrals are solved by standard integral techniques for the valence basis functions giving rise to additional matrix elements in standard *ab initio* or density functional theory (DFT) schemes at the SCF level.

There are basically two current approaches in molecular applications for approximating V^{PP}: (1) the model core potential (MCP) one, also its extension to the *ab initio* model potential (AIMP) [72, 73] and (2) the semi-local pseudopotential (PP) approximation [74, 75].

In the MCP, or more advanced AIMP, approximations [72, 73], V^{PP} is represented by an adjustable local potential and a projection operator. This potential is constructed so that the inner nodal structure of the pseudo-valence orbitals is conserved, thus closely approximating all-electron valence AOs. Scalar relativistic effects are directly taken into account by relativistic operators such as Douglas-Kroll (DK) one. SO effects can be included with the use of the SO operator, V^{SO}. The resulting one-electron integrals are then easily solved for Gaussian functions. The methods are implemented in some commercial packages and can be applied to most of the elements of the Periodic Table, except of the heaviest, where such potentials still need to be constructed.

In the effective core potential (ECP) approximation, V^{PP} is represented by a semi-local potential [74]. Unlike in the MCP methods, there are no core functions and the pseudo-valence orbitals are nodeless for the radial part, which is an essential approximation. The semi-local ansatz gives rise to rather complicated integrals over the Gaussian functions compared to the MCP methods, though efficient algorithms were developed for their solution. Relativistic and SO effects are treated by relativistic one-electron PPs (RPP) [76]

$$V^{RPP} = \sum_{l,j,m_j} V_{lj}(r)\left|ljm_j\right\rangle\left\langle ljm_j\right|, \qquad (10)$$

or relativistic scalar and SO effects can be separated in the following way

$$V^{RPP} = V^{AREP} + V^{SO}, \qquad (11)$$

where the scalar V^{AREP} is

$$V^{\mathrm{AREP}} = \sum_{l,m_j} V_l(r)|lm_l\rangle\langle lm_l|. \tag{12}$$

The V^{AREP} is usually fitted to one-component (scalar relativistic) or two (four)-component all-electron DHF relativistic atomic wave functions or energies. Such potentials for elements Am through 118 were generated, e.g., by Nash et al. [77]. The ECPs are implemented in the program packages such as Gaussian, Molpro, MOLCAS, or Turbomole, and in the solid-state program CRYSTAL (see [71] and references therein).

Energy-adjusted PPs use atomic spectra (energies) for generating V^{PP} or V^{RPP} [75]. To achieve high accuracy, a large number of valence states has to be taken into account in the fitting procedure, which technically can be demanding and computer time expensive. SOPPs are obtained by adding V^{SO} to V^{AREP} (Eq. 12). These PPs, also including QED effects, were generated for the transactinides till Z = 118 [78, 79].

There are several other PPs differing in the way of fitting pseudopotential parameters. Among these are the popular quasirelativistic (QR) PPs of Hay and Wadt, which are implemented, for example, in the commercial program package "Gaussian" though have not yet been developed for the transactinides [80, 81].

More recently, generalized relativistic effective core potentials, GRECPs, have been developed [82]. An improvement over the original idea of V^{PP} is the division of the valence space into an outer core part and a valence part, and introduction of a special technique to correct an error introduced by smoothing orbitals in the core region. This could give more accurate results than V^{PP} provided a small core definition is used. The method is not widely used, as GREPs are not yet developed for all elements of the Periodic Table, and it has not yet been implemented in standard program packages. It was applied to some simplest heaviest elements molecules.

PPs are also used for 1D, 2D and 3D infinite systems (polymers, surfaces and the bulk). In the solid-state calculations, PPs are constructed from Kohn–Sham rather that Hartree–Fock equations. An overview of this class of the PP methods is given elsewhere [71].

4.3.3 Relativistic Density Functional Theory

DFT is based on the knowledge of the ground state electron density, which uniquely determines the Hamiltonian and, therefore, the ground state energy and other properties [83, 84]. Due to its relative simplicity, DFT became extremely useful in the application to large molecules, clusters, solutions and solids. Systems with the large number of atoms can be treated with sufficient accuracy. The computing time in the DFT for a system of many atoms, N_{at}, grows as N_{at}^2 or N_{at}^3, while in traditional methods, where the many-electron wave function $\Psi(r_1 \ldots r_N)$ is

used, as exp(N_{at}). DFT methods are alternative and complementary, both quantitatively and conceptually, to the traditional ones.

For the relativistic case [85, 86] in the non-collinear spin-polarize (SP) formalism, the Kohn–Sham equation for the total energy lying in the basis of the calculational algorithms is

$$E = \sum_{i=1}^{M} n_i \langle \phi_i | \hat{t} | \phi_i \rangle + \int V^N \rho \mathrm{d}^3 \vec{r} + \frac{1}{2} \int V^H \rho \mathrm{d}^3 \vec{r} + E^{\mathrm{xc}}[\rho, \vec{m}] + \sum_{p>q} \frac{Z_p Z_q}{|\vec{R}_p - \vec{R}_q|} \tag{13}$$

with the electron density

$$\rho(\vec{r}) = \sum_{i=1}^{M} n_i \phi_i^+(\vec{r}) \phi_i(\vec{r}) \tag{14}$$

and the magnetization density

$$\vec{m}(\vec{r}) = -\mu_B \sum_{i=1}^{M} n_i \phi_i^+(\vec{r}) \beta \vec{\Sigma} \phi_i(\vec{r}), \tag{15}$$

where ϕ_i are 4c-Dirac spinors. In Eqs. 13–15, $\hat{t}$ is the Dirac kinetic operator, μ_B is the Bohr-magneton, $V^N$is the nuclear potential, $V^H$is the electronic Hartree potential, and E^{ex} is the exchange correlation energy functional. The 4c spin operator $\vec{\sum} = \left(\sum_x, \sum_y, \sum_z\right)$ is built from the 2c Pauli matrix σ.

Application of the variational principle with the constraint that the number of electrons in the system should be conserved leads to the single particle Kohn–Sham equations in their non-collinear form

$$\left\{ \vec{t} + V^N + \tilde{V}^H + \frac{\delta E^{\mathrm{xc}}[\rho, \vec{m}]}{\delta \rho} - \mu_B \beta \vec{\Sigma} \frac{\delta E^{\mathrm{xc}}[\rho, \vec{m}]}{\delta \vec{m}} \right\} \phi_i = \varepsilon_i \phi_i. \tag{16}$$

According to the SP formalism, nearly each electron is treated by its own wavefunction with a quantum number j and magnetic number m_j. (The collinear approximation is also implemented in the method). This permits treatment of open shell system.

Usually, self-consistent, all-electron calculations are performed within the relativistic local density approximation (LDA). The general gradient approximation (GGA), also in the relativistic form, RGGA, are then included perturbatively in $E^{xc}(\rho, \vec{m})$. The accuracy depends on the adequate knowledge of the potential, whose exact form is, however, unknown. There is quite a number of these potentials and their choice is dependent on the system. Thus, PBE is usually favored by the physics community, PBE0, BLYP, B3LYP, B88/P86, etc., by the chemical community, while LDA is still used extensively for the solid state.

There are two 4c-DFT SP methods based on the solution of Eq. 13. They were extensively used for the heaviest elements. The first one [87] utilizes numerical

4*c* wave functions as a basis set. (The basis set optimization procedure is described in [87]). In the present form, it allows for treating explicitly very large systems such as clusters of up to more than hundred atoms and is, therefore, suitable for treatment of adsorption phenomenon on surfaces of solids. A possibility to treat the large number of atoms economically is foreseen via an embedded cluster procedure [88] (Fig. 7).

The second 4*c*-DFT code is the Beijing Density Functional (BDF) one [89]. As basis sets, 4*c* numerical atomic spinors obtained by finite-difference atomic calculations are used for cores, while basis sets for valence spinors are a combination of numerical atomic spinors and kinetically balanced Slater-type functions. Both the 4*c*-DFT [87] and 4*c*-BDF [89] methods give very similar results.

Earlier, the intrinsically approximate 4*c* Dirac-Slater discrete variational, DS DV, code of Ellis and Rosen [90] with the Slater $E^{\mathrm{ex}} = -3C[3\rho(r)/8\pi]^{1/3} = 0.7$ was used for calculations of transactinide compounds (see [6] for a review). Even though the method was inaccurate in calculating total and, hence, dissociation energies, it provided accurate IPs, EAs and electron transition energies.

2*c*-DFT methods are a cheaper alternative to the 4*c* ones, with a comparable accuracy [91]. One version is available as a part of the Amsterdam Density Functional (ADF) program package [92]. Calculations were performed on some transactinide molecules.

A one-component quasirelativistic DFT method, also a part of the ADF package [92], was extensively used in the calculations for transition element and actinide compounds. (Earlier, the quasirelativistic Hartree–Fock-Slater (QR HFS) method was widely used for such calculations [93]). In this method, the Hamiltonian contains relativistic corrections already in the zeroth-order and is therefore called the zeroth-order regular approximation (ZORA) [94, 95]. The spin operator is also included in the ZORA Fock operator [96]. Other popular quasirelativistic 2*c*-DFT methods are based on the DKH approximation [97, 98] and implemented in many program packages. The following codes should also be mentioned: of Rösch [99, 100], Ziegler [101], and Case and Young [102]. They were, however, not used for the heaviest elements. A review on relativistic DFT methods for solids can be found in [103].

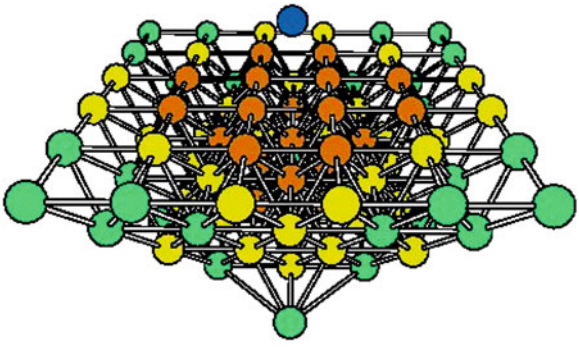

Fig. 7 Embedded M'-M_n system. (The embedded M_n cluster is shown in *red*)

Table 2 Accuracy of different molecular methods showing the importance of relativistic and correlation effects on the equilibrium bond length, R_e (in Å), dissociation energy, D_e (in eV), and vibrational frequency, ω_e (in cm^{-1}), of AuH

Method	R_e	D_e	ω_e	Ref.
HF (NR)	1.831	1.08	1464	[104]
HF (NR) MP2	1.711	1.90	1695	[104]
DHF	1.570	1.78	2067	[104]
DHF MP2	1.497	3.11	2496	[104]
DK CCSD(T)	1.525	2.92	2288	[106]
PP CCSD(T)	1.527	3.21	2306	[107]
RECP CCSD(T)	1.510	3.31	2330	[108]
DFT DKH	1.539	3.33	2330	[99]
DFT ZORA (MP)	1.537	3.33	2258	[109]
4*c*-BDF	1.537	3.34	2259	[109]
Experiment	1.524	3.36	2305	[110]

Accuracy of various relativistic, non-relativistic, correlated and non-correlated methods [99, 104–109] in comparison with experiment [110] is demonstrated in Table 2 for AuH, a sort of a test molecule (see also [111]). Both the PP/RECP and DFT methods seem to perform rather well for this molecule. The data of Table 2 also demonstrate the importance of relativistic and electron correlation effects. Thus, relativistic effects diminish the equilibrium bond length (R_e) by 0.26 Å (the HF–DF difference without correlation), or by 0.21 Å [the (HF + MP2) − (DF + MP2) difference with correlation], and enlarge the dissociation energy (D_e) by 0.70 eV (the HF–DF difference without correlation), or by 2.21 eV [the (HF + MP2) − (DF + MP2) difference with correlation]. Correlation diminishes R_e on the DF level by 0.07 eV, but enhances D_e by 1.34 eV. Thus, even for AuH correlation amounts almost to 50% of the chemical bond strength. These data also demonstrate that there is no additivity of correlation and relativistic effects.

5 Atomic Properties of the Transactinides

Electronic configurations, ionization potentials, atomic/ionic radii, polarizabilities and stability of oxidation states are important chemical properties, whose knowledge is indispensable in assessing similarity of the heaviest elements to their lighter homologs in the chemical groups.

5.1 Electronic Configurations

Predictions of chemical properties of elements Z = 104 through Z = 172 in the ground states made on the basis of DF and DS calculations up to 1975 are summarized in [1, 2]. DF ground states are also reported for Z = 111 through 132 [22]. MCDF calculations for ground and excited states of elements Rf through Hs are

published in [24–29], and for ground states of elements Z = 119–164 in [30]. Excited states of elements Z = 119–169 were also predicted at the MCDF level of theory [31]. The DC(B) CC ground and some excited states were calculated for Rf [112], elements 111–120 [48, 113–133] and 121–122 [34, 35]. DFT + QED calculations were reported for ground states of elements 121–131 [134].

MCDF calculations [23] have shown that Lr is the first element where the strong relativistic stabilization of the $7p_{1/2}$ electron results in a ground state electronic configuration, $7s^27p_{1/2}$ ($^2P_{1/2}$), different to that of Lu, $7s^26d$ ($^2D_{3/2}$). More accurate DCB CCSD calculations [122] confirmed this result. The next excited state of Lr, $7s^26d_{3/2}$ ($^2D_{3/2}$), was found to lie at 0.16 eV higher in energy in good agreement with the "corrected" value of 0.186 eV of the MCDF calculations [23].

For Rf, MCDF calculations [24, 25] have again shown a different electronic configuration, $7s^26d7p$ ($^3D_2$), than the one of Hf, $6s^25d^2$ ($^3F_2$). The $7s^26d7p$ ground state of Rf was, however, not confirmed by more accurate DCB CCSD calculations [112]. Inclusion of correlation effects of higher orders (f-electrons) in the CCSD calculations resulted in the inversion of the $7s^26d7p$ and $7s^26d^2$ states, with the latter being more stable.

Various calculations have shown that the relativistic stabilization of the 7s-AO in the 7th period results in the availability of the $7s^2$ electron pair in the ground and first ionized states of the 6d and 7p elements, $6d^q7s^2$ and $7s^27p^q$, respectively (Tables 3 and 4). This is in contrast to the 6th period, where Pt and Au have different, $5d^q6s$, ground states, or Ta, W, Os and Hg have different, $d^{q-1}s$, the 1+ ionized states. (The non-relativistic configuration of element 111 is, for example, $6d^{10}7s$ [113]). The relativistic stabilization of the 7p electrons manifests itself in some excited states different than those of lighter homologs, e.g., $6d7s^27p$ ($^3D_2$) of Rf lying 0.3 eV higher in energy in contrast to the $6d^27s^2$ ($^3F_3$) state of Hf.

For elements 119 and 120, the calculations have given the 8s and $8s^2$ states beyond the 118 core, respectively, as ground. Element 121 has an $8s^28p_{1/2}$ state in difference to Ac, $7s^26d$, due to the relativistic stabilization of the $8p_{1/2}$ AO, according to the DCB FSCC calculations [34]. Due to the same reason, the lowest state of the element 121 anion is $8s^28p^2$ compared to the $7s^27p6d$ state of Ac^-. For element 122, the DCB CCSD calculations [35] have given the $8s^27d8p_{1/2}$ ground state in contrast to the $7s^26d^2$ state for Th: the relativistic stabilization of the $8p_{1/2}$ orbital is responsible for such a change. All these calculations (except of the MCDF ones for Rf) agree on the ground states of elements up to $Z = 121$. They, however, start to disagree at $Z > 121$ (see Table 1), as was discussed in Sect. 2.

5.2 *Ionization Potentials, Electron Affinities and Oxidation States*

Non-relativistic (HF) and relativistic (DF) AO energies [21] of elements 104 through 118 are shown in Fig. 8. They are helpful in understanding ionization

Table 3 Electronic configurations, stable oxidation states and single ionization potentials of Rf through Cn

Element	Rf[b]	Db[c]	Sg[c]	Bh[c]	Hs[c]	Mt[d]	Ds[d]	Rg[b]	Cn[b]
Chemical group	4	5	6	7	8	9	10	11	12
Stable oxidation States[a]	**4**,3	**5**,4,3	**6**,4	7,5,4,3	**8**,6,4,3	3,6,1	6,4,2,0	**5**,3,-1	**4**,2,**0**
M	$6d^27s^2$	$6d^37s^2$	$6d^47s^2$	$6d^57s^2$	$6d^67s^2$	$6d^77s^2$	$6d^87s^2$	$6d^97s^2$	$6d^{10}7s^2$
IPi, eV	6.01	6.9	7.8	7.7	7.6	8.7	9.6	10.6	11.97
M^+	$6d7s^2$	$6d^27s^2$	$6d^37s^2$	$6d^47s^2$	$6d^57s^2$	$6d^67s^2$	$6d^77s^2$	$6d^87s^2$	$6d^97s^2$
IP* eV	14.37	16.0	17.9	17.5	18.2	(18.9)	(19.6)	(21.5)	22.49
M^{2+}	$7s^2$	$6d^3$	$6d^37s$	$6d^37s^2$	$6d^57s$	?	?	?	$6d^87s^2$
IP_3, eV	23.8[c]	24.6	25.7	26.6	29.3	(30.1)	(31.4)	(31.9)	(32.8)
M^{3+}	7s	$6d^2$	$6d^3$	$6d^27s^2$	$6d^37s^2$	?	?	?	?
IP_{4j} eV	31.9[c]	34.2	35.4	37.3	37.7	(40)	(41)	(42)	(44)
M^{4+}	[Rn]	6d	$6d^2$	$6d^27s$	$6d^2\ s^2$	($6d^5$)	($6d^6$)	($6d^7$)	($6d^8$)
IPs, ev		44.6	47.3	49.0	51.2	(51)	(53)	(55)	(57)
M^{5+}		[Rn]	6d	$6d^2$	$6d^3$				
IP_6, eV			59.2	62.1	64.0				
M^{6+}			[Rn]	6d	$6d^2$				
IP_7, ev				74.9	78.1				
M^{7+}				[Rn]	6d				
IPs, eV					91.8				

[a] bold = most stable states in the gas phase, underlined = most stable in solutions; [b] CCSD calculations: Rf [112]; Rg [113]; Cn [114]; [c] MCDF calculations: Rf [24, 25]; Db [26], Sg [27], Bh and Hs [28]; [d] DF calculations [1, 2]. The values of the IP in the parentheses are extrapolations, see [2]

Table 4 Atomic properties of element 112 through 120 (selected values)

Property	Cn	113	F1	115	Lv	117	118	119	120
Group	12	13	14	15	16	17	18	1	2
Electr. conf.	$d^{10}s^2$	$7s^27p$	$7s^27p^2$	$7s^27p^3$	$7s^27p^4$	$7s^27p^5$	$7s^27p^6$	$8s^1$	$8s^2$
Oxid. state	4,2,0	1,3	2	1,3	2,4	3,1,5,−1	4,2,6	1	2
IP, eV	11.97[a]	7.306[b]	8.626[c]	5.579[d] 5.553[e]	6.881[f]	7.638[g]	8.914[h]	4.788[i]	5.838[j]
EA, eV	0[a]	0.68(5)[b]	0[k]	0.383[d] 0.368[e]	0.905[f]	1.589[g]	0.056[l]	0.663[m]	0.019[j]
α, a.u.	27.40[n]	29.85[o]	30.59[n] 31.0[s]	(66)[p]	(61.17)[p]	(54.24)[p]	46.33[h]	169.00[r]	162.6[j]
AR, Å	1.71[n]	1.22[o]	1.75[n]	2.0[e]	–	1.76[u] 1.77[v]	2.41[h]	2.40[t]	2.0[t]
R_{vdW}, Å	1.99[n]	1.84[o]	2.08[n]	2.46[e]	–	–	2.41[h]	–	–

[a] Ref. [114]; [b] [115]; [c] DCB IHFSCC[129]; [d] [117]; [e] [123]; [f] DCB XIHFSCC[124]; [g] DC CCSD (T) [124]; [h] DCFSCC[119]; [i] DCB FSCC [120]; [j] DCB XIHFSCC (+ QED for IP) [125];[k] [129, 140];[l] [48]; [m] [121]; [n] [127];[o] [126];[p] estimated via a correlation with $R_{max}(np_{3/2})^3$ [130]; [r] DK CCSD(T) [131, 132]; [s] Kramers-restricted (KR) DC [133]; [t] [2]; [u] MCDF [137]; [v] $1/2R_e(M_2)$[91]

process and trends in ionization potentials. The latter, experimental in the case of the 6th row elements, and calculated (best values) in the case of the 7th row elements of the Periodic Table are given in Tables 3, 4 and are shown in Fig. 9.

The DF and DS IPs of elements 104 through 166 are given in [1, 2]. Multiple MCDF IPs of Rf through Hs, Cn, Fl and 117 are presented in [24–28, 135–137], and the first MCDF IPs of elements 113–119 are in [29]. IP(114) was also calculated using relativistic HF MBPT [138], and IPs and EAs of 7p elements were calculated using a multireference (MR) CI method [55]. The DC(B) CC IPs are reported for elements Rf, Rg-122 [34, 35, 48, 112–127]. The accuracy of various calculations of IPs of Pb and Fl is demonstrated in Table 5 [2, 60, 116, 129, 136, 138–140], where the highest level of theory is DCB IHFSCC [116, 129].

The calculated IP(Rf) is smaller than IP(Hf), because the 6d electron of Rf is weaker bound than the 5d one of Hf. For Db and Sg, IPs should be similar to those of Ta and W, due to the similar energies of the ionized electrons in each pair of the homologs. This is, indeed, the case shown by the calculations. IP(Bh) should be smaller than IP(Re). From Hs through Cn, IP of the 6d elements should, however, be larger than IPs of Os through Hg due to the more bound 6d electron in the heaviest elements in comparison with the 6s one in the lighter homologs. The MCDF calculations for Hs [28] and DF ones for Mt [1, 2] have, however, given lower values than expected. For Ds through Cn, the calculated values are larger than those of Pt through Hg, as anticipated. More accurate calculations than the DF and MCDF ones are, therefore, needed for the midst of the 6d-series.

IPs of elements 113 and 114 are also larger than those of Tl and Pb, respectively, due to the relativistically stabilized $7p_{1/2}$ AO. The relativistic stabilization of the $np_{1/2}$ AO in group 13 and 14 is responsible for a trend reversal in the decreasing IPs beyond In and Sn, respectively [126, 127]. IPs of elements 115 through 118 are, on the contrary, smaller than those of Bi through At, and are the

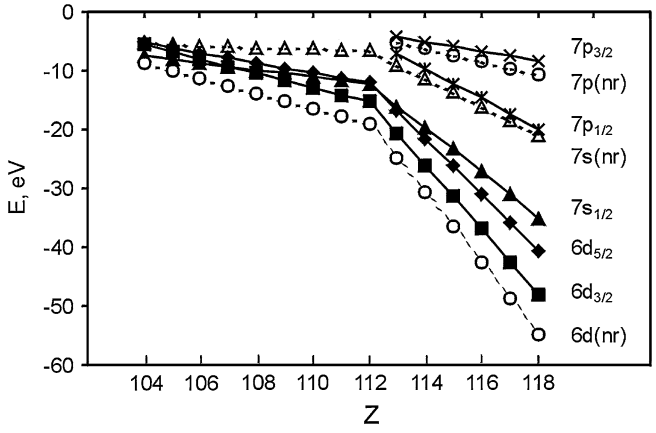

Fig. 8 Relativistic (DF, *solid lines*) and non-relativistic (HF, *dashed lines*) orbital energies of elements 104 through 118. The data are from [21]. From [11]

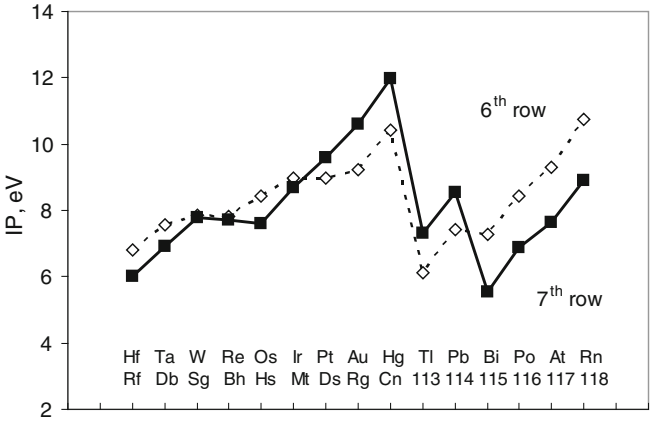

Fig. 9 Ionization potentials of the 6th row elements (*dashed line*, experimental values [141, 142]) and 7th row elements (*solid line*, calculated values, see Tables 3 and 4)

Table 5 A comparison of various calculations of IPs (in eV) of Pb and Fl

Method	Pb	Fl	Ref.
DF	–	8.9 (8.5[a])	[2]
MCDF	7.036	8.125 (8.275[a])	[136]
2*c*-ECP CCSD(T)	7.156 (7.30 fit)	8.529 (8.68[a])	[139]
rel. HF MBPT	7.433	8.487	[138]
CASMC/CI[b]	–	8.419	[60]
DFC CCSD(T)	–	8.36	[140]
DCB IHFSCC	7.484	8.539	[116]
DCB IHFSCC[c]	7.459	8.626	[129]
Exp.	7.417	–	[141]

[a] Extrapolated value; [b] Relativistic Complete Active Space Multiconfiguration/Configuration Interaction method; [c] with a more extended and balanced basis set than in [116]

smallest in their groups, due to the relativistically destabilized $7p_{3/2}$ AO. The drop of the *solid line* in Fig. 9 from element 114 to 115 reflects the magnitude of the 7p AO SO splitting. Overall, Cn has the largest IP in the 7th period, and also in group 12, indicating its largest inertness, while element 118 has a relatively low IP, the lowest in group 18, indicating its maximal chemical activity in this group. It should also be the most electropositive element out of all noble gases.

An upturn in IPs is observed in group 1 from Sc to element 119 and in group 2 from Ba to element 120 due to the relativistic stabilization of the outer $ns_{1/2}$ electrons [143, 144] (Figs. 10, 11). IPs of elements 119 and 120 are relativistically increased, e.g., from 3.31 eV to 4.53 eV for element 119, as DK CCSD calculations show [131, 132].

The IP(121) of 4.447 eV, a DCB FSCC value [34], is the highest in group 3. The DCB IH FSCC value of IP(122) of 5.595 eV [35] is lower than IP(Th) of

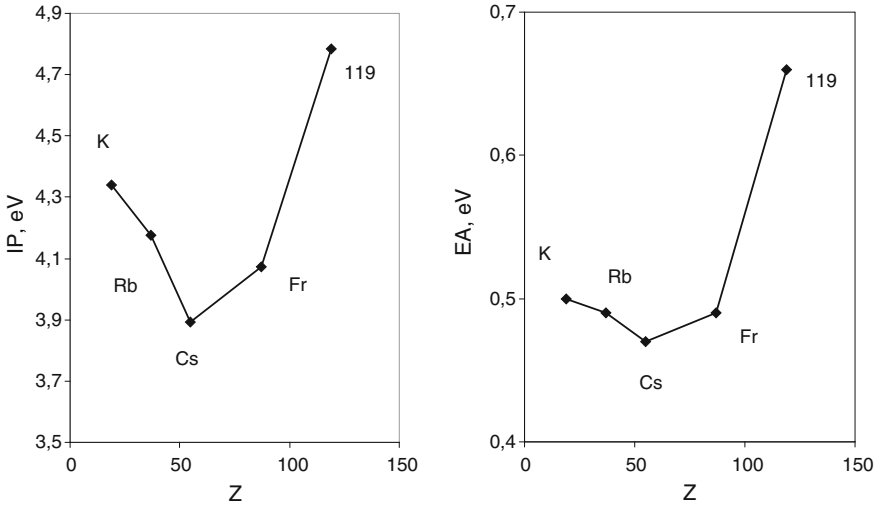

Fig. 10 Ionisation potentials, IP, and electron affinities, EA, of group-1 elements. The data for K through Fr are experimental [141, 142], while those for element 119 are DCB CC calculations [120, 121] (see Table 4). Reprinted with permission from [144]. Copyright 2012 Elsevier

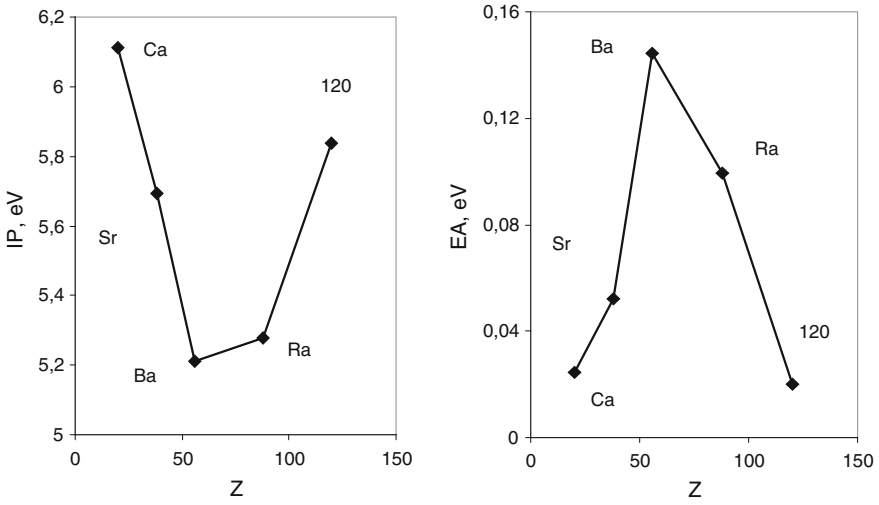

Fig. 11 Ionisation potentials, IP, and electron affinities, EA, of group-2 elements. The data for Ca through Ra are experimental [141, 142], while those for Ra (EA) and element 120 are DC CC calculations [125] (see Table 4). Reprinted with permission from A. Borschevsky, V. Pershina, E. Eliav, U. Kaldor, J. Chem. Phys. **136**, 134317 (2012). Copyright 2012 American Institute of Physics

6.52 eV due to the more bound $8p_{1/2}$ electron of element 122 than the 6d one of Th. The DF and DS values of IPs of even heavier elements can be found in [1, 2].

According to MCDF calculations [25–28], multiple IP should decrease in groups 4 through 8 (Fig. 12). The reason for that is the proximity of the valence 7s and 6d orbitals and relativistic destabilization of the latter with increasing Z in the groups (Fig. 8). That makes energies of the electron transitions between the (n–1)d and ns levels smaller than of the corresponding transitions in their 4d and 5d homologs, resulting in an enhanced stability of the maximum oxidation states.

IPs of internal conversion electrons (1s and 2s) of Cn, Fl, and elements 116 (livermorium, Lv) and 118 were predicted to an accuracy of a few 10 eV using DHF theory and taking into account QED and nuclear-size effects [44]. The $K_{\alpha 1}$ transition energies for different ionization states of Mt were calculated using the same approach and compared with recent experiments on the α-decay of ^{272}Rg [45].

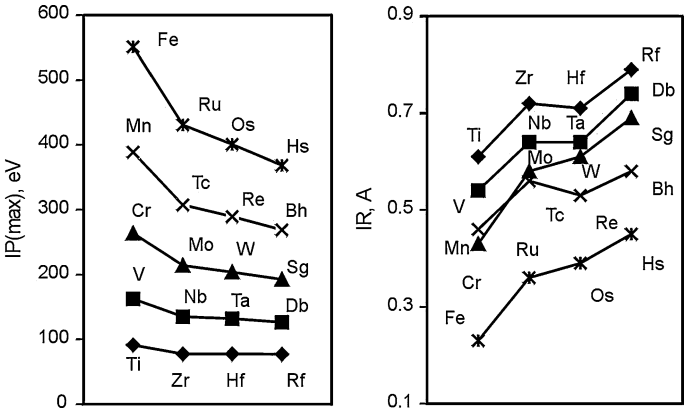

Fig. 12 Ionization potentials to the maximal oxidation state (IP_{max}) and ionic radii (IR) for Rf through Hs obtained from the MCDF calculations [24–28]. From [11]

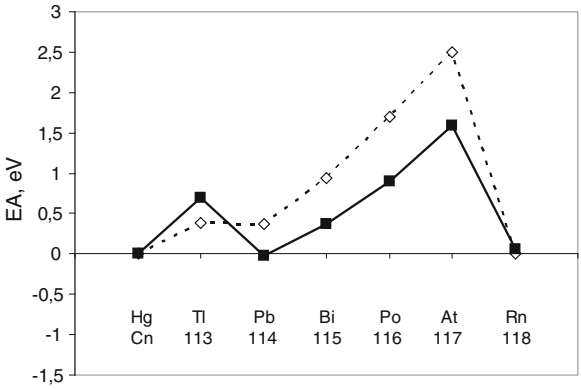

Fig. 13 Electron affinities of the 6th row (open rhomboids connected by the *dashed line* are experimental values [142]) and the 7th row elements of the Periodic Table (filled *squares* connected by the *solid line* are DC(B) CC calculated values, see Table 4)

Electron affinities were calculated for a few of the heaviest elements (Table 4 and Fig. 13). No bound anion was found for Cn by DCB FSCC calculations [114]. EA(113) was shown to be larger than EA(Tl) due to the relativistic stabilization of the $7p_{1/2}$ AO [115]. For Fl having a quasi-closed $7s^2 7p_{1/2}^2$ shell, a negative EA was obtained at various levels of theory (−0.02 eV at DC FSCC [128], −0.215 eV at DHF MRCI [55]), which might be due to the limited, though very large, basis sets. (The negative value has, of course, no physical sense). Thus, it was concluded that Fl has no EA [128]. A zero EA was also obtained by the DHF(B) CCSD(T) calculations [140]. EAs of elements 115 through 117 are smaller than those of the lighter homologs due to the relativistic destabilization of the $7p_{3/2}$ AOs. Element 118 has a positive EA of 0.058 eV, according to the DCB FSCC + QED calculations [48, 118]. The reason for that is the relativistic stabilization of the 8s AO.

EA of element 119 is the largest is group 1 because of the relativistic stabilization of the ns AO (Fig. 10). Also, due to the same reason, a reversal of the decreasing trend in EA beyond Cs is observed in this group. In group 2, on the contrary, EA increases from Ca to Ba, while a reversal of the trend occurs beyond Ba, so that EA of element 120 is about that of Ca (Fig. 11). This trend was explained by the one in the energies of the vacant AOs of a mixed $np_{1/2}$ and (n–1)d character [143] and polarizabilities of the group-2 atoms [125]: Since the extra

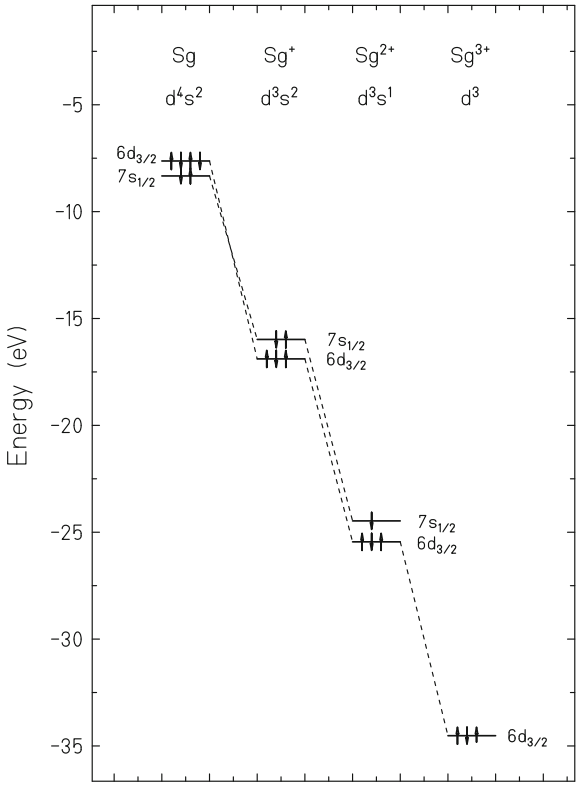

Fig. 14 MCDF orbital energies of the neutral through the third ionized state of Sg. Reprinted with permission from V. Pershina, E. Johnson, B. Fricke, J. Phys. Chem. A **103**, 8463 (1999). Copyright 1999 American Chemical Society

electron is bound to the atom due to the strong correlation (polarization) interaction, the smallest α of element 120 results in its smallest EA. Thus, correlation effects were shown to be very important to stabilize the element 120 negative ion.

Using IP and EA, absolute electronegativities χ were predicted for group 1 and 2 elements including 119 and 120, respectively [143, 144]. They show a reversal of the decreasing trend at Cs and Ba in these groups, respectively. Thus, element 119 should be more electronegative than K, and element 120 should be as electronegative as Ca. EA of element 121 of 0.569 eV should be the highest in group 3, according to the DCB FSCC calculations [34].

Predicted oxidation states of elements Rf through 120 are given in Tables 3, 4. As was mentioned, the proximity of the valence 7s and 6d AOs (Fig. 8) results in the stability of the highest oxidation states at the beginning of the 6d series. For the same reason, lower oxidation states will be unstable there. Thus, e.g., the step-wise ionization process results in the $6d^2$ and not the $7s^2$ configuration for Db^{3+} or Sg^{4+} (see Fig. 14 for Sg, as an example) [145]. Since the 6d AOs of the 6d elements are more destabilized than the (n–1)d AOs of the 4d and 5d elements, the Db^{3+} and Sg^{4+} will even be less stable than Ta^{3+} and W^{4+}.

The destabilization of the 6d AOs at the end of the 6d series is also the reason for the 6d electrons to be chemically active. As a consequence, an increase in the stability of the higher oxidation states is expected, e.g., of the 3+ and 5+ states of Rg and 4+ state of Cn. The 0 state will, however, be predominant in Cn due to its closed-shell structure.

The large relativistic stabilization of the $7s^2$ electrons and, hence, a large 7s–7p gap hindering hybridization, see Fig. 8, is the reason for an enhanced stability of lower oxidation states at the beginning of the 7p-series. Thus, the 1+ oxidation state will be more important for element 113 than the 3+ state.

Due to the relativistic stabilization of the two $7p_{1/2}$ electrons of Fl, the 2+ state should predominate over the 4+ one to a greater extent than in the case of Pb. The 6d AOs should be still accessible for hybridization for elements 113 and 114 and should take part in bonding leading to the formation of compounds of these elements in higher oxidation states like, e.g., $113F_5$ or FlF_6. For elements 115 through 118, on the contrary, lower oxidation states should be more stable than those of the lighter homologs due to the inaccessibility of the relativistically stabilized $7p_{1/2}$ AO for bonding. For element 115, the 1+ state should be more important due to the SO destabilized $7p_{3/2}$ electron. The 3+ state should also be possible, while 5+ not. For Lv, a decrease in the stability of the 4+ oxidation state is expected due to the large SO splitting of the 7p AOs, and the 2+ state should be important because of the two destabilized $7p_{3/2}$ electrons. For element 117, the 1+ and 3+ oxidation states should be the most important, while the 5+ and 7+ states less. The 1- state of element 117 having one-electron hole on the $7p_{3/2}$ AO should, therefore, be less important (its EA is the smallest in the group). For element 118, 2+ and 4+ states are possible, while the 6+ one will be less important, because of the strong binding of the $7p_{1/2}$ electrons. Oxidation states of heavier elements are discussed in [1, 2].

5.3 Atomic/Covalent/Ionic Radii and Polarizability

Radii, atomic (AR) and ionic (IR), are defined by the maximum of the radial charge density, R_{max}, of the outer valence AO in a neutral, or ionized atom, respectively. They were, therefore, estimated in most cases via a correlation between these quantities in the chemical groups. (The DF R_{max} of AOs of elements up to Z = 120 are tabulated by Desclaux [21]). The MCDF R_{max} and defined on their basis AR and IR for Rf through Hs and their lighter homologs in the chemical groups in various oxidation states are given in [23–28], for elements 112 and 114 in [135, 136], and for element 117 in [137]. (The radii for homologs are given in [146–148]). Van der Waals radii, R_{vdW}, in some cases were also estimated via a correlation with R_{max}, AOs as well as from calculations of bond lengths in molecules bound by dispersion forces, like, e.g., Cn_2 [127]. AR of elements Rf through Rg are given in [2], AR and R_{vdW} of elements Cn through 120 are in Table 4. Covalent radii (CR) were obtained for elements till Z = 118 from calculated bond lengths in some covalent compounds [149, 150].

These data show that AR of the 6d elements (the same is valid for R_{vdW}) should be smaller than those of their 5d congeners, with the maximum effect on Rg and Cn undergoing the strongest 7s AO contraction in the respective groups. In group 13 and 14, AR and R_{vdW} exhibit a reversal of the increasing trend at In and Sn, respectively, as that in $R_{max}(np_{1/2})$-AO, so that elements 113 and 114 should have smaller radii than those of the 6p homologs. The reason for that is the relativistic contraction of the $np_{1/2}$ AOs. In elements 115 through 118, the radii should be larger than those of their lighter homologs due to the increasing expansion of the $np_{3/2}$ AOs. In group 1 and 2, a reversal of the increasing trend in AR should occur at Cs and Ba, so that AR of elements 119 and 120 are about AR of Rb and Sr, and those of elements 165 and 166 are about AR of K and Ca, respectively (Fig. 15) [2, 143, 144]. The reason for the trend reversal is the increasing relativistic stabilization of the ns AO. The shell-contraction effects are, however, much smaller in the group-1 series of elements compared to the group-11 ones.

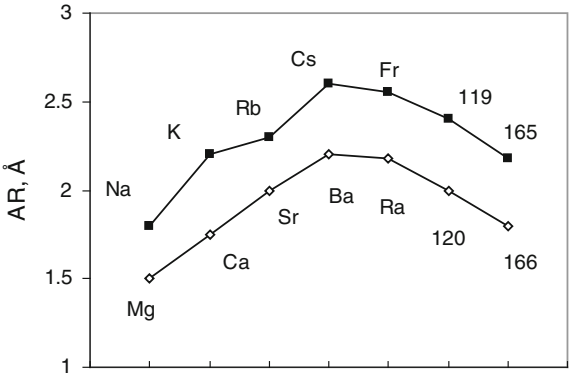

Fig. 15 Atomic radii of alkali and alkaline earth elements. The data for Na through Cs and Mg through Ra are experimental ones [146]. The data for the heaviest elements are from DC and DF calculations (see Table 4). From [13]

Table 6 Estimated ionic radii for CN = 6 (in Å) of Rf through Hs in the maximum oxidation states [24–28]. Experimental data [148] are for the lighter elements

Group 4		Group 5		Group 6		Group 7		Group 8[a]	
Ti^{4+}	0.61	V^{5+}	0.54	Cr^{6+}	0.44	Mn^{7+}	0.46	Fe^{8+}	0.23
Zr^{4+}	0.72	Nb^{5+}	0.64	Mo^{6+}	0.59	Tc^{7+}	0.57	Ru^{8+}	0.36
Hf^{4+}	0.71	Ta^{5+}	0.64	W^{6+}	0.60	Re^{7+}	0.53	Os^{8+}	0.39
Rf^{4+}	0.79[b]	Db^{5+}	0.74[b]	Sg^{6+}	0.65[b]	Bh^{7+}	0.58	Hs^{8+}	0.45

[a] For CN = 4; [b] a correlation of IR with the $\langle \bar{r}_{nl} \rangle$of the 6p AO s gives IR of 0.74 Å for Rf^{4+} , 0.66 Å for Db^{5+} , and 0.63 Å for Sg^{6+} [152]. More realistic values obtained from the geometry optimization of molecular compounds are 0.76 Å for Rf^{4+} and 0.69 Å for Db^{5+}

The IR of group-4 through 8 elements in their highest oxidation states for the coordination number, CN, equal to 6 are given in Table 6 and Fig. 12. They are almost equal for the 4d and 5d elements due to the lanthanide contraction (of 0.020 Å), which is roughly 86% a nonrelativistic effect: The diminished shielding of the nucleus charge by the 4f electrons causes the contraction of the valence shells. The IR of Rf through Hs are about 0.05 Å larger than IR of their 5d congeners. This is due to an orbital expansion of the outer $6p_{3/2}$ AOs responsible for the size of the ions. The IR of the 6d elements are, however, still smaller than IR of the actinides due to the actinide contraction (0.030 Å). The latter is larger than the lanthanide contraction and is mostly a relativistic effect. This is due to the fact that the 5f shell is more diffuse than the 4f shell, so that the contraction of the outermore valence shells is increased by relativity to a larger extent in the case of the 6d elements as compared to the 5d elements. The DF and HF calculations [151] for the 5d and 6d elements with and without the 4f and 5f shells, respectively, have shown that the shell-structure contraction is, indeed, enhanced by relativistic effects and that the orbital and relativistic effects are not additive.

IR of the 119^+ and 120^{2+} ions were determined via a correlation with $R_{max}[(n–1)p_{3/2}]$ AO in group 1 and 2, respectively [143, 144]. In contrast to the trend in AR in these groups (Fig. 15), the IR reveal a steady increase with Z stipulated by the expansion of the outermost $(n–1)p_{3/2}$ AOs in these ions.

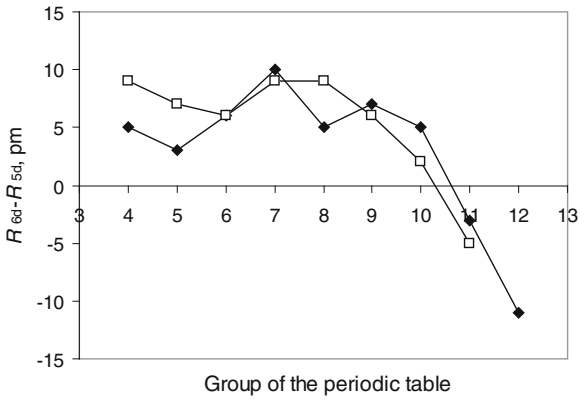

Fig. 16 The difference in the lengths of the single (filled rhomboids) and triple (open *squares*) bonds between the 6d and 5d metals [149, 150]. From [13]

Single and triple bond CR for the group-4 through 8 6d-elements were found to be about 0.06 Å on the average larger than CR of the 5d elements [149, 150] (Fig. 16), in agreement with the IR (Table 6). (The triple bond CR are slightly larger, 0.08 Å on the average). An important finding of those works is a decrease in the CR_{6d}-CR_{5d} difference starting from group 9, reaching negative values in groups 11 and 12, as a result of the relativistic bond contraction caused by the relativistic stabilization of the ns AO. This was called a "transactinide break" [149, 150].

Static dipole polarizabilities (α) were calculated most accurately at the DC CC level of theory for elements Cn through Fl, elements 118 through 120 [119, 125–127, 131, 132]. For elements 115 through 117, α were determined via a correlation with R^3_{max} of the outermost valence AOs in the chemical groups [130]. Results are given in Table 4 and Fig. 17 in comparison with experimental polarizabilities of the homologs in the 6th period.

According to the DC CC calculations [127], polarizability of Cn should be the smallest in group 12 due to the relativistic contraction of the 7s AO. Polarizabilities of element 113 and Fl are also smaller than those of In and Tl, and Sn and Pb, respectively, due to the relativistic stabilization of the $7p_{1/2}$ AO [126, 127]. A reversal of the trends in α is observed in group 13 and 14 beyond In and Sn, respectively, similarly to that in AR, or $R_{max}(np_{1/2})$-AO. A steep increase in α (Fig. 17) from element 114 to 115 reveals the magnitude of the 7p AO SO effect, since the highest occupied (HO) AO in Fl is $7p_{1/2}$, while it is $7p_{3/2}$ in element 115. Thus, the trend becomes opposite in groups 15 through 18 to those in groups 13 and 14, so that for elements 115 through 118, α is the largest in the respective chemical groups due to the largest $R_{max}(np_{3/2})$-AO.

For element 119, α is relativistically decreased from 693.9 to 165.98 a.u., as calculated at the DK CCSD(T) level of theory [131, 132]. A reversal of the increasing trend in α is predicted in groups 1 and 2 beyond Cs and Ba, so that α of elements 119 and 120 are about those of Rb and Ca, respectively [125, 143, 144]. The reason for the trend reversal is the increasing relativistic contraction of the ns AO.

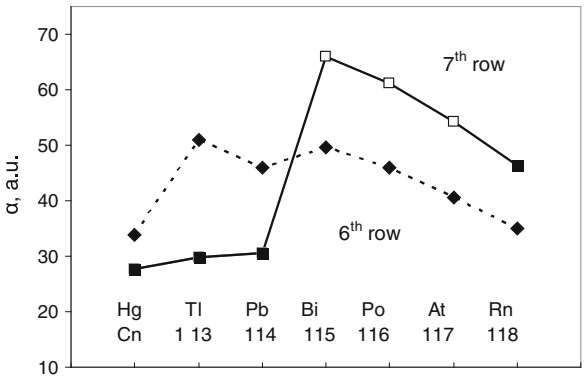

Fig. 17 Polarizabilities of the 6th row (filled rhomboids connected by the *dashed line* are experimental values [142]) and 7th row elements of the Periodic Table (*filled squares* connected by the *solid line* are DC calculated values, open ones are obtained via a correlation with R^3_{max} of their outer AO, see Table 4)

Table 7 Polarizabilities, α (in a.u.), of Hg and Cn calculated within different approximations

Atom	Method	α				Ref.
		HF	MP2	CCSD	CCSD(T)	
Hg	NR PP	82.25	–	–	37.83	[153]
	AR PP	44.78	28.33	35.26	34.42	[153]
	ECP	32.46	27.13	28.82	28.48	[139]
	DC	44.90	27.47	35.31	34.15	[127]
	exp.	–	–	–	33.91	[154]
Cn	NR PP	107.85	–	–	74.66	[153]
	AR PP	29.19	23.57	25.84	25.82	[153]
	ECP	30.30	27.67	28.61	28.68	[139]
	DC	29.46	25.11	27.66	27.64	[127]

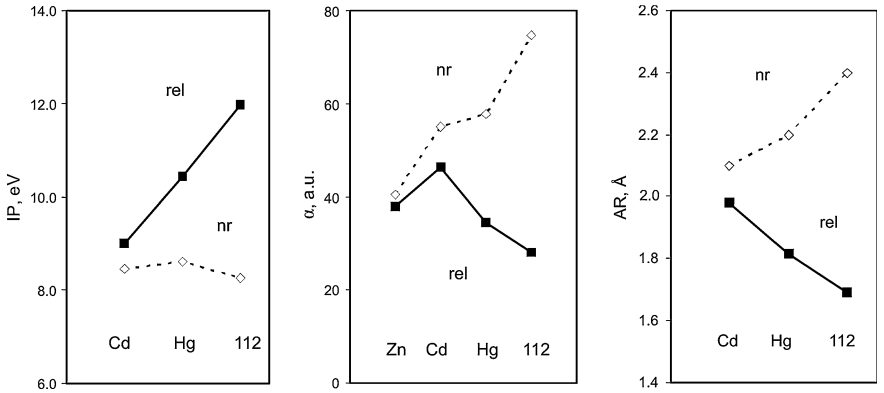

Fig. 18 Relativistic (*solid lines*) and non-relativistic (*dashed lines*) ionization potentials, IP, atomic radii, AR, and polarizabilities, α, of group-12 elements. Reprinted with permission from [155]. Copyright 2000 Elsevier

Finally, Table 7 demonstrates the influence of relativistic and correlation effects on α shown by various calculations—nonrelativistic (NR), average relativistic (AR, i.e., without spin–orbit) PP, relativistic ECP and DC; without electron correlation Hartree–Fock (HF), and with correlation at the different levels of theory (MP2, CCSD and CCSD(T))—for Hg and Cn, as an example. One can see that relativistic effects essentially decrease α of both species, with the effect being much more pronounced for the heavier element (a relativistic decrease from 74.7 to 25.8 a.u., as is shown by the PP CCSD(T) calculations [153]). Correlation effects also decrease α in both cases much more at the nonrelativistic level than at the relativistic. Correlation effects on α of group 13 and 14 elements are similar to those of group-12 elements.

Influence of relativistic effects on atomic properties of group-12 elements, as the most interesting case, is shown in Fig. 18. Thus, relativistic effects are

responsible for the largest IP and smallest both α and AR of Cn in group 12. This means that Cn should be chemically rather inert, much more than the lighter homologs in the group.

6 Electronic Structures and Properties of Gas-Phase Compounds of the Heaviest Elements. The Role of Relativistic Effects

6.1 Rf Through Hs (Elements 104 Through 108)

Elements at the beginning of the 6d series form halides, oxyhalides, oxides and other compounds similarly to their lighter homologs in the chemical groups. Their electronic structures and chemical properties such as ionicity, covalence, bonding, geometrical configurations, thermochemical stability, as well as the influence of relativistic effects on those properties, have been studied in a number of theoretical works. Many of them were also devoted to predictions of the behavior of such compounds in gas-phase chromatography experiments (see "Gas-Phase Chemistry of Superheavy Elements").

6.1.1 Hydrides of Rf and Sg

Group-4 and 6 hydrides, MH_4 (M = Ti, Zr, Hf, and Rf) and MH_6 (M = Cr, Mo, W, and Sg) are the simplest systems which were used in the past as models to study influence of relativistic effects on molecular properties. The early DF one-center expansion (DF-OCE) calculations [156–158] showed relativistic effects to decrease the bond length of RfH_4 and SgH_6, so that $R_e(RfH_4)$ is only 0.03 Å larger than $R_e(HfH_4)$, and $R_e(SgH_6)$ is 0.06 Å larger than $R_e(WH_6)$. The relativistic contraction of orbitals and of bond lengths were shown to be two parallel, but largely independent effects. The calculations revealed a decrease in the dissociation energy of RfH_4 as compared to that of HfH_4 and a slight increase in it of SgH_6 as compared to that of WH_6.

6.1.2 Group-4 Through 8 Halides, Oxyhalides and Oxides

Halides and oxyhalides of the elements at the beginning of the 6d series were studied extensively using a variety of methods, mostly DFT and PPs. The 4*c*-DS DV and DFT calculations were performed for the following compounds: MCl_4 (M = Ti, Zr, Hf, and Rf) [159], MCl_5, $MOCl_3$, MBr_5 and $MOBr_3$ (M = Nb, Ta, and Db) [160–164], MCl_6, $MOCl_4$, MO_2Cl_2 (M = Mo, W, and Sg) [165–167], MO_3Cl (M = Tc, Re, and Bh) [168], and MO_4 (M = Ru, Os, and Hs) [169, 170].

The RECP CCSD calculations were performed for halides and oxyhalides of Rf through Sg, such as $RfCl_4$, MCl_6, $MOCl_4$, MO_2Cl_2, MO_3 (M = W and Sg), MCl_5,

and MBr_5 (M = Ta and Db) [171]. Results of *ab initio* non-correlated DF calculations were reported for $RfCl_4$ and HsO_4 [172, 173].

Results until 1999 are overviewed in [6–9]. For later reviews including more accurate calculations, see [10–14].

Various properties of the transactinide compounds were predicted on the basis of these calculations. Thus, optimal geometries and stability of compounds (dissociation energies) were predicted with a sufficient accuracy. Moreover, electronic density distribution and type of bonding were defined. Some other spectroscopic

Table 8 Bond lengths (in Å) of halides, oxyhalides and oxides of group 4–8 elements as a result of the 4*c*-DFT [159–170] and RECP CCSD(T) [171] calculations in comparison with experiment

Group	Molecule	RECP CCSD(T)		4*c*-DFT[a]		Exp.[b]	
		$M–O/L_{ax}$	$M-L_{eq}$	$M–O/L_{ax}$	$M-L_{eq}$	$M–O/L_{ax}$	$M-L_{eq}$
4	$ZrCl_4$	–	–	–	2.344	–	2.318
	$HfCl_4$	–	–	–	2.344	–	2.317
	$RfCl_4$	–	2.381		2.402	–	–
5	$NbCl_5$	–	–	*2.34*	*2.24*	2.338	2.241
	$TaCl_5$	–	–	*2.37*	*2.23*	2.369	2.227
	$DbCl_5$	–	–	*2.42*	*2.28*	–	–
	$NbOCl_3$	–	–	*1.66*	*2.24*	1.68	2.276
	$TaOCl_3$	–	–	*1.67*	*2.25*	–	–
	$DbOCl_3$	–	–	*1.72*	*2.30*	–	–
	$NbBr_5$	–	–	2.500	2.449	–	–
	$TaBr_5$	2.481	2.435	2.495	2.444	2.473	2.412
	$DbBr_5$	2.536	2.499	2.548	2.496	–	–
	$NbOBr_3$	–	–	1.704	2.442	1.694	2.429
	$TaOBr_3$	–	–	1.716	2.440	–	–
	$DbOBr_3$	–	–	1.788	2.484	–	–
6	$MoCl_6$	–	–	–	*2.25*	–	–
	WCl_6	–	2.319	–	*2.26*	–	2.26
	$SgCl_6$	–	2.359	–	*2.32*	–	–
	$MoOCl_4$	–	–	*1.658*	*2.279*	1.658	2.279
	$WOCl_4$	1.67	2.317	*1.685*	*2.280*	1.685	2.28
	$SgOCl_4$	1.72	2.364	*1.747*	*2.340*	–	–
	MoO_2Cl_2	–	–	*1.698*	*2.259*	1.698	2.259
	WO_2Cl_2	1.700	2.282	*1.710*	*2.270*	1.710	2.270
	SgO_2Cl_2	1.749	2.339	*1.772*	*2.330*	–	–
	WO_3	1.735	–	–	–	–	–
	SgO_3	1.777	–	–	–	–	–
7	TcO_3Cl	–	–	1.69	2.30	–	–
	ReO_3Cl	–	–	1.71	2.28	1.761	2.23
	BhO_3Cl	–	–	1.77	2.37	–	–
8	RuO_4	–	–	1.712	–	1.706	–
	OsO_4	–	–	1.719	–	1.711	–
	HsO_4	–	–	1.799	–	–	–

[a] *Italics*—estimates for the heaviest elements on the basis of IR; [b] for experimental values see the corresponding references in the theoretical works [159–171]

Table 9 Atomization energies, D_e, (in eV), ionization potentials, IP, (in eV), dipole moments, μ (in D), polarizabilities, α (in a.u.), of group 4–8 compounds as a result of various calculations

Group	Molecule	D_e[a]	IP[b]	μ	α	Method	Ref.
4	$ZrCl_4$	21.68	–	–	–	DFT	[159]
		20.32	11.94	–	10.14	BH	
	$HfCl_4$	21.14	–	–	–	DFT	[159]
		20.53	12.03	–	–	BH	
	$RfCl_4$	19.50	10.96	–	–	DFT	[159]
		18.80	-			RECP	[171]
5	$NbCl_5$	*19.25*	10.77	–	–	DS DV	[160]
	$TaCl_5$	*19.46*	10.73	–	–	DS DV	[160]
	$DbCl_5$	17.76	10.83	–	–	DS DV	[160]
	$NbOCl_3$	*21.6*	11.60	0.91	–	DS DV	[163]
	$TaOCl_3$	*22.52*	11.57	0.99	–	DS DV	[163]
	$DbOCl_3$	20.82	11.64	1.27	–	DS DV	[163]
	$NbBr_5$	18.32	9.35	–	172.1	DFT	[164]
		17.86				BH	
	$TaBr_5$	19.41	9.33	–	167.3	DFT	[164]
		18.92				BH	
	$DbBr_5$	18.86	9.37	–	167.0	DFT	[164]
	$NbOBr_3$	20.53	–	–	–	DFT	[164]
	$TaOBr_3$	21.43	–	–	–	DFT	[164]
	$DbOBr_3$	20.36	–	–	–	DFT	[164]
6	$MoCl_6$	–	11.06	–	–	DS DV	[165]
	WCl_6	*21.7*	11.13	–	–	DS DV	[165]
		19.9				RECP	[171]
	$SgCl_6$	20.05	11.17	–	–	DS DV	[165]
		19.9				RECP	[171]
	$MoOCl_4$	*20.54*	–	0.14	–	DS DV	[166]
	$WOCl_4$	*22.96*	–	0.49	–	DS DV	[166]
		21.5		0.24		RECP	[171]
	$SgOCl_4$	*21.24*	–	1.03	–	DS DV	[166]
		21.0		0.77		RECP	[171]
	MoO_2Cl_2	*21.08*	–	1.04	–	DS DV	167
	WO_2Cl_2	*23.5*	–	1.35	–	DS DV	[167]
		21.5		1.51		RECP	[171]
	SgO_2Cl_2	21.6	–	1.83	–	DS DV	[167]
		21.0		2.39		RECP	[171]
	WO_3	18.9	–	–	–	RECP	[171]
	SgO_3	17.8	–	–	–	RECP	[171]
7	TcO_3Cl	23.12	12.25	0.93	33.33	DFT	[168]
	ReO_3Cl	24.30	12.71	1.29	39.88	DFT	[168]
		23.76				BH	
	BhO_3Cl	22.30	13.05	1.95	50.61	DFT	[168]
8	RuO_4	27.48	12.21	–	58.07	DFT	[170]
		19.11	**12.19**		**58.64**	exp.	
	OsO_4	27.71	12.35	–	55.28	DFT	[170]
		21.97	**12.35**		**55.13**	exp.	
	HsO_4	28.44	12.29	–	68.88	DFT	[170]

[a] *Italics*—"experimental" values (calculated via a Born-Haber, BH, cycle); [b] **bold**—measurements

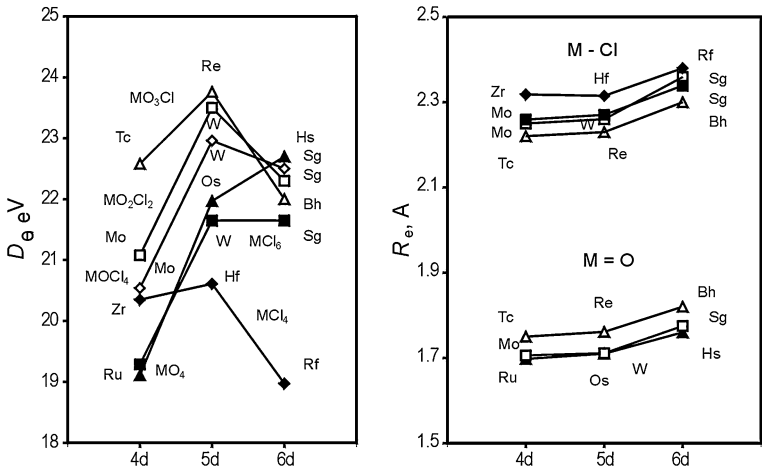

Fig. 19 Atomization energies, D_e, (experimental for the 4d and 5d elements and calculated for the 6d elements) and bond lengths, R_e, for various halides, oxides and oxyhalides of group-4 to 8 elements (see the data in Tables 8 and 9)

properties such as IPs, EAs, energies of electron transitions, polarizabilities and dipole moments were obtained for the stable geometries. Many works were devoted to the study of relativistic effects (both scalar ones and SO interaction) on all those properties by performing additional non-relativistic calculations and comparing them with the relativistic ones. Some works were also devoted to the study of influence of correlation effects on various properties, particularly on bonding. For that purpose, molecular calculations using the DF (HF) approximation (i.e., without correlation), as well as at various levels of electron correlation were performed.

The calculated dissociation energies were used to predict stability of various compounds of the transactinides (at experimental conditions). Using some other properties, like, e.g., polarizabilities, dipole moments and geometrical configurations, volatility of species for gas-phase chromatography experiments were predicted with the use of physico-chemical adsorption models (see further).

Results of the 4*c*-DFT and RECP calculations of various properties—optimized geometries (R_e and bond angles), D_e, IP, α, and μ—of the halides, oxyhalides and oxides of group-4 through 8 elements are summarized in Tables 8, 9. The D_e and R_e are also depicted in Fig. 19.

Overall, very good agreement is observed between the 4*c*-DFT and RECP calculations, as well as between the calculated and experimental values, especially for the bond lengths and geometries. The DFT dissociation energies are slightly overestimated as compared to the experiment, however, they follow perfectly the trends, so that they are rather reliable. Some other properties, including the electronic density distribution, e.g., effective charges, are also nicely reproduced by the calculations. Therefore, predictions for the heaviest elements should be highly reliable.

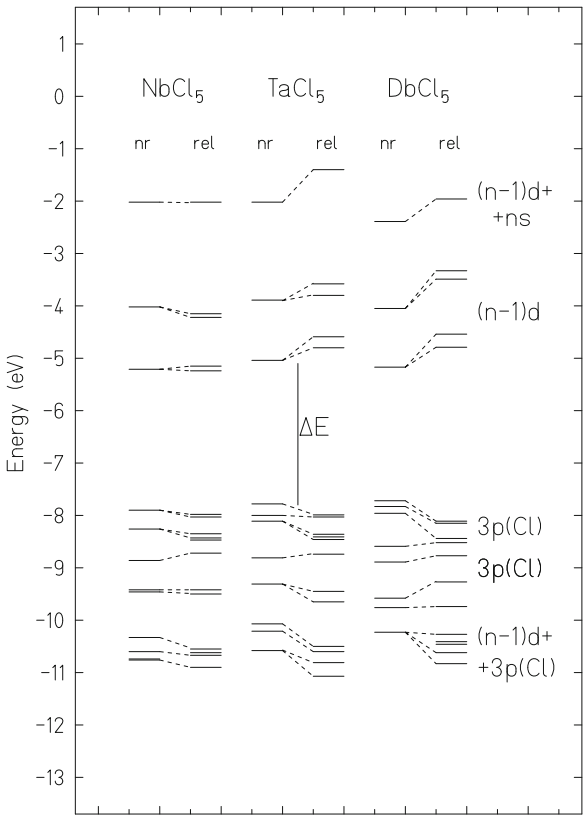

Fig. 20 Relativistic (rel) and non-relativistic (nr) energy levels in MCl_5 (M = Nb, Ta, and Db) obtained from the DS DV calculations. ΔE is the HOMO–LUMO gap. Reprinted with permission from V. Pershina and B. Fricke, J. Chem. Phys. **99**, 9720 (1993). Copyright 1993 American Institute of Physics

The calculations have shown that compounds of the 6d elements are, indeed, homologs of the lighter congeners in the chemical groups and that bonding is defined preferentially by the participation of the valence 6d AOs, with an admixture of the 7s and $7p_{1/2}$ AOs.

A typical schemes of the molecular energy levels of the d-element compounds including those of the transactinides in the relativistic and non-relativistic cases are shown in Fig. 20 for MCl_5 (M = Nb, Ta, and Db), as an example [161]. One can see that the MO schemes, as well as the MO composition (see [160] and [161]), are similar for all the three molecules: the set of bonding MOs is topped by the HOMOs of the preferentially ligand, 3p(Cl), character. Separated from them by the energy gap, ΔE (the HOMO–LUMO gap), lying higher in energy, are the vacant levels of the metal (n–1)d character.

Due to the similarity in the electronic structures, molecular properties of MCl_5 (M = Nb, Ta, and Db) are then also similar. Thus, e.g., IPs defined by the energies of the HOMOs do not differ much (Table 9). Some other properties, like EAs, defined by the LUMOs, or charge-transfer electron transitions change smoothly from the Nb to Db molecule.

The influence of relativistic effects on the MO energies of the group-5 MCl_5, being also typical, is seen from the same Fig. 20 [161].

Thus, relativistic effects increase the HOMO energies (their absolute values), which results in an increase in the molecular IPs. They also decrease the energies (absolute values) of the vacant levels of the (n–1)d character, including LUMOs, which results in a decrease in the EAs. Both effects, consequently, result in an increase in the energies of the electron charge-transfer transitions from the levels of the ligand character to those of the metal character, E[3p(Cl) → (n–1)d(M)]. Since the latter is associated with the reduction of the metal, such an increase leads to an increase in the stability of the maximum oxidation state, i.e., 5+ in group 5. This is demonstrated by a correlation between E[3p(Cl) → (n–1)d(M)] and reduction potentials $E°$(V–IV) for MCl_5 (M = V, Nb, Ta, and Db) in Fig. 21. Thus, non-relativistically, Db^{5+} would have been even less stable than Nb^{5+}. Similar correlations can be shown for compounds of group 4–8 elements in the highest oxidation states. Thus, in groups 4 through 8, relativistic effects increase the stability of the maximum oxidation state.

The RECP and DFT calculations (Tables 8, 9, Fig. 19), in agreement with each other, established that R_e are similar for the 4d and 5d compounds due to the lanthanide contraction, while those of the 6d compounds are about 0.05–0.06 Å larger. (One can also see from Table 8 that the bond lengths estimated on the basis of IR of the heaviest elements in the early DS DV calculations are very realistic). This is in line with their larger IR and CR (see Sect. 5.3). Such an increase in R_e is explained by the orbital and relativistic expansion of the (n–1)d AOs in the groups.

The D_e were shown to increase from the 4d to the 5d compounds and decrease from the 5d to the 6d element compounds for almost all types of species except of group-8 MO_4. In [160–168], such a decrease in D_e of the 6d element compounds was explained by a decrease in the ionic contribution to bonding, while the covalent one steadily increases in the groups. D_e obtained as a sum of the ionic and covalent contributions to chemical bonding calculated within the DS DV scheme turned out to be rather accurate [160–167].

A decrease in ionicity and increase in covalence in groups 4–8 are seen from decreasing Mulliken effective charges, Q_M, and increasing overlap populations (OP), serving as a measure of covalence (Fig. 22). A comparison of results of relativistic and nonrelativistic calculations shows that the reason for this trend is increasingly important relativistic effects. Figure 23 shows relativistic and non-relativistic values of Q_M and OP for MCl_5 (M = V, Nb, Ta, and Db), as an example [161], which change in an opposite way from Ta to Db. A partial OP analysis (Fig. 24) shows that such an increase in covalence (total OP) is due to the increasing contribution of all the relativistic valence AOs, while the contribution of the non-relativistic ns and $np_{1/2}$ AOs decreases from Ta to Db. (In the case of the (n–1)d AOs, the relativistic and nonrelativistic trends are the same, because relativistic effect only enhances the orbital one).

RECP CCSD(T) calculations for the group-6 oxyhalides, with and without SO coupling [171], have shown that larger SO effects on the 6d AOs result in a decrease in D_e of the 6d compounds of 1–1.5 eV in comparison with the 5d ones

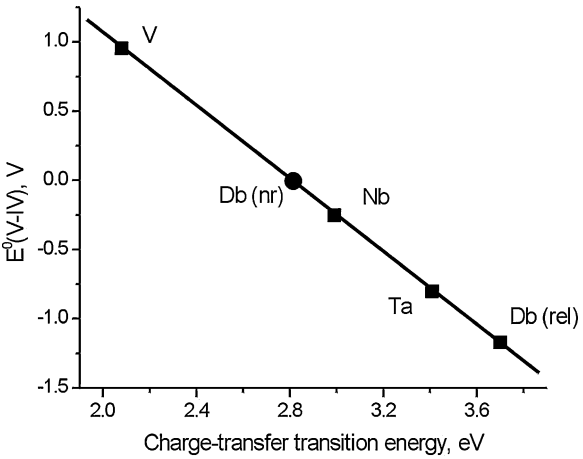

Fig. 21 Correlation between reduction potentials $E°$(V–IV) and energies of the lowest charge-transfer transitions E[3p(Cl) → (n–1)d(M)] in MCl_5 (M = V, Nb, Ta and Db). The non-relativistic value for Db is shown with a filled *circle*. Reproduced from [9]

(Table 10). The effects are larger for the Sg compounds than for the Rf ones due to an increasing $6d_{3/2}$-$6d_{5/2}$ splitting.

Thus, relativistic effects are responsible for the continuation of trends in IP, EA, covalence and stabilities of oxidation states in the groups in going over from the 5d to the 6d elements. (The SO effects are, however, responsible for a trend reversal in D_e). The non-relativistic description of these properties would give opposite and, therefore, wrong trends.

In [171], the importance of electron correlation on Q_M, OP, μ and D_e was demonstrated on the example of group-6 MO_2Cl_2 (Table 10). Correlation effects were shown to significantly decrease Q_M and μ, and increase D_e accounting, e.g., for about 65% in $D_e(SgO_2Cl_2)$. The effects on D_e were found to be larger in the W compounds than in the Sg ones and they become more significant as the number of oxygen atoms increases.

Both the DFT and RECP calculations predict an increase in the stability of compounds of the 6d elements with increasing number of oxygen atoms, e.g., from $SgCl_6$ to $SgOCl_4$ and to SgO_2Cl_2, as is experimentally known for the lighter homologs Mo and W. Thus, SgO_2Cl_2 was recommended in [167] as the most stable type of oxychloride for high-temperature gas phase experiments. $SgCl_6$ and $SgOCl_4$ were shown to be unstable with respect to the loss of Cl transforming into compounds of Sg^V [165, 166].

Among other important trends, one should mention a decrease in the metal–ligand bond strength of the halides with increasing group number, in addition to a decrease in it from the 5d to the 6d compounds within the same group [165]. Thus, $SgCl_6$ was shown to be unstable. Consequently, $BhCl_7$ should not exist. This is also connected with a decrease in the relative stability of the maximum oxidation state along the transactinide series, see Fig. 5 in [165].

Similarly to the chlorides, the trend in the stability of group-5 MBr_5 was predicted from the 4*c*-DFT calculations as Nb < Db < Ta [164]. However, for $MOBr_3$ the trend in the stability is given as Db < < Nb < Ta (see Table 9). Thus,

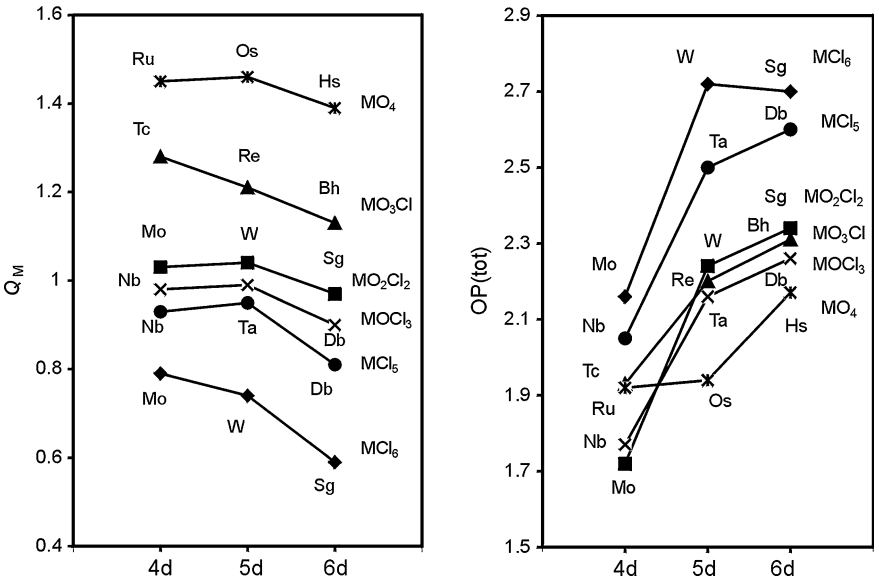

Fig. 22 Effective charges (Q_M) and total overlap populations (OP) in group-4 through 8 (oxy)halides and oxides obtained as a result of the Mulliken population analysis in the DFT calculations [160–170]

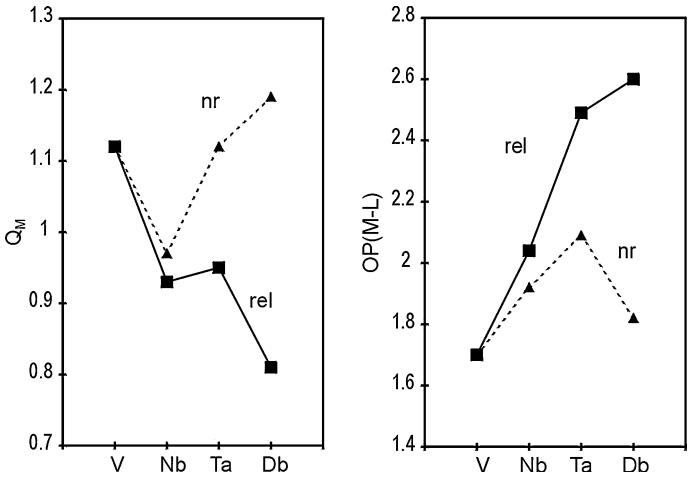

Fig. 23 Relativistic (rel) and non-relativistic (nr) effective charges, Q_M, and overlap populations, OP, in MCl_5 (M = V, Nb, Ta, and Db). L denotes the ligand. The data are from [161]

it was concluded that Db should not have a preference to form oxygen-containing compounds, in difference to the earlier expectations [163]; see also "Gas-Phase Chemistry of Superheavy Elements".

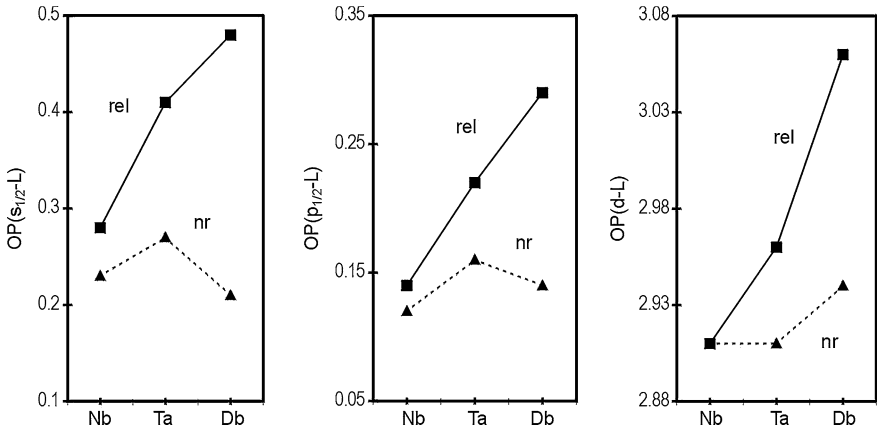

Fig. 24 Relativistic (rel) and non-relativistic (nr) partial overlap populations in MCl_5 (M = Nb, Ta, and Db). L denotes valence orbitals of the ligand. The data are from [161]

Table 10 Correlation and SO effects on the electronic density distribution (Q_M and OP), dipole moments, μ (in D), and atomization energy, D_e (in eV), of MO_2Cl_2 (M = W and Sg)

	Molecule	RECP		DFT
		HF(AREP)[a]	SO-CCSD(T)[b]	DS DV[c]
Q_M	WO_2Cl_2	2.18	1.71	1.08
	SgO_2Cl_2	1.94	1.52	0.97
OP	WO_2Cl_2	2.14	2.03	2.23
	SgO_2Cl_2	2.72	2.55	2.34
μ	WO_2Cl_2	1.70	1.51	1.35
	SgO_2Cl_2	2.64	2.39	1.83
D_e	WO_2Cl_2	11.7	22.2	23.8
	SgO_2Cl_2	14.2	21.0 (22.5[d])	21.8

[a] Average Relativistic, i.e., without SO and correlation [171]; [b] with SO effects and correlation [171] [c] fully relativistic [167]]; [d] without SO effect

Stability of MO_3Cl (M = Tc, Re and Bh) should follow the trend Bh < Tc < Re, according to the 4*c*-DFT calculations [168].

The 4*c*-DFT calculations have also shown that group-8 MO_4 molecules should be all very similar and stable, with the following trend in D_e: RuO_4 < OsO_4 < HsO_4 [169]. However, calculations with larger basis sets, like those used in [170], had to be performed to provide a more accurate value of $D_e(HsO_4)$. $R_e(HsO_4)$, very accurately calculated in [170], should also be larger than R_e of RuO_4 and OsO_4, as in compounds of group 4–7 elements. For these molecules, influence of relativistic effects on properties important for gas-phase experimental investigations was studied in detail [169, 170]. Figure 25 show relativistic and non-relativistic IPs, α, and R_e of these molecules. One can see that relativistic

effects decrease R_e, increase IPs (with the strongest effect on HsO_4) and decrease α. They do, however, not change trends in these properties in the group, since those for the relativistic and non-relativistic (n–1)d AOs are the same. The shape of the IP and α plots with a peak at Os reflects the "zigzag" behavior of the (n–1)d AOs (see Fig. 1 in [169]).

There are also *ab initio* DF [173] and the infinite-order regular approximation with modified metric method (IORAmm/HF) [174] theoretical studies of the electronic structures of MO_4 (M = Os and Hs). These works, however, revealed some deficiency of the calculations that resulted in the prediction of a wrong trend in properties from Os to Hs, as compared to the more accurate calculations [170] and the experiment (see below, as well as discussions in [169]).

All the group 5–7 oxyhalides, as low-symmetry compounds, have dipole moments (see Table 9). As the data show, μ increases from the 4d to 5d and further to 6d compounds, which is connected with an increasing metal–ligand separation. Both relativistic and correlation effects decrease μ (Table 10) due to a decrease in the molecular size and increase in IPs.

The PP calculations were also performed for DbO, along with NbO and TaO. Relativistic effects were shown to stabilize the $^2\Delta_{3/2}$ ground state electronic configuration in DbO, as that in TaO, in contrast to the $^4\Sigma^-$ state of NbO [175, 176].

6.1.3 Other Group-4 Through 8 Compounds

The DS DV calculations were performed for $M(CO)_6$ (M = Mo, W, Sg, and U) [177]. $Sg(CO)_6$ was found to be very similar to $W(CO)_6$ and different from $U(CO)_6$. Bond lengths in covalent compounds of the type MX (M = Rf through element 118; X = H, N, B, and C) and some others were calculated using various approaches, mostly by ADF ZORA (see [149, 150] for a summary). As was mentioned in Sect. 5.3, R_e of the Rf through Hs compounds are about 0.05 Å larger than of their 5d counterparts in good agreement with IR and bond lengths in other types of compounds (Fig. 16).

6.1.4 Predictions of Volatility of Group-4 Through 8 Compounds

Identification of the heaviest elements by studying their volatility is a difficult task. Several quantities are associated with this physical phenomenon, which are not necessarily interrelated. Thus, in gas-phase chromatography experiments, a measure of volatility is either a deposition temperature in a thermochromatography column, T_{ads}, or the temperature of the 50% of the chemical yield, $T_{50\%}$, observed on the outlet of the isothermal column (see "Experimental Techniques" and "Gas-Phase Chemistry of Superheavy Elements", as well as [178]). From these temperatures, an adsorption enthalpy, ΔH_{ads}, is deduced using adsorption models [179], or Monte Carlo simulations [180, 181]. The ΔH_{ads} is supposed to be related to the sublimation enthalpy, ΔH_{sub}, of the macroamount (see "Thermochemical Data from Gas-Phase Adsorption and Methods of their Estimation"). The usage of a correlation between

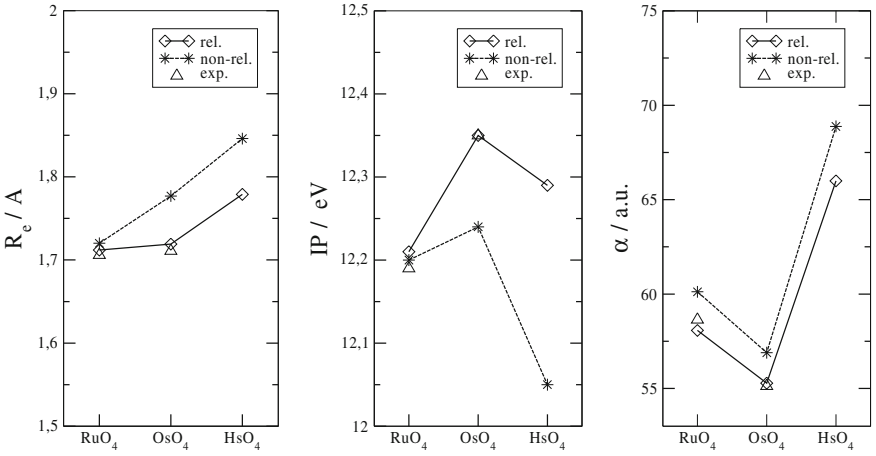

Fig. 25 Relativistic (rel.) and nonrelativistic (non-rel.) bond lengths, R_e, ionization potentials, IP, and polarizabilities, α, of MO_4 (M = Ru, Os, and Hs). Reprinted with permission from V. Pershina, J. Anton, T. Jacob, Phys. Rev. A **78**, 032518 (2008). Copyright 2008 American Physical Society

ΔH_{ads} and ΔH_{sub} is, however, restricted to some groups and types of compounds, while generally not allowed (see below). In macrochemistry, a measure of volatility is an equilibrium vapor pressure over a substance, P_{mm}. Boiling points, T_b, and enthalpy of evaporation, ΔH_{evap}, basically correlate with P_{mm}.

Another difficulty comes from the fact that the studied chemical species are not known. Their composition is usually judged by analogy with the chemical behavior of lighter homologs in the chemical groups. Beside the low statistics of just a few events, a difficulty arises with respect to the interpretation of results, since the surface of the column is not well known. It is often modified with aerosol transport particles or halogenating agents, so that the mechanisms of adsorption and the nature of chemical or physical interactions can only be assumed [178]. Thus, available experimental data are sometimes contradictory and do not correlate with a single property or an electronic structure parameter of the adsorbate.

To determine ΔH_{ads} of a heavy molecule on a complex surface is still a formidable task for quantum chemical calculations. Fully relativistic methods for calculating systems of the heaviest elements interacting with a (complex) surface are not yet available. Especially difficult is the prediction of the physisorption phenomenon caused by weak interactions, where the DFT generally fails.

In the past, DS DV calculations were helpful in establishing some correlation between electronic structure parameters and volatility of halides, oxyhalides and oxides known from macrochemistry [6, 11]. It was established, e.g., that covalent compounds (having higher OP) are more volatile than ionic, and that molecules with dipole moments interact more strongly with a surface than without those, and that the sequence in the adsorption energy is defined by the sequence in dipole moments.

Lately, predictions of the interaction energy of heaviest element molecules with inert surfaces (quartz, silicon nitride, also modified) were made with the use of physisorption models [155, 168–170]. These models are based on the principle of intermolecular interactions subdivided into usual types of long-range forces: dipole–dipole, dipole-polarizability and van der Waals (dispersion) one. Molecular properties required by those models are then calculated with the use of most accurate relativistic methods.

Thus, e.g., for a molecule with a zero dipole moment adsorbed on a dielectric surface by van der Waals forces, the following model of the molecule-slab interaction is used [155]:

$$E(x) = -\frac{3}{16}\left(\frac{\varepsilon - 1}{\varepsilon + 2}\right)\frac{\alpha_{\mathrm{mol}}}{\left(\frac{1}{IP_{\mathrm{slab}}} + \frac{1}{IP_{\mathrm{mol}}}\right)x^3}, \tag{17}$$

where IP_{slab} and IP_{mol} are ionization potentials of the slab and molecule, ε is the dielectric constant of the surface material, and x is molecule-surface separation distance. In a comparative study, x for a lighter element is deduced from the known ΔH_{ads}, while that for a heaviest element is estimated using the difference in their molecular size.

Using this model, ΔH_{ads} of, e.g., group-8 tetroxides on a silicone nitride surface of detectors of a chromatography column were predicted [170]. Since the RuO_4, OsO_4 and HsO_4 molecules are very similar, a very high accuracy of the calculated properties (see Table 9) was required in order to give reliable ΔH_{ads}. The 4*c*-DFT calculations performed with extremely large basis sets revealed an inversion of the trend in α and IPs beyond Os (Fig. 25). Such a trend reversal results in the trend reversal in $-\Delta H_{ads}$, $RuO_4 > OsO_4 < HsO_4$, according to Eq. 17 (Fig. 26). This is in agreement with the experimentally observed trend in $-\Delta H_{ads}$: $OsO_4 < HsO_4$ [182]. Also, the calculated ΔH_{ads} of HsO_4 of -45.1 kJ/mol proved to be in excellent

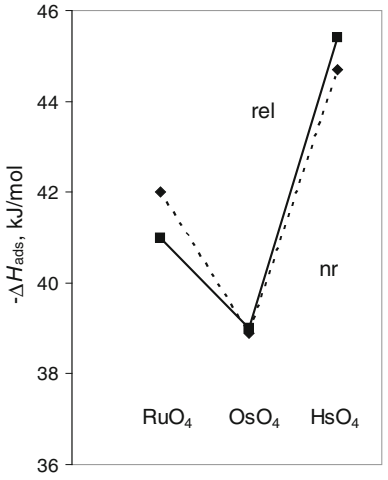

Fig. 26 Relativistic (*solid line*) and nonrelativistic (*dashed line*) adsorption enthalpies of MO_4 (M = Ru, Os, and Hs) on silicon nitride [170]

agreement with the measured ΔH_{ads} of -46 ± 2 kJ/mol. The trend reversal in the molecular properties and ΔH_{ads} is explained by the trend reversal in energies of the (n–1)d AOs at Os (see Fig. 1 in [169]). Relativistic effects were shown to have no influence on the trend in $\Delta H_{ads}(MO_4)$ (Fig. 26), as they have no influence on the trends in the molecular properties (Fig. 25), since relativistic and nonrelativistic (n–1)d AOs change in the same way with increasing Z in group 8 [170].

In [183], thermodynamic equations are given allowing for prediction of T_{ads} of an atom or molecule with respect to T_{ads} of a homolog in a comparative study. One of those equations is shown here for the case of mobile adsorption of molecules with a rotational degree of freedom:

$$e^{-\Delta E_A/\mathrm{RT}} \frac{1}{t_{1/2}^{A} r_A d_A T_A^{1/2} m_A^{1/2}} = e^{-\Delta E_B/\mathrm{RT}} \frac{1}{t_{1/2}^{B} r_B d_B T_B^{1/2} m_B^{1/2}}. \quad (18)$$

Here $t_{1/2}$ is half-life of the central atom isotope, r is molecular radius, d is the metal–ligand distance, T is adsorption temperature, m is mass, and ΔE is adsorption energy of a heaviest molecule A with respect to its lighter homolog B. Predictions of $T_{ads}(HsO_4)$ with respect to $T_{ads}(OsO_4)$ were made in [183], as an example. In the same work, various measures of volatility are critically compared, showing that in a comparative study, the most adequate measure of it (in macrochemistry) is the ratio of adsorption/desorption constants, K_{ads}/K_{des}.

For predictions of adsorption of molecules with non-zero dipole moments, equations taking into account long-range interactions, such as molecular dipole-surface charge, dipole-induced dipole, and van der Waals one were deduced. Thus, e.g., the interaction energy of a molecule with a surface charge is [168]

$$E(x) = -\frac{2Qe\mu_{mol}^2}{x^2} - \frac{Q^2 e^2 \alpha_{mol}}{2x^4} - \frac{3}{2} \frac{\alpha_{mol}\alpha_{slab}}{\left(\frac{1}{IP_{mol}} + \frac{1}{IP_{slab}}\right)}, \quad (19)$$

where μ, IP_{mol} and α_{mol} belong to the molecule and those with index "slab" to the surface; Q is a charge of the surface atom and x is the molecule-surface distance. Using this equation, ΔH_{ads} of group-7 MO_3Cl on a quartz surface of the chromatography column covered with HCl were predicted [168]. The 4*c*-DFT calculated molecular properties required by the model are given in Table 9. Main contributions to the total *E(x)* are given in Table 11 indicating an increase in the energies of all three types of interactions from Tc to Bh. $\Delta H_{ads}(BhO_3Cl) = -78.5$ kJ/mol and $\Delta H_{ads}(TcO_3Cl) = -48.2$ kJ/mol were then determined with

Table 11 Contributions to the interaction energy *E(x)* of the MO_3Cl molecules (M = Tc, Re, and Bh) with Cl^Q (surface) for $Q = {}^-0.4$. From [168]

Molecule	μ-Qe $E10^{16}$ x^2, eV cm^2	α-Qe $E10^{32}$ x^4, eV cm^3	α-α(Cl) $E10^{48}$ x^6, eV cm^6
TcO_3Cl	2.23	5.69	379.06
ReO_3Cl	3.10	6.81	460.65
BhO_3Cl	4.67	8.64	591.17

respect to $\Delta H_{ads}(ReO_3Cl) = -61$ kJ/mol, so that the sequence in volatility was predicted as $TcO_3Cl > ReO_3Cl > BhO_3Cl$. This trend is caused by increasing μ in this row. The predicted sequence and the ΔH_{ads} values are in excellent agreement with the experimental ones of -51 ± 2 kJ/mol for TcO_3Cl and -77 ± 8 kJ/mol for BhO_3Cl [184].

Similarly, a trend in adsorption of group-6 MO_2Cl_2 on a modified quartz surface was predicted as Mo < W < Sg due to increasing dipole moments in this row (Table 9), so that the trend in volatility is Mo > W > Sg [167]. This was also confirmed by results of isothermal gas-phase chromatography experiments [185, 186].

The physisorption adsorption mechanism could, however, not explain results of the gas-phase chromatography experiments with pure halides of group-4 and 5 elements. Thus, e.g., experiments on the chlorides and bromides of group-5 elements, using both thermo- and isothermal chromatography techniques [187–190] revealed that volatility of the Nb and Ta halides is similar, while that of Db is lower. Taking into account the predicted sequence in volatility (as P_{mm} of MBr_5 over the solid) Nb < Ta < Db [162], this unexpected behavior was explained by the formation of either oxyhalides MOL_3, or the $KMBr_5L$ (L = Cl, Br) salt on a quartz surface modified with aerosol transport KCl or KBr particles. To test this assumption, a new theoretical study on the prediction of the adsorption behavior of group 5 bromides at the given experimental conditions was undertaken in [164].

First, it was shown that $DbBr_5$ should, indeed, be formed at the experimental conditions, while $DbOBr_3$ should not (see dissociation energies in Table 9). Further on, the calculations have shown that if the MBr_5 molecule approaches a KCl or KBr surface along the z axis, physisorption described by Eq. 17 occurs. If the molecule, however, approaches such a surface by one of the facets, the MBr_6^- complex is formed (Fig. 27), where an additional Br atom comes from the surface.

The 4c-DFT calculated energies of the $MBr_5 \rightarrow MBr_5L^-$ (L = Br, Cl) reaction with respect to those of Nb, are given in Table 12. The latter are in excellent agreement with the $TaBr_5$-$NbBr_5$ and $DbBr_5$-$NbBr_5$ differences in the experimental ΔH_{ads}, so that the sequence in the strength of the complexes should indeed

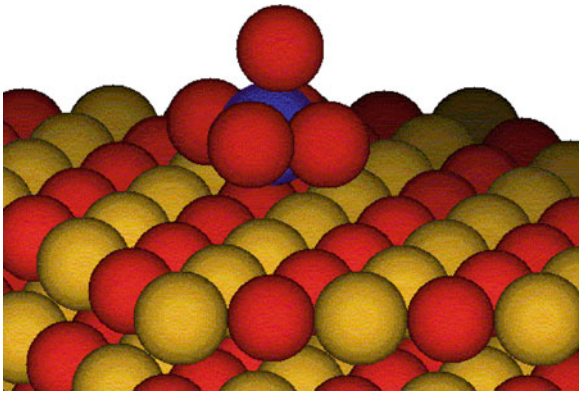

Fig. 27 Formation of MBr_6^- on the KBr surface. Reprinted with permission from V. Pershina, J. Anton, J. Chem. Phys. **136**, 034308(7) (2012). Copyright 2012 American Institute of Physics

Table 12 Energies of the $MBr_5 \rightarrow MBr_5L^-$ (L = Br, and Cl) reaction with respect to those of Nb, $\Delta\Delta E$, as well as relative values (with respect to those of Nb) of measured ΔH_{ads} (in eV)

Reaction energy	Nb	Ta	Db
$\Delta\Delta E(MBr_5 \rightarrow MBr_6^-)$/Nb	0	−0.09	−0.21
$\Delta\Delta E$ $(MBr_5 \rightarrow MBr_5Cl^-)$/Nb	0	−0.09	−0.25
$-\Delta H_{ads}[SiO_2/KCl]/Nb$[a]	0	−0.08	−0.29
$-\Delta H_{ads}[SiO_2/KBr]/Nb$[b]	0	−0.08	+0.19

[a] Experiment [188]; [b] experiment [190], see "Gas-Phase Chemistry of Superheavy Elements"

be Nb < Ta < Db. Thus, obviously, MBr_5L^- (L = Br, Cl) are formed on the KBr/KCl surface in the "one-atom-at-a-time" experiments [187–189]. In this case, the complex of Db should be the strongest, which means that $DbBr_5$ should be the least volatile among the homologs.

The latest experiments on the adsorption of the group-5 pentabromides on the quartz surface (presumably modified with KBr aerosol particles) [190] have, however, shown the following sequence in the adsorption energy $DbBr_5 < NbBr_5 < TaBr_5$, in contrast to the former experiments [188] and recent theoretical predictions [164]. This new experimental result has not yet found its explanation.

6.1.5 Solid State of the 6d Elements

Solid-state calculations were performed on the Rf metal [191]. The structural and electronic properties were evaluated by the first principles DFT in scalar relativistic formalism with and without SO coupling and compared with its 5d homolog Hf. It is found that Rf should crystallize in the hexagonal close packed structure as Hf. However, under pressure, it should have a different sequence of phase transitions than Hf: *hcp* → *bcc* instead of *hcp* → *ω* → *bcc*. An explanation is offered for this difference in terms of the competition between the band structure and the Ewald energy contributions.

6.2 Mt and Ds (Elements 109 and 110)

The group-9 and 10 elements Mt and Ds, respectively, have received little attention so far. The position of these elements in the Periodic Table suggests that they should be noble metals. Volatile hexafluorides and octafluorides might be produced and used for chemical separation experiments. The DS DV calculations for DsF_6 indicate that DsF_6 should be very similar to PtF_6, with very close values of IPs [192]. Relativistic effects were shown to be as large as ligand-field splitting.

Bond lengths in MtH_3, MtC^-, DsH_2, and DsH_3 were calculated using the ADF ZORA program [149, 150]. Using the same method, electronic structures of DsC and DsCO were calculated in [193] suggesting that these compounds are chemically similar to the corresponding 5d homologs.

6.3 Rg (Element 111)

A special interest in the chemistry of Rg is explained by the expectation of unusual properties of its compounds caused by the maximum of the relativistic contraction and stabilization of the 7s AO in this group. The electronic structure of the simplest molecule RgH, a sort of a test system like AuH, was studied at various levels of theory [194–198]. The most representative results are shown in Table 13. (More extended tables are given elsewhere [8, 194, 197]). One can see that a very high accuracy of the calculations is needed to predict the correct trend in R_e from AuH to RgH, because the values are very similar. The 4*c*-DFT R_e [198] is in excellent agreement with the DHF CCSD(T) one [197], as one of most accurate.

The data of Table 13 demonstrate the importance of relativistic and correlation effects on the properties of RgH. A study of influence of relativistic effects on properties of these molecules was performed in [194], see Fig. 28. A comparison of the relativistic (DF or ARPP) with the non-relativistic (HF or NRPP) calculations shows that bonding is considerably increased by relativistic effects doubling the dissociation energy, though the SO splitting diminishes it by 0.7 eV (the ARPP CCSD—SOPP CCSD difference). Thus, it was established, in agreement with the BDF calculations [109], that the trend to an increase in D_e from AgH to AuH should be reversed from AuH to RgH (Fig. 28). The PP CCSD calculations have found that R_e(RgH) is substantially shortened by relativity, $\Delta R_e = -0.4$ Å, and it is the smallest in the series AgH, AuH and RgH, so that the trend to a decrease in R_e is continued with RgH [194]. The BDF calculations [109] have, however, shown R_e(RgH) to be slightly larger than R_e(AuH). The different trends in R_e obtained in these two types of the calculations are connected with a different contribution of the contracted 7s and expanded 6d orbitals to bonding (though the

Table 13 Bond length, R_e (in Å), dissociation energy, D_e (in eV), and force constant, k_e (in mdyn Å^{-1}), as well as vibrational frequency of the bond, ω_e (in cm^{-1}), in the parentheses, for RgH calculated using various approximations in comparison with AuH

Molecule	Method	R_e	D_e	k_e (ω_e)	Ref.
AuH	exp.	1.5236	3.36	3.14	[110]
RgH	HF	2.015	0.90	1.01	[194]
	NRPP CCSD(T)	1.924	1.83	1.11	[194]
	DF	1.520	1.56	4.66	[194]
	ARPP	1.505	2.32	4.98	[194]
	ARPP CCSD(T)	1.498	3.79	4.77	[194]
	SOPP CCSD(T)	1.503	3.05	4.72	[194]
	PP CCSD(T)	1.529	2.83	(2642)	[195]
	SC PP CCSD(T)[a]	1.512	2.87	(2668)	[196]
	DHF CCSD(T)	1.523	2.83	4.23	[197]
	4*c*-BDF	1.546	2.77	3.66	[109]
	SO ZORA(MP)	1.530	2.87	4.26	[109]
	4*c*-DFT	1.520	2.85	(2804)	[198]

[a] Shape-consistent (SP)

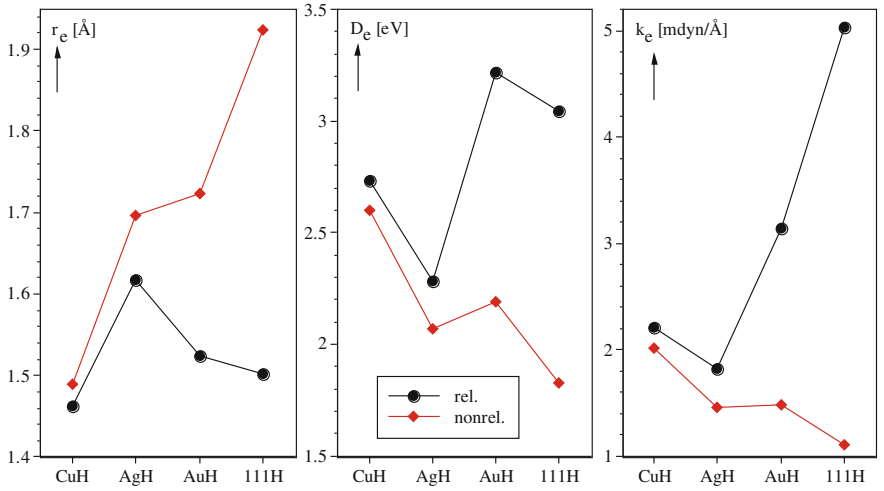

Fig. 28 Nonrelativistic and relativistic bond lengths, r_e (see also Table 13 for various values for RgH), dissociation energies, D_e, and force constants, k_e, of the group-11 hydrides. Reprinted with permission from [194]. Copyright 1996 Elsevier

6d contribution was found to de predominant in both cases). In [109], much larger SO effects were found on R_e (SO increased) and k_e (SO decreased) of RgH. The trend to an increase in k_e was found to be continued with RgH having the largest value of all known diatomic molecules [194]. The μ was shown to be relativistically decreased from AgH to AuH and to RgH indicating that RgH is more covalent and element Rg(I) is more electronegative than Au(I) [109, 194].

Results of the 4*c*-BDF [109] and 4*c*-DFT calculations [198] for other dimers, AuX and RgX (X = F, Cl, Br, O, Au, Rg), indicate that relativistic effects follow a similar pattern to that for RgH except for RgF and RgO, where SO splitting increases D_e. The PP calculations for RgH, RgLi and RgF [197] have, however, shown that SO effects on R_e are very small, but they are large for D_e, decreasing it in all the cases, in difference to the BDF calculations for RgF [109]. Scalar relativistic effects increase D_e(RgLi), but decrease D_e(RgF). They decrease R_e by about 0.4 Å in all the cases. The singlet state was found to be the ground for Rg_2 in comparison with the triplet [198]. The dissociation energy was found to change in the following order: $Au_2 > RgAu > Rg_2$.

In order to study the stability of higher oxidation states, energies of the $MF_6^- \rightarrow MF_4^- + F_2$ and $MF_4^- \rightarrow MF_2^- + F_2$ (M = Cu, Ag, Au, and Rg) decomposition reactions were calculated at the PP MP2 and CCSD levels of theory [199]. Relativistic effects were shown to stabilize higher oxidation states in the high-coordination compounds of Rg due to the destabilization of the 6d AOs and their larger involvement in bonding. RgF_6^- was shown to be the most stable in this group. SO coupling stabilizes the molecules in the following order: $RgF_6^- > RgF_4^- > RgF_2^-$. This order is consistent with the relative involvement of the 6d electrons in bonding for each type of molecule.

6.4 Cn (Element 112)

6.4.1 Relativistic Effects in Group 12 of the Periodic Table

Group-12 elements have all closed-shell $(n–1)d^{10}ns^2$ ground states. Along with the increasing relativistic stabilization of the ns AO in the group (Fig. 3), this results in the fact that the elements become more inert with increasing Z. Thus, bulk Hg is known to be a liquid, however, very different from a condensed noble gas. In the case of Cn, relativistic effects are further amplified, so that this element was expected to be a volatile liquid, or a gas. This was originally assumed by Pitzer in 1975 [200], who found out that the very high excitation energy of 8.6 eV from the s^2 closed shell into the sp valence state of Cn will not be compensated by the energy gain of the chemical bond formation. Thus, Cn should reveal a noble gas character. The high inertness of Cn has also been demonstrated by other atomic properties, such as the highest IP, smallest AR and polarizability in group 12, as discussed in Sect. 5 (Fig. 18).

Experimentally, an inertness/reactivity of Cn was supposed to be investigated by studying its volatility with respect to that of Hg and Rn as adsorption on a gold surface (gold plated detectors) of the chromatography column used in gas-phase chromatography experiments [201–203] ("Gas-Phase Chemistry of Superheavy Elements"). The questions to the modern electronic structure theory, therefore, were: Is Cn metallic in the solid state, or is it more like a solid noble gas? What is its ΔH_{sub}? How volatile and reactive towards gold is the Cn atom in comparison with Hg and Rn?

6.4.2 Van der Waals Systems. Volatility as Sublimation

Homonuclear dimers. In the first approximation, bonding in the solid state of an element is described by bonding in its homonuclear dimer, M_2. Knowledge of the latter was, therefore, important to estimate ΔH_{sub} of the bulk Cn. Moreover, Hg_2 and Cn_2 have been of a special interest in chemical theory in testing the accuracy of quantum chemical methods in treating closed-shell interactions. Accordingly, electronic structures of these dimers were calculated with the use of a various methods, such as 4*c*-BDF, ECP CCSD(T), QP PP CCSD(T) [204] and 4*c*-DFT [155, 198]. Results are summarized in Table 14 and Fig. 29.

Table 14 Bond lengths, R_e (in Å), and dissociation energies, D_e (in eV), of Hg_2 and Cn_2

Method	Hg_2		Cn_2		Ref.
	R_e	D_e	R_e	D_e	
4*c*-BDF (PBE)	3.439	0.053	3.089	0.156	[204]
4*c*-BDF (PBESIC)	3.904	0.025	3.363	0.075	[204]
QR PP CCSD(T)	3.769	0.044	3.386	0.097	[204]
4*c*-DFT (B88/P86)	3.63	0.01	3.45	0.05	[198]
exp.	3.63	0.043	–	–	[110, 205]

The calculations have shown that even though bonding both in Hg_2 and Cn_2 is preferentially of van der Waals type, a partial overlap occurs. The 6d-AOs are active and mixing up with the 7s-AOs of Cn in the HOMO.

Both the DFT and PP calculations agree on an increase in D_e of about 0.04 eV from Hg_2 to Cn_2 with the corresponding bond shortening, in line with the smaller R_{max}[7s(Cn) AO] in comparison with R_{max}[6s(Hg) AO] (Fig. 3). Thus, due to the relativistic 7s AO contraction, Cn_2 should be more stable than Hg_2. This suggests that the bulk of Cn should be more bound than that of Hg (liquid).

Solid state. LDA DFT (non-relativistic, scalar relativistic, SR, and 4*c*-relativistic) band structure calculations were performed on the Cn solid state [206]. The results have shown that Cn prefers the *hcp* structure (as that of Zn and Cd) in difference to Hg (*fcc*). Thus, it should differ from its lighter homolog Hg on a structural level and resemble the solid-state noble gases. A cohesive energy of 1.13 eV (109 kJ/mol) was obtained for Cn at the SR level of theory, which is larger than that of Hg (0.64 eV) and is an order of magnitude larger than those of the solid noble gases. This result is consistent with the larger $D_e(Cn_2)$ with respect to $D_e(Hg_2)$ (see Table 14). Thus, from a theoretical point of view, ΔH_{sub} of 22 kJ/mol obtained via an extrapolation in group 12 [207] is obviously underestimated, as such an extrapolation in this group is not grounded. It was also concluded that Cn is not a metal, but rather a semiconductor with a band gap of at least 0.2 eV. (The LDA results were considered as a lower bound). In this sense, Cn resembles the group 12 metals more closely than it does the noble gases.

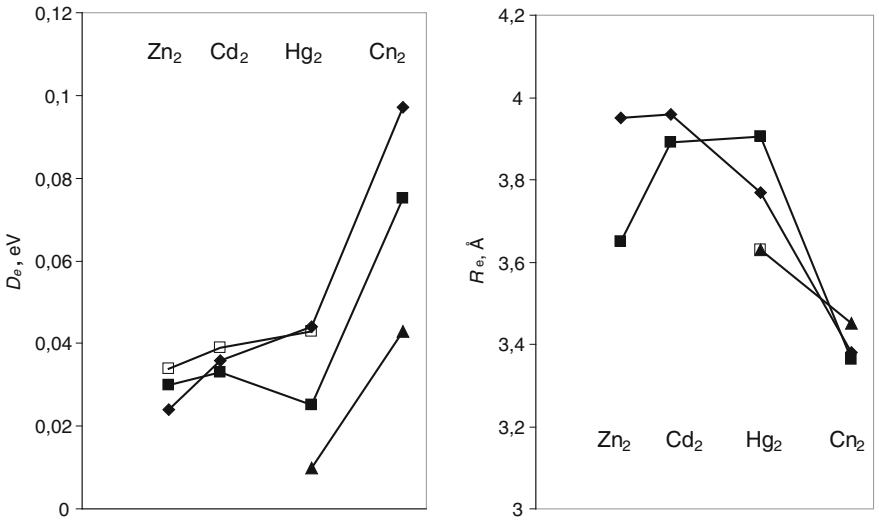

Fig. 29 QR PP CCSD(T) (*filled rhomboids*), 4*c*-BDF (PBESIC) (*filled squares*), 4*c*-DFT (B88/P86) (*filled triangles*) and experimental (*open squares*) dissociation energies, D_e, and bond lengths, R_e, of the group-12 dimers (see Table 14). Reprinted with permission from V. Pershina, Radiochim. Acta, **99**, 459 (2011). Copyright 2011 Oldenbourg Wissenschaftsverlag GmbH

Adsorption on inert surfaces. The knowledge of ΔH_{ads} of Cn on inert surfaces such as quartz and ice (that can be formed in the chromatography column at very low temperatures) was also required for interpreting results of the gas-phase chromatography experiments. With this aim in view, ΔH_{ads} of Hg and Cn, as well as of Rn for comparison, on these surfaces were estimated using a physisorption model (Eq. 17) and DCB FSCC calculated atomic properties [127]. The obtained $-\Delta H_{ads}$ of Hg of 40.5 kJ/mol on quartz and of 25.20 kJ/mol on ice are in good agreement with the experimental values of 42 ± 2 kJ/mol and 25.5 ± 2 kJ/mol, respectively [208, 209]. For Cn, $-\Delta H_{ads} = 43.2 \pm 0.2$ kJ/mol on quartz and $-\Delta H_{ads} = 26.3 \pm 0.1$ kJ/mol on ice were predicted. Thus, Cn was expected to be more strongly bound than Hg by van der Waals forces and to be deposited on ice in the thermochromatography column at slightly higher temperatures than Hg.

By using relativistic *vs.* non-relativistic values of the atomic properties (Fig. 18), the influence of relativistic effects on ΔH_{ads} and the trend in group 12 was elucidated [155]. The trend in ΔH_{ads} was shown to be defined by the trend in AR, since trends in α and IP cancel each other (see Eq. 17). Thus, due to the relativistically more contracted AR(Cn) than AR(Hg), $-\Delta H_{ads}$ of Cn is larger than that of Hg, while non-relativistically, it is the other way around.

6.4.3 Volatility as Measured in Gas-Phase Chromatography Experiments. Interaction with Metals

Heteronuclear dimers. In the simplest approximation, a gold surface can be approximated by only one gold atom. Thus, in order to estimate binding energies of Cn with noble metals, electronic structure calculations were first performed for HgM and CnM, where M = Ag, Au, Pt, Pd, and Cu using the 4*c*-DFT method [210]. It was demonstrated that Cn forms a chemical bond with Au primarily due to the overlap between the double occupied 7s(Cn) AO and single occupied 6s(Au) AO, as well as between the $6d_{5/2}$(Cn) AO and $5d_{5/2}$(Au) AO. Thus, CnAu should be chemically bound having a $\sigma^2\sigma^{*1}\ ^2\Sigma^+$ ground state configuration with two electrons in the bonding and one in the antibonding MOs (Fig. 30).

Overall, Cn should be about 0.2 eV weaker bound with a transition metal atom M than Hg and the bonds should be longer. The latter is a result of the participation of the more expanded 6d(Cn) AOs than the 5d(Hg) AOs in bonding. Among M, bonding with Pd should be the strongest, while with Ag the weakest.

The influence of relativistic effects on properties of MAu (M = Hg and Cn) was studied in [155]. Relativity is shown to increase D_e(HgAu) by 0.13 eV, but to decrease it by about the same amount (0.12 eV) in CnAu due to the contraction of the 7s(Cn) AO. This makes trends in the nonrelativistic *vs.* relativistic D_e values opposite from HgAu to CnAu, so that $D_e^{nr}(CnAu) > D_e^{nr}(HgAu)$, while $D_e^{rel}(CnAu) < D_e^{rel}(HgAu)$. R_e is decreased by relativity in both systems and the trends are the same both for the non-relativistic and relativistic R_e.

Interaction with gold clusters. In [211–213], 4*c*-DFT calculations were performed for Hg and Cn interacting with gold clusters, Au_n. Since the structure of the

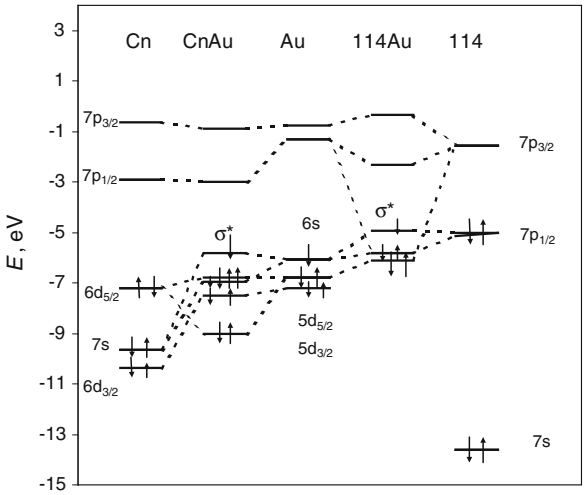

Fig. 30 Bond formation (principal MOs) of the CnAu and FlAu molecules. Reprinted with permission from V. Pershina, Radiochim. Acta, **99**, 459 (2011). Copyright 2011 Oldenbourg Wissenschaftsverlag GmbH

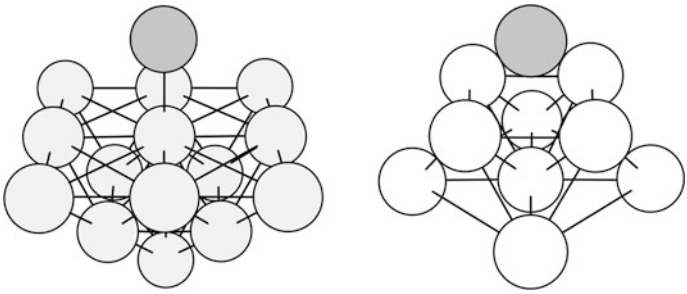

Fig. 31 The M-Au_{14} and M-Au_9 systems simulating adsorption of M in the on-top and hollow sites on the Au(100) surface, respectively. Reprinted with permission from V. Pershina, T. Bastug, Chem. Phys. **311**, 139 (2000). Copyright 2000 Elsevier

gold surface used in the chromatography experiments is not known, two types of ideal surfaces, Au(100) and Au(111), were considered. In the first case, the surface was simulated by the medium-size Au_n clusters and embedded clusters, Au_nAu_m [211, 212]. The ad-atom was positioned at all possible adsorption sites: on-top, bridge and hollow (see Fig. 31 for the on-top and hollow positions on small clusters and Fig. 7 for the on-top position on an embedded cluster). The convergence in E_b(M-Au_nAu_m) with the cluster size was reached for $n > 29$ and $m = 156$ [212].

The obtained potential energy curves are shown in Fig. 32. It was found out that both Cn and Hg adsorb preferentially at the bridge position, and E_b(Cn-Au_n) should be 0.38 eV smaller than E_b(Hg-Au_n) for this position.

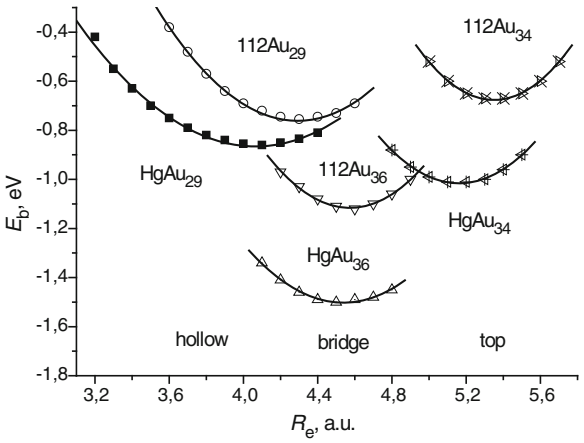

Fig. 32 The 4*c*-DFT calculated potential energy curves for the M-Au$_n$Au$_{156}$ systems (M = Hg and Cn) in the three adsorption positions of M: on-top, hollow and bridge [212]

The difference in the binding energies between Hg-Au$_n$ and Cn-Au$_n$ was calculated as 0.38 eV for the bridge position. With respect to the measured $-\Delta H_{ads}$(Hg) of 1.03 eV on gold [208, 209], this gives $-\Delta H_{ads}$(Cn) = 0.67 eV. This value is in reasonably good agreement with the measured $-\Delta H_{ads}$(Cn) = $0.54^{+0.2}_{-0.01}$ eV (52^{+20}_{-4} kJ/mol) [202, 203]. The obtained absolute values of E_b of Hg and Cn are, however, larger than the experimental $-\Delta H_{ads}$ indicating that the Au(100) surface is obviously a loose approximation for the real one.

Thus, next, adsorption of Cn on the Au(111) surface was considered at the 4*c*-DFT level of theory [213]. The Au(111) surface was modeled by the large Au$_n$ clusters, where the convergence in E_b(M-Au$_n$) with the cluster size was reached for n = 95 for the top, n = 94 for the bridge, n = 120 for the hollow-1 and n = 107 for the hollow-2 positions. The bridge position was found again preferential for Hg, while hollow-2 for Cn. The obtained E_b(Cn-Au$_n$) of 0.46 eV turned out to be in good agreement with the experimental $-\Delta H_{ads}$(Cn) of $0.54^{+0.2}_{-0.01}$ eV [203], indicating that the Au(111) ideal surface is close to the real one.

Works on RECP and 2*c*-DFT (SO corrected) calculations for Hg and Cn interacting with small gold clusters (n = 1–4, and 10) arrived at the same conclusion that the Cn-Au$_n$ bonding is about 0.2 eV weaker than the Hg-Au$_n$ one [214–217].

In [155], the influence of relativistic effects on adsorption of Hg and Cn on gold was investigated on the example of small ad-atom-gold clusters modelling adsorption at the on-top and hollow positions (Fig. 31). Relativistic effects were shown to define the trend to a decrease in E_b(M-Au$_n$) from Hg to Cn, even though they increase E_b(M-Au$_n$) both in the Hg and Cn systems, especially at the hollow position due to the involvement of the 6d(Cn) AOs in bonding. This makes the difference in E_b(M-Au$_n$) between Hg and Cn very small. Relativistic effects were shown to decrease R_e, the distance of the ad-atom to the surface, in all the cases.

Figure 33 summarizes the most interesting cases of the group-12 elements chemistry: D_e(M$_2$), ΔH_{sub}(M), D_e(MAu), E_b(M-Au$_n$) and ΔH_{ads}(M) on gold. Thus,

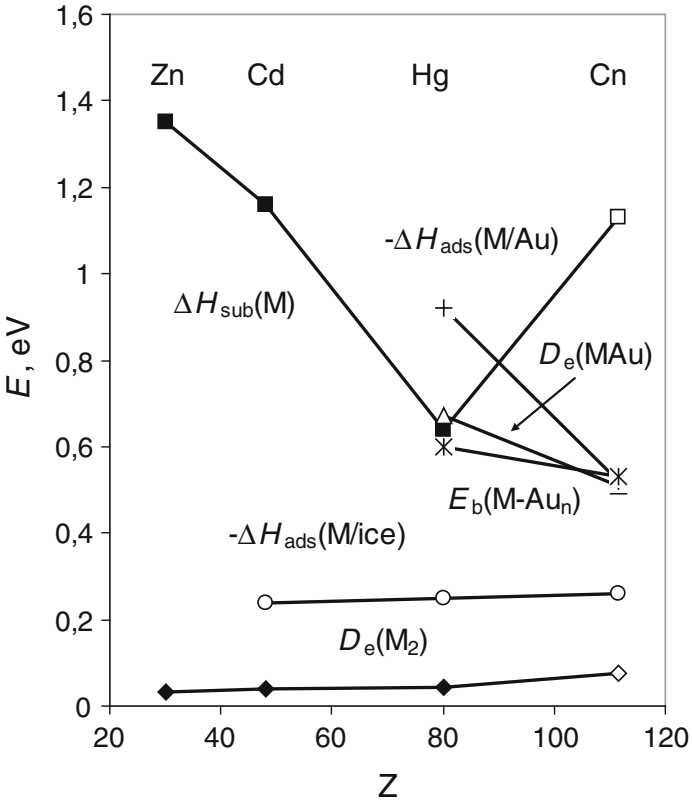

Fig. 33 Binding energies of group-12 elements M (M = Zn, Cd, Hg, and Cn) in various systems: $D_e(M_2)$ (*rhomboids*), $-\Delta H_{ads}$(M/ice) on ice (*circles*), ΔH_{sub}(M) of solids (*squares*), D_e(MAu) (*triangles*); E_b(M-Au$_n$) (*stars*); experimental $-\Delta H_{ads}$(M/Au) on gold (*crosses*). Filled symbols are experimental values, open ones are calculations. Reprinted with permission from V. Pershina, Radiochim. Acta, **99**, 459 (2011). Copyright 2011 Oldenbourg Wissenschaftsverlag GmbH

Cn should be stronger bound by van der Waals forces than Hg both in M_2, solid state and adsorbed state on an inert surface, and this is a relativistic effect caused by the contraction of the 7s(Cn) AO. The M-Au bonding, chemical in nature, should, on the contrary, decrease from Hg to Cn due to the gradual stabilization of the ns AO in group 12. This suggests that a linear correlation between ΔH_{sub} and $-\Delta H_{ads}$ (as that used in [203]) is not valid in this group due to the different type of bonding in these two cases. Therefore, obtained on the basis of this correlation $\Delta H_{sub}(Cn) = 38^{+10}_{-12}$ kJ/mol ($0.39^{+0.1}_{-0.12}$eV), as well as $\Delta H_{sub}(Cn) = 22$ kJ/mol (0.23 eV) obtained via a straightforward extrapolation in group 12 [207] are, obviously, underestimated.

The main conclusion of both the theoretical and experimental studies is that Cn interacts with gold by chemical forces due to the overlap between the valence

orbitals. It forms a metal–metal bond upon adsorption, though weaker than that of Hg, due to relativistic effects. Thus, it behaves like a typical d-element, but not like an inert gas, which is in agreement with its position in group 12 of the Periodic Table.

6.4.4 Other Compounds

The relativistic contraction of the 7s AO is expected to manifest itself also in properties of other Cn compounds. The PP calculations [153] have shown that the relativistic bond length contraction in CnH^+ is similar to that in RgH, and that $R_e(CnH^+)$ is the smallest among all others, CdH^+, HgH^+ and CnH^+, and is similar to $R_e(ZnH^+)$, in agreement with the GRECP calculations [218]. (The RECP CCSD(T) calculations [139] for HgH^+ and CnH^+ have, however, given a larger R_e for the latter compound). Another interesting point is that, in contrast to the group-11 hydrides, the trend in the dissociation energies from Cd to Hg is continued with Cn, i.e., $D_e(CdH^+) < D_e(HgH^+) < D_e(CnH^+)$, while $D_e(AgH) < D_e(AuH) > D_e(RgH)$ [139, 151, 218]. The reason for this difference is greater relativistic effects in CnH^+ than in RgH.

The second (DK2) and third-order DK (DK3) method was also applied to CnH, CnH^+ and CnH^- [219]. It was shown that scalar relativistic effects on the properties of CnH^- are similar to those on 113H and are smaller than those on CnH^+ and CnH. The DK results for CnH differ, however, from the GRECP ones [218]: according to the former, $R_e(HgH) < R_e(CnH)$, and $D_e(HgH) > D_e(CnH)$, while the latter give $R_e(HgH) > R_e(CnH)$, and $D_e(HgM) \approx D_e(CnH)$ (see discussions in [218]).

As was mentioned above, the destabilization of the 6d AOs should result in their larger involvement in bonding. Thus, high-coordination compounds of Cn should be stable and higher oxidation states should be observed. The PP CCSD(T) calculations of the energies of the $MF_4 \rightarrow MF_2 + F_2$ and $MF_2 \rightarrow M + F_2$ (M = Zn, Cd, Hg, and Cn) decomposition reactions supported this assumption [153]. The results are depicted in Fig. 34.

Thus, the 2+ state is important for all three molecules, ZnF_2, CdF_2, and HgF_2, though the first two are more stable than HgF_2. The latter decomposes at 645 °C. The small energy of the decomposition reaction of MF_2 into M and F_2 confirms the prediction that Cn will be more inert than Hg, though the difference to Hg is not that large. A comparison with non-relativistic results shows that this is a pure relativistic effect: non-relativistically, CnF_2 would have been by far more stable (comparable to CdF_2) with decomposition energy of 509.8 kJ/mol.

The 4+ oxidation state is not known for Zn, Cd, and Hg. Results of the PP calculations suggested that HgF_4 should be thermodynamically stable [220, 221]. The energy of the decomposition reaction of CnF_4 of 129.5 kJ/mol indicates that the molecule should be thermodynamically more stable than HgF_4 [153] (Fig. 34). However, no definite conclusion about the existence of CnF_4 can be drawn, since its decomposition energy is between 100 and 200 kJ/mol: experimentally, few

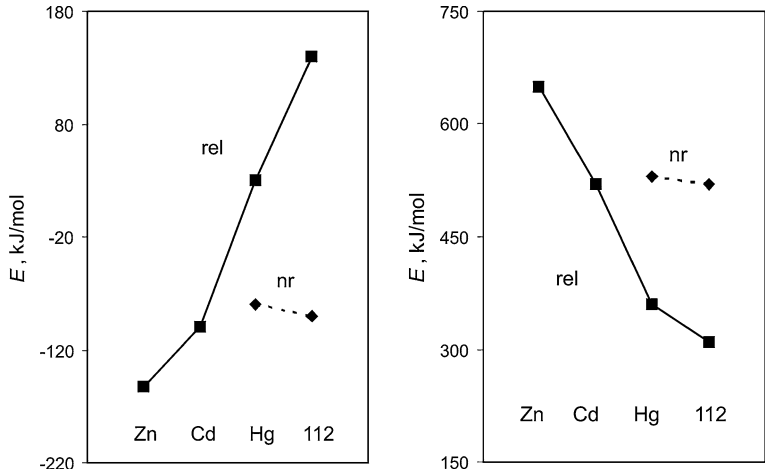

Fig. 34 Relativistic (*solid lines*) and nonrelativistic (*dashed lines*) energies of the decomposition reactions $MF_4 \rightarrow MF_2 + F_2$ and $MF_2 \rightarrow M + F_2$ (M = Zn, Cd, Hg, and Cn). Re-drawn from the data of [153]

compounds with the energy below 100 kJ/mol are known in the solid state. Nonrelativistically, CnF_4 would be definitely unstable with the energy of the decomposition reaction of −93.9 kJ/mol. SO coupling increases energies of both reactions significantly.

A Mulliken population analysis for MF_2 and MF_4 (M = Hg and Cn) suggests that the 6d AOs of Cn are involved in bonding to a larger extent than the 5d AOs of Hg [153]. It was also found that the addition of F^- ions to HgF_2 and to HgF_4 is energetically favorable [220, 221]. By analogy, it is assumed that in combination with appropriate polar solvent, CnF_5^- and/or CnF_3^- may be formed [153].

6.5 7p Elements

6.5.1 Adsorption on Inert Surfaces and Volatility of Atoms

In the 7p elements, the 7s electrons are bound more tightly than the 6s ones in the 6p elements, so they will not take part in the chemical bond formation (Fig. 8). Also, a large SO splitting of the 7p shell into the *nlj* subshells will result in differences in the chemical behavior in comparison with lighter homologs having a complete *nl* shells [1, 2].

Early extrapolations from lighter homologs in the chemical groups have shown that elements 113 through 117 should have smaller ΔH_{sub}, or formation (standard) enthalpies of gaseous atoms, $\Delta H_f(g)$, than their lighter homologs [207], which means that the bulk of the heaviest elements is less bound.

Flerovium, like Cn, was in this sense of particular interest due to the relativistic stabilization of the $7p_{1/2}$ AOs resulting in the quasi-closed shell $7s^27p_{1/2}^2$ ground state and, therefore, inaccessibility of these electrons for chemical bonding. The arguments of Pitzer, similar to those used for Cn, namely, that the $p_{1/2}^2 \rightarrow p^2$ promotion energy to the metal valence state of Fl will not be compensated by the metal–metal bond formation, led to the conclusion that this element should be a relatively inert gas, or a volatile liquid bound by van der Waals forces [200].

Experimentally, volatility of the 7p elements at the beginning of the series, i.e., those with a sufficiently long half-life, is supposed to be studied using gas-phase chromatography techniques. First results were already reported for Fl [222, 223]. Test experiments were conducted on the nearest homolog of element 113, Tl [224].

In order to guarantee transport of elements 113 and 114 from the target chamber to the chemistry set up through Teflon or polyethelene (PE) capillaries, their ΔH_{ads} on these materials need to be known. They were predicted using DC(B) CC calculated atomic properties (Table 4) and a physisorption model of Eq. 17 [126, 127]. The obtained ΔH_{ads} of these elements and their homologs in the groups on these surfaces (also on quartz) are shown in Figs. 35, 36. The ΔH_{ads} were shown to exhibit a trend reversal beyond In in group 13 and beyond Sn in group14 due to the trend reversal in the atomic IP, AR, and α (Figs. 35, 36). The extremely small α of elements 113 and 114, caused by the contraction of the $7p_{1/2}$ AO, is the main reason for their low ΔH_{ads} on inert surfaces. This will allow for easy transport of these elements through the Teflon or PE capillaries.

Adsorption of element 118 and lighter noble gases on various surfaces was also a subject of theoretical investigations with possible future applications. It was interesting to know if it is possible to separate this element from its lighter homologs in group 18 on a specific surface using a chromatography technique. Accordingly, using the DC(B) CC calculated atomic properties (Table 4) and Eq. 17, van der Waals coefficients C_3 and ΔH_{ads} of Ne through element 118 on noble metal (Au and Ag) and non-metal (quartz, ice, Teflon and graphite) surfaces were obtained in [119]. Results for some surfaces are shown in Fig. 37. The C_3 coefficients were shown to steadily increase in group 18, while the increase in $-\Delta H_{ads}$ from Ne to Rn does not continue with element 118: even though α increases in the group (Fig. 37). However, AR $= R_{vdW}$ also increases in this group making ΔH_{ads} of element 118 almost equal to that of Rn (see Eq. 17). It was, therefore, predicted that experimental distinction between Rn and element 118 by adsorption on these surfaces will be impossible. A proper material for separating element 118 could probably be charcoal; further study is needed to test this assumption.

6.5.2 Homonuclear Dimers and Volatility as Sublimation

Homonuclear dimers. Keeping in mind that bonding in M_2 is related to bonding in the solid state, ΔH_{sub} were estimated for the entire series of the 7p elements and their 6p homologs on the basis of the 4*c*-DFT calculations of $D_e(M_2)$ [225, 226].

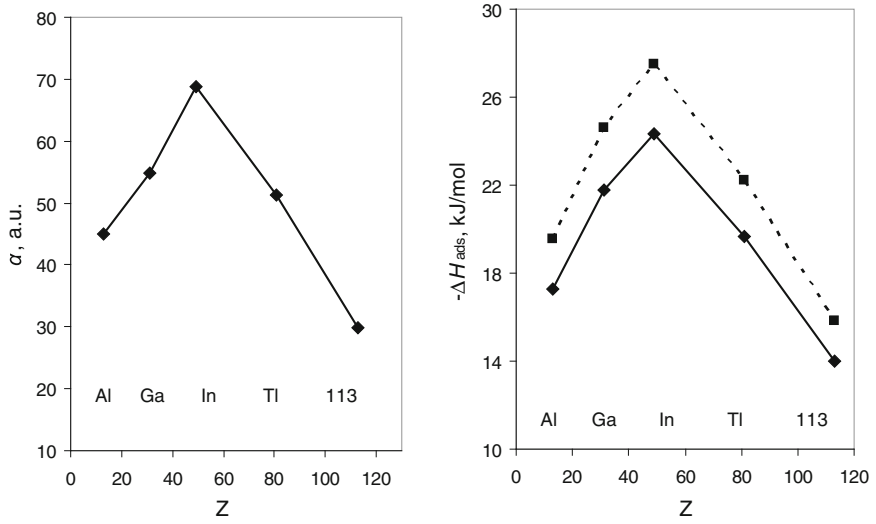

Fig. 35 Polarizabilities, α, and adsorption enthalpies, $-\Delta H_{ads}$, of group-13 elements on Teflon (*solid line*) and polyethylene (*dashed line*): $-\Delta H_{ads}(113)$ is 14 kJ/mol on Teflon and 16 kJ/mol on PE [126]

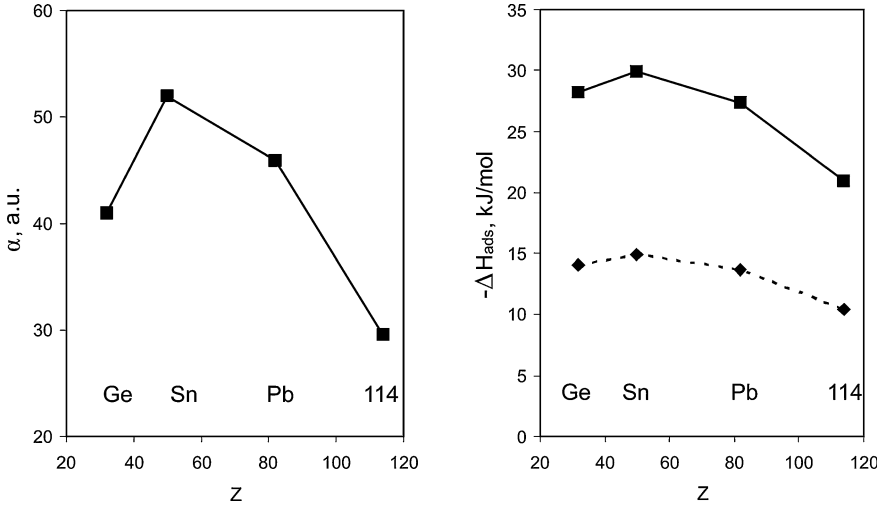

Fig. 36 Polarizabilities, α, and adsorption enthalpies, $-\Delta H_{ads}$, of the group-14 elements on quartz (*solid line*) and Teflon (*dashed line*): $-\Delta H_{ads}(Fl)$ is 21 kJ/mol on quartz and 10.4 kJ/mol on Teflon [127]. From [13]

Some other calculations were also performed for these species: *ab initio* DF for $(113)_2$ [227], 4*c*-BDF, 2*c*-SO ZORA and DC MP2-DFT for the element 113–118 dimers [91, 228–233], and RECP ones for the Fl and element 118 dimers [139].

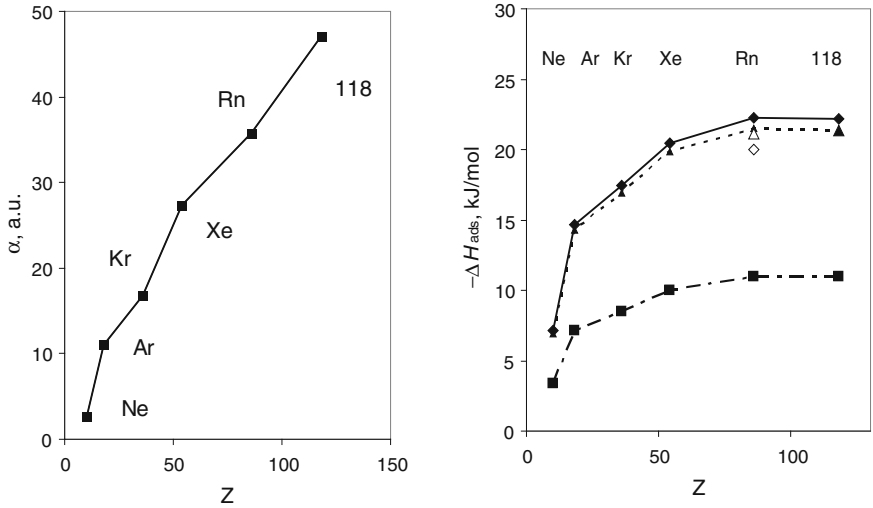

Fig. 37 Polarizabilities, α, and adsorption enthalpies, $-\Delta H_{ads}$, (filled symbols are calculations) of the noble gas atoms on quartz (*rhomboids*, *solid line*), ice (*triangles*, *dashed line*) and Teflon (*squares*, *dashed-dotted line*). Experimental data are for Rn on quartz (an *open rhomboid*) and on ice (an *open triangle*). From [119]

The obtained $D_e(M_2)$ are shown in Fig. 38 [225]. All the 7p-element homonuclear dimers of group-13 through 17 were shown to be weaker bound than their 6p homologs, with the difference in the binding energy between them decreasing from group 15 onwards and a reversal of the trend in group 18, so that $D_e[(118)_2] > D_e(Rn_2)$.

According to *ab initio* DF calculations, $(113)_2$ should be weakly bound because the $7p_{1/2}$ electron yields a weak bond having $2/3\pi$ bonding and $1/3\sigma$ antibonding character [227].

A special case is Fl_2, as that of Cn_2. It was of particular interest due to the strong stabilization and contraction of the $7p_{1/2}$ AO and, therefore, assumed van der Waals nature of the $7p_{1/2}^2$-$7p_{1/2}^2$ bonding. In order to test this hypothesis at the MO level of theory, the electronic structures of Pb_2 and Fl_2 were calculated within various approximations. Results are summarized in Table 15 and shown in Fig. 39.

All the calculations agree on the fact that Fl_2 is stronger bound than a typical van der Waals system. At the 4*c*-DFT level of theory, it is slightly more strongly bound than Cn_2, but much more weakly than Pb_2. A Mulliken population analysis indicates that both the $7p_{1/2}$ and $7p_{3/2}$ AOs of Fl take part in the bond formation: the HOMO of σ character is composed of the $7p_{1/2}$ (98%) and $7p_{3/2}$ (2%) AOs [225, 226]. The participation of the more expanded $7p_{3/2}$(Fl) AO in bonding in comparison with the $6p_{3/2}$(Pb) AO explains an increase in R_e from Pb_2 to Fl_2 (Fig. 39). SO effects were shown to decrease D_e, but increase R_e in both systems [228].

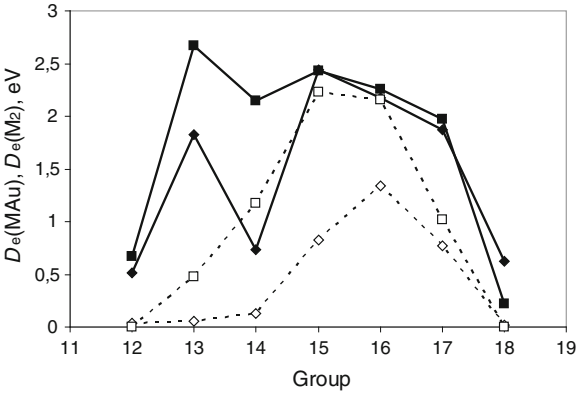

Fig. 38 Calculated dissociation energies of MAu and M_2 (M are elements Hg/Cn through Rn/118). Filled and open *squares* are D_e(MAu) and $D_e(M_2)$ of the 6p elements, respectively, while filled and open rhomboids are D_e(MAu) and $D_e(M_2)$ of the 7p elements, respectively. Reprinted with permission from V. Pershina, A. Borschevsky, J. Anton, T. Jacob, J. Chem. Phys. **133**, 104304 (2010). Copyright 2010 American Institute of Physics

Table 15 Bond lengths, R_e (in Å), dissociation energies, D_e (in eV), and vibrational frequencies, ω_e (in cm^{-1}), of Pb_2 and Fl_2

Molec.	Method	R_e	D_e	ω_e	Ref.
Pb_2	ECP CCSD(T)	3.06	0.64	111	[228]
	RECP CCSD(T)	2.98	0.68	–	[139]
	4*c*-BDF	2.98	1.14	108	[228]
	2*c*-DFT SO ZORA	2.97	1.16	106	[229]
	4*c*-DFT	2.97	1.18	107	[225, 226]
	exp.	2.93	0.86	110	[234]
	exp.	–	1.17	–	[235]
Fl_2	ECP CCSD(T)	3.73	0.07	26	[228]
	4*c*-BDF	3.49	0.12	50	[228]
	2*c*-DFT SO ZORA	3.46	0.12	40	[229]
	4*c*-DFT	3.49	0.13	26	[225, 226]

In $(115)_2$, the $7p_{3/2}$ electrons become active and form a $3/2_u(\pi_u)$ bonding, so that D_e is larger that D_e of $(113)_2$ and Fl_2 [225, 230]. They are also active in Lv_2, but the D_e is larger than that of $(115)_2$ in difference to the 6th period where $D_e(Po)_2 < D_e(Bi_2)$. Thus, the maximum in $D_e(M_2)$ in the 7th row of the Periodic Table is shifted towards group 16 with respect to group 15 in the 6th and upper rows (Fig. 38). This is a pronounced relativistic effect caused by the very large SO splitting of the 7p AOs. As a result of the stabilization of the $7p_{1/2}$ AOs, the system of the highest bonding-antibonding MOs in M_2 consists of only four MOs composed of the $7p_{3/2}$ AOs, so that the half-filled shell (with 4 electrons) falls on Lv_2. In contrast, the $6p_{1/2}$ and $6p_{3/2}$ AOs are not so well separated energetically from each other and form a set of six highest bonding-antibonding MOs, so that the half-filled shell (with 6 electrons) falls on Bi_2 [225].

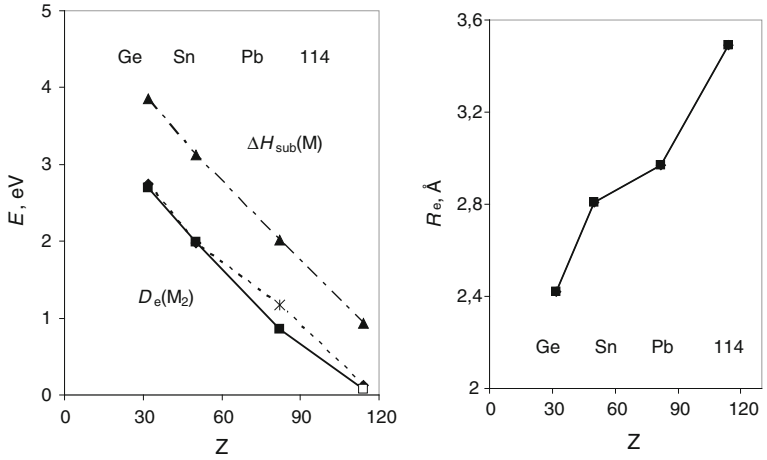

Fig. 39 Dissociation energies, $D_e(M_2)$, (experimental for Ge_2 through Pb_2: Two points for Pb_2 are two different experimental values [234, 235]; and calculated for Fl_2: two points are two different types of calculations, 4*c*-DFT [226] and RECP CCSD(T) [228]); sublimation enthalpies, $\Delta H_{sub}(M)$ [142], and calculated bond lengths, $R_e(M_2)$ [226], where M = Ge, Sn, Pb, and Fl. From [13]

Analogously to the lighter homologs, element 117 should also form $(117)_2$. The calculations found a considerable π bonding character [231, 232]. The bonding is weaker than that of Lv_2 due to the larger number of antibonding electrons. Finally, in $(118)_2$ bonding is of van der Waals type, since the number of bonding and antibonding electrons is the same. It is, however, stronger than that of Rn_2 [139, 225, 233]. This is explained by the larger α of element 118 (46.3 a.u.) than of Rn (35.04 a.u.) [119]. The MO population analysis indicated that no 8s(118) AO takes part in the bond formation in $(118)_2$ [225].

Sublimation (atomization) enthalpies. Solid-state calculations using periodic DFT codes for the 7p elements are still problematic due to very large SO effects on their valence electron shells. An easier way to obtain $\Delta H_f(g)$ is via a correlation with $D_e(M_2)$ in the respective chemical groups. $\Delta H_f(g)$ estimated in this way [225] and those predicted via a linear extrapolation in the groups [207] are given in Table 16, in good agreement with each other. One can see that the $\Delta H_f(g)$ decreases almost linearly with Z in these groups and the values for the 7p elements are the smallest (see Fig. 39 for group 14, as an example).

In [236], E_{coh} of Fl was predicted from SR and SO-GGA-DFT solid-state calculations. The obtained value of 0.5 eV (48.2 kJ/mol), the SO-PW91 result, is in reasonable agreement with the estimates of [207, 225] (Table 16). SO effects were shown to lower E_{coh} and lead to structural phase transitions for the solid Fl (the *hcp* structure in contrast to the *fcc* for Pb). In a nonrelativistic world, all group-14 elements would adopt a diamond structure. An increase in the solid-state nearest-neighbor distance is found from Pb to Fl, as that in their homonuclear dimers, indicating that the nature of the chemical bond in the crystal is similar to that of M_2.

Table 16 Standard enthalpies, $\Delta H_f(g)$ (in kJ/mol), of the 7p elements

Method	E113	Fl	E115	Lv	E117
Extrapolation[a]	138.1	70.3	146.4	92.1	83.7
Correlation[b]	144.7	70.4	152 ± 12	101.3	91.7

[a] Ref. [207]; [b] Ref. [225]

6.5.3 Intermetallic Dimers and Interaction with Metals

Heteronuclear dimers. In order to estimate ΔH_{ads} of the 7p elements on gold, 4*c*-DFT calculations for the MAu dimers were performed in [226, 237]. The obtained D_e(MAu) for the 7p and 6p elements in comparison with $D_e(M_2)$ are shown in Fig. 38. One can see that in groups 13 and 14, D_e(MAu) of the 7p elements are smaller than D_e of the 6p homologs (see also Fig. 40 for group 14 elements, as an example), while in groups 15 through 17, they are about the same. This is in contrast to the trends in $D_e(M_2)$ in these groups, where $D_e(Bi_2) >> D_e[(115)_2]$, $D_e(Po_2) >> D_e(Lv_2)$, and $D_e(At_2) > D_e[(117)_2]$. The relatively strong M-Au bonding of elements 115 through 117 with gold is explained by the relativistic destabilization of the $7p_{3/2}$ AOs fitting energetically better to the 6s(Au) AO, thus making—together with the $7p_{1/2}$ AO—a full σ-bond in MAu in difference to M_2, where only the $7p_{3/2}$ AOs are involved in bonding [225]. In group 18, a reversal of the trend takes place, so that $D_e(118Au) > D_e(RnAu)$, in agreement with the trend in $D_e(M_2)$. This is due to the relativistically more destabilized $7p_{3/2}(118)$ AO than the $6p_{3/2}(Rn)$ AO, thus better overlapping with the valence AOs of gold.

According to results of the calculations, Fl should be stronger bound with gold than Cn [213, 237]. This is due to the fact that in FlAu—even though both FlAu

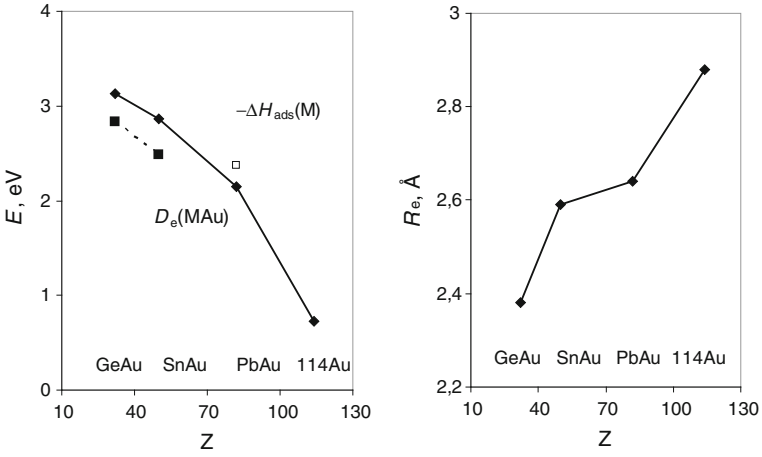

Fig. 40 Dissociation energies, D_e, (*solid line*—calculations [226], *dashed line*—experiment) and calculated bond lengths, R_e, in MAu (M = Ge, Sn, Pb, and Fl). A measured $-\Delta H_{ads}$ of Pb on gold is shown with an open *square*. Reprinted with permission from V. Pershina, Radiochim. Acta, **99**, 459 (2011). Copyright 2011 Oldenbourg Wissenschaftsverlag GmbH

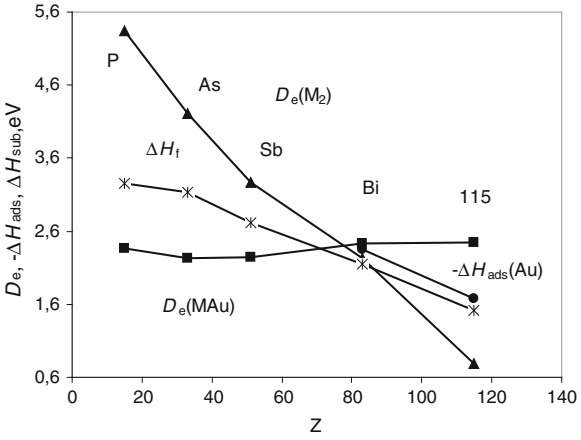

Fig. 41 Calculated dissociation energies, D_e, of MAu (*squares*) [237] and M_2 (*triangles*) [225], formation enthalpies, $\Delta H_f(g)$, of the group 15 elements (*stars*) (for P though Bi are from [142], while for element 115 from [225]) and semi-empirical $-\Delta H_{ads}$ of Bi and element 115 on gold (*circles*) [238]. Reprinted with permission from V. Pershina, A. Borschevsky, J. Anton, T. Jacob, J. Chem. Phys. **133**, 104304 (2010). Copyright 2010 American Institute of Physics

and CnAu are open shell systems with one antibonding σ^* electron—the electron density is donated from the lying higher in energy $7p_{1/2}$(Fl) AO to the 6s(Au) AO, while in CnAu, some excitation energy is needed to transfer some electron density from the closed $7s^2$ shell of Cn to the open 6s shell of Au (Fig. 30).

The calculations have also revealed that the M-Au bond strength *does not decrease linearly with Z* in group 15, 16 and 17. Figure 41 shows, e.g., that in group 15, $D_e(M_2)$ and $\Delta H_f(g)$ decrease, while D_e(MAu) slightly increases with Z. Also, in group 14, a decrease in D_e(MAu) is not strictly linear with Z (Fig. 40).

The 4*c*-DFT calculations were also performed for group-14 intermetallic dimers MM', where M' are group-10 and 11 metals Ni, Pb, Pt, Cu, Ag and Au [226]. (Some of them were supposed to be used as electrode materials in electrochemical deposition experiments [239]). Bonding of Fl with Pt was found to be the strongest, while that with Ag and Ni—the weakest. The trends in D_e and R_e of PbM' and FlM' as a function of M' were shown to be determined by the trends in the energies and R_{max} of the valence (n–1)d AO of the M' atoms, respectively, and are similar for PbM' and FlM' (except for M' = Ni).

Adsorption on gold. The calculated metal–metal bonding in the dimers was used to predict ΔH_{ads} of the heaviest elements on the corresponding metal surfaces. (For lighter elements, semi-empirical ΔH_{ads} are given in [238]). In [240], $-\Delta H_{ads}$ of element 113 on gold of 82 kJ/mol was estimated with respect to the measured $-\Delta H_{ads}$(Tl) of 240 ± 5 kJ/mol [224] using a difference in their D_e(MAu) calculated within the 4*c*-DFT approximation. This gives a preliminary value of $-\Delta H_{ads}(113) = 158.6$ kJ/mol, which is very close to 164.4 kJ/mol predicted via semi-empirical models [238].

In [241], adsorption of the element 113 atom and Tl on a gold surface was modeled by cluster calculations. The 2*c*-DFT calculations were performed for the M-Au$_n$ (M = Tl and element 113, and $n_{max} = 20$) systems, with the gold clusters simulating the Au(100) and Au(111) surfaces. The results show that the difference in the binding energy, E_b(M-Au$_n$), between Tl and element 113 stays within ± 15 kJ/mol of 82 kJ/mol obtained in [240] for MAu. Thus, the cluster calculations performed on a larger scale [241] confirmed the estimate made on the basis of D_e(MAu) [240], so that $-\Delta H_{ads}(113)$ can be finally given as 159 ± 15 kJ/mol.

In [226], $-\Delta H_{ads}$ of Fl on gold of 91 kJ/mol was estimated with respect to the measured $-\Delta H_{ads}$ of Pb [242] using a difference in D_e(MAu) between Pb and Fl.

Also, extensive 4*c*-DFT calculations were performed for M = Pb and Fl interacting with large Au$_n$ clusters simulating the Au(111) surface [213]. All possible adsorption positions were considered. Both Pb and Fl were found to prefer the bridge one, where the convergence in E_b(M-Au$_n$) with the cluster size was reached for $n = 94$. The calculated E_b values turned out to be in very good agreement with experimental data for Pb [242] (Table 17 and Fig. 42) indicating that the Au(111) surface is obviously close to the real one. The obtained $-\Delta H_{ads}$(Fl) of 68.5 kJ/mol is indicative of formation of a chemical bond of Fl with gold. A comparison with group-12 Hg and Cn [213] shows that the trend in E_b(M-Au$_n$) should be Cn < Hg < Fl << Pb (Fig. 42), exactly as that for D_e(MAu) of these elements. Since Hg dissolves into the gold surface gaining another ~0.3 eV [238], the trend in $-\Delta H_{ads}$ should be Cn < Fl < Hg << Pb.

Calculations for the Cn-Au$_n$ and Fl-Au$_n$ systems with the use of other relativistic DFT methods [214–217] came to the same conclusion that Fl should form a rather strong chemical bond with gold, stronger than Cn (Table 17).

Results of the first experiment on adsorption of Fl on gold have, however, given a rather low $-\Delta H_{ads}$ of 34^{+54}_{-11} kJ/mol ($0.35^{+0.6}_{-0.1}$ eV). A conclusion was drawn that this value "suggests the formation of a weak physisorption bond between atomic 114 and a gold surface" [222]. For Cn, it was, however, concluded that "the stronger (than van der Waals—V.P.) adsorption interaction of Cn with gold

Table 17 The Cn-Au$_n$ and Fl-Au$_n$ binding energies (in eV) simulating interactions of M with the Au(100) and Au(111) surfaces (bold values are for the preferential positions)

Method	n	Position	Surface	Cn	Fl	Ref.
4*c*-DFT	1	Top	–	0.51	0.73	[213]
2*c*-DFT	1	Top	–	0.47	0.72	[214–216]
SO DFT	3	Top, bridge	–	0.47	0.77	[214–216]
2*c*-DFT	26	Bridge	Au(100)	0.33	0.55	[216]
2*c*-DFT	37	Hollow-2	Au(111)	–	0.49	[217]
4*c*-DFT	95	Top	Au(111)	0.30	0.47	[213]
4*c*-DFT	94	Bridge	Au(111)	0.42	**0.71**	[213]
4*c*-DFT	107	Hollow-2	Au(111)	**0.46**	0.59	[213]
$-\Delta H_{ads}$ (exp.)	∞	Unknown	Unknown	$0.54^{+0.2}_{-0.04}$	$0.35^{+0.6}_{-0.1}$ ≥ Cn	[202, 222] [223]

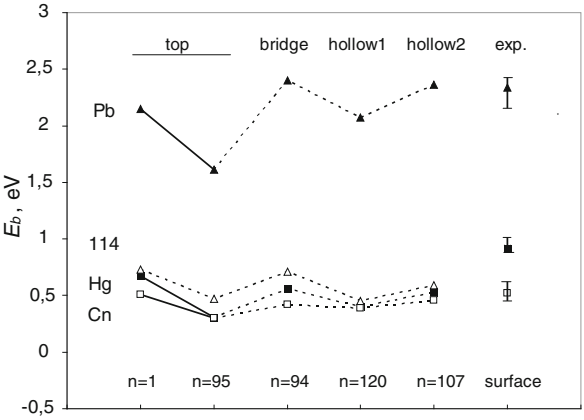

Fig. 42 The 4*c*-DFT calculated binding energies of Pb, Hg, Cn, and Fl with gold clusters in comparison with experimental $-\Delta H_{ads}$ of Pb, Hg and Cn on gold [203, 208, 209, 242]. Reprinted with permission from V. Pershina, J. Anton, T. Jacob, J. Chem. Phys. **131**, 084713 (2009). Copyright 2009 American Institute of Physics

involves formation of a metal bond, which is behavior typical of group-12 elements" [202, 203]. Thus, according to the conclusions of [222], Fl should be chemically more inert than Cn. The subsequent experiment by Yakushev et al. on the adsorption of Fl, conducted at a lower background of interfering products, registered two events of this element adsorbed on gold at room temperature [223]. Such a relatively high T_{ads} is indicative of the chemisorption process and formation of a metal–metal bond. The preliminary estimate of ΔH_{ads} supports the theoretical conclusion that Fl should be at least as reactive as Cn. Further experiments should shed more light on this interesting case.

A summary of the chemical properties of group-14 elements considered above is given in Fig. 43. For elements of this group, a decrease in all types of interactions is observed with increasing Z, so that Fl is the most weakly, but *chemically* bound element in all types of the compounds.

Finally, it is worth comparing properties of Cn and Fl, as both of them were expected to be very inert. Thus, on inert surfaces, Cn should about 6 kJ/mol more strongly adsorb by van der Waals forces than Fl, since $R_{vdW}(Cn) < R_{vdW}(Fl)$. The M–M chemical bond in Fl_2 should be somewhat stronger than that in Cn_2, of preferentially van der Waals character, according to the DFT calculations. (However, *ab initio* DF correlated calculations for both systems would give a more grounded basis for such a comparison). In intermetallic compounds, Fl should be more strongly bound than Cn by chemical forces, since the $7p_{1/2}$(Fl) AO is more readily available for bonding than the 7s(Cn) AO, and the $7p_{3/2}$ AO takes part in the bond formation as well. Also, it should adsorb more strongly than Cn on transition metal surfaces, both by chemical forces. For the solid state of Cn and Fl, a straightforward comparison of cohesive energies obtained by the different DFT calculations [206, 236] is, however, problematic.

In groups 15 through 17, approximately equal D_e(MAu) of the 6p and 7p counterparts suggest that the heaviest elements should adsorb on gold as almost strongly as their lighter homologs, while element 118 should adsorb even more strongly than Rn [237].

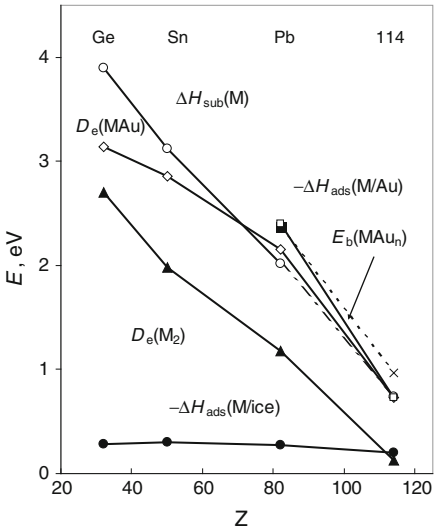

Fig. 43 Calculated dissociation energies D_e of M_2 (filled *triangles* [225]) and MAu (*open rhomboids* [237]); calculated binding energies E_b(M-Au$_n$) (open *squares* [213]); ΔH_{sub}, experimental for Ge, Sn, and Pb, [142] and extrapolated for Fl (*open circles*); experimental $-\Delta H_{ads}$(Pb) on gold (*filled square*) [242]; an estimated $-\Delta H_{ads}$(Fl) (a *cross*) [226]; and calculated $-\Delta H_{ads}$(M) on ice (*filled circles*) [127]. Reprinted with permission from V. Pershina, Radiochim. Acta, **99**, 459 (2011). Copyright 2011 Oldenbourg Wissenschaftsverlag GmbH

At the end of this section, it is again worth discussing validity of the correlation between ΔH_{ads} on some metals and ΔH_{sub} of macroamounts of the adsorbent. As one can see, in groups 13 and 14 there is some, although nonlinear, correlation between these quantities, as that between D_e(MAu) and D_e(M_2) (see, e.g., Fig. 40 for group-14 elements). In groups 15 through 17, no correlation between ΔH_{sub}(M) and $-\Delta H_{ads}$(M) on gold is, however, expected, since M–M and M-Au bonding changes in a different way with Z (see, e.g., Fig. 41 for group-15 elements). There is also no correlation between these quantities in the 6th and 7th periods (see Fig. 10 of [237]). Thus, the case of the 7p elements with strong relativistic effects on their electron shells shows that ΔH_{sub}(M) obtained via a correlation with $-\Delta H_{ads}$(M) can give erroneous results. Also, linear extrapolations of properties such as D_e(MAu) or $-\Delta H_{ads}$(M) from the lighter homologs in the groups should not be used.

6.5.4 Other Compounds of the 7p Elements

Hydrides. DHF, DFC, PP, RECP and 2*c*- and 4*c*-DFT calculations were performed for MH (M = 113–118) [139, 198, 228–230, 243–250] and $113H_3$ [251] and their lighter homologs in the chemical groups. An aim of these studies was the investigation of the influence of relativistic effects on molecular spectroscopic properties. Most representative results are shown in Table 18 and Fig. 44.

Table 18 Bond lengths, R_e (in Å), dissociation energies, D_e (in eV), and SO effects, Δ(SO), on them in MH (M = 113–117) from the RECP calculations [246–248]

Molecule	R_e	ΔR_e(SO)	D_e	ΔD_e(SO)
TlH	1.927	−0.021	1.98	−0.47
113H	1.759	−0.206	1.46	−0.93
PbH	1.884	0.001	1.61	−0.71
FlH	1.972	0.068	0.43	−2.18
BiH	1.836	0.019	2.24	0.08
115H	2.084	0.206	1.82	−0.23
PoH	1.784	0.031	2.27	−0.29
LvH	1.988	0.171	1.81	−0.63
AtH	1.742	0.032	2.31	−0.68
117H	1.949	0.171	1.79	−1.04
RnH	4.387	−0.025	1.84 meV	0.05 meV
118H	3.857	−0.407	5.50 meV	1.94 meV

According to these calculations, in 113H, the 6d and 7s AOs of element 113 participate little in bonding and all the effects are defined by the $7p_{1/2}$ shell. A large relativistic contraction of the $7p_{1/2}$ AO results in a large contraction of the 113-H bond. The SO bond contraction, ΔR_e(SO), is about −0.2 Å. Such a bond contraction is not found in the other MH (M = elements 114–118) (Fig. 44): For FlH through 118H, both the relativistically contracted $7p_{1/2}$ and expanded $7p_{3/2}$ AOs take part in the bond formation, with the contribution of the $7p_{1/2}$ AO gradually decreasing along the 7p series, so that the bonds are longer than those of the homologous MH (M = Pb through Rn). The dissociation energies D_e(MH) (M = 113 through 117) are reduced by the large SO effects (Table 18), with the lowest one at FlH. They also decrease from the 6p to 7p element hydrides. $113H_3$ becomes less stable towards the decomposition into 113H and H_2 than the lighter homologs [251]. In 118H, the van der Waals bond is stabilized by about 2.0 meV by SO effects, with ΔR_e(SO) = −0.025 Å [247]. Trends in the stability of the hydrides were predicted as follows: RnH < < HgH < PbH and 118H < < FlH < CnH.

The RECP CCSD(T) calculations for PbH^+ and FlH^+ have also given a 50% weaker and shorter bond in the latter due to the contraction of the $7p_{1/2}$ AO [139]. The trend for single-charge ions of group 18 is $D_e(RnH^+) > D_e(118H^+)$ and $R_e(RnH^+) < R_e(118H^+)$.

CAS-SCF/SOCI RECP calculations for FlH_2 demonstrated breakdown of the conventional singlet (X^1A_1) and triplet ($^3B_1$) states due to the large relativistic, including SO, effects [252]. The SO effects are shown to destabilize FlH_2 by almost 2.6 eV.

In LvH_2, the SO interaction was found to lengthen the Lv-H bond and lead to a significant H-Lv-H bond angle increase in comparison with PoH_2 according to the RECP calculations [253]. It was concluded that there is a rehybridization of the valence 7p AO with a "supervalent" 8s AO of Lv.

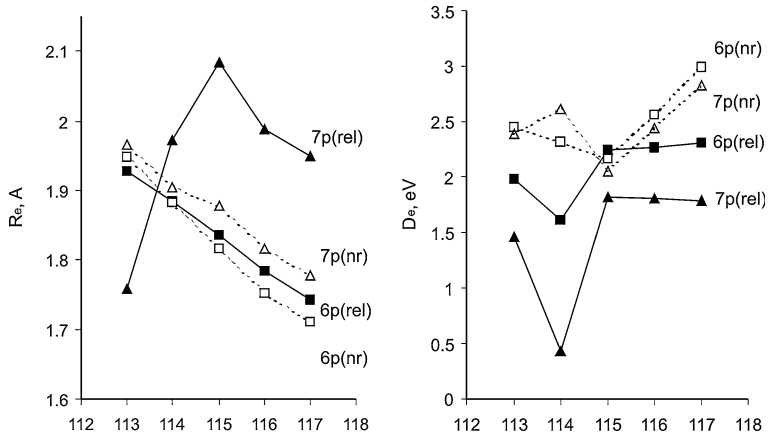

Fig. 44 Bond lengths, R_e, and dissociation energies, D_e, for the 6p- (Tl through At) and 7p-elements (113 through 117) hydrides, MH [228, 246–249]. From [14]

Oxides, hydroxides, halides and halogeno-complexes. Element 113. Results of the 4*c*-DFT calculations have shown Tl and element 113 to form a stable MOH molecule with D_e of 3.68 eV for Tl and 2.42 eV for element 113 [240]. Thus, in the gas-phase chromatography experiments, 113OH should be formed in a pure oxygen flow by analogy with TlOH [224]. $-\Delta H_{ads}$ of 113OH on gold is expected to be lower than $-\Delta H_{ads}$ of the element 113 atom.

PP, DCB, RECP and 4*c*-DFT calculations were performed for MF (M stands for all group 13 metals) [198, 243, 244]. The results show increasing R_e and μ_e from TlF to 113F, in contrast to the decreasing values from TlH to 113H. These different trends in R_e and μ_e for the MF compounds as compared to MH are explained by a more ionic nature of the MF molecules.

A theoretically interesting case is the (113)(117) molecule. The DF calculations have shown that in this molecule both the low-lying $7p_{1/2,1/2}$(113) AO and the destabilized $7p_{3/2,1/2}$(117) AO contribute to electron transfer to the group 13 atom [254]. Thus, rather than the single electron of the group 13 atom completing the valence p shell of the group 17 atom, the electron flow is more the other way around: the high-lying $7p_{3/2,1/2}$ shell donates into the low-lying $7p_{1/2,1/2}$ shell of the group 13 atom. This results in a reversal of the dipole direction and a change of the sign of μ_e.

As in Cn, the relativistic destabilization of the 6d AOs is expected to influence properties of high-coordination compounds of element 113. This was confirmed by the PP and RECP calculations for $113X_3$ (X = H, F, Cl, Br, and I) [74, 244]. As a consequence of the involvement of the 6d AOs, a T-shaped rather than trigonal planar geometric configuration was predicted for these molecules showing that the valence shell electron pair repulsion (VSEPR) theory is not applicable to the heaviest elements. Relativistic effects on bond angles were assumed to be small. However, if Jahn–Teller distortions are involved, relativistic effects may significantly change bond angles, as was shown for AtF_3 [255].

A stable high-coordination compound of element 113, $113F_6^-$, with the metal in the 5+ oxidation state is also foreseen in [244]. $113F_5$ will probably be unstable since the energy of the decomposition reaction $113F_5 \rightarrow 113F_3 + F_2$ is less than −100 kJ/mol. The calculated energies of the reaction $MX_3 \rightarrow MX + X_2$ (M = B through element 113) suggest a decrease in the stability of the 3+ oxidation state in this group.

Element 114 (flerovium, Fl). Electronic structures of FlX (X = F, Cl, Br, I, O) and FlO_2 were calculated using 2*c*-RECP CCSD(T), 2*c*-DFT SO ZORA and 4*c*-BDF methods [228, 229]. Better agreement with experiment for the known compounds of Pb was shown by the RECP CCSD(T) results. Trends in R_e and D_e for the halides and oxides from Pb to Fl were found to be similar to those for the hydrides. In contrast to PbO_2 (D_e = 5.60 eV), FlO_2 (D_e = 1.64 eV) was predicted to be thermodynamically unstable with respect to the decomposition into the metal atom and O_2. According to results of these calculations Fl should not react with O_2 at the experimental conditions, as was theoretically shown in [127].

The *ab initio* DF and PP calculations [256] for the decomposition reactions $MX_4 \rightarrow MX_2 + X_2$ and $MX_2 \rightarrow M + X_2$ (M = Si, Ge, Sn, Pb, and Fl; X = H, F, and Cl) also predicted a decrease in the stability of the 4+ oxidation state in group 14. The instability was shown to be a relativistic effect (see Fig. 45 for MH_4, as an example). The neutral state was found to be more stable for Fl than for Pb. As a consequence, Fl is expected to be less reactive than Pb, but about as reactive as Hg. This is in agreement with the predicted adsorption of Fl on gold that should be much weaker than that of Pb and slightly weaker than that of Hg [213] (Table 17 and Fig. 42). The possibility of the existence of FlF_6^{2-} was also suggested in [256].

Elements 116–117. Estimates of formation enthalpies of MX_2 and MX_4 (X = F, Cl, Br, I, SO_4^{2-}, CO_3^{2-}, NO_3^-, and PO_4^{3-}) for Po and Lv made on the basis of MCDF atomic calculations confirmed the instability of the 4+ state of Lv [257]. The chemistry of Lv is expected to be mainly cationic: an ease of formation of the divalent compounds should approach that of Be or Mn, and tetravalent compounds, e.g., LvF_4, should be formed with the most electronegative atoms.

Influence of SO effects on molecular structure of MX_2 (X = F, Cl, Br, I, At, and element 117) of Lv and its lighter homologs was studied with the use of the quasirelativistic 2*c*-HF and DFT ECP methods [258]. The results have shown that

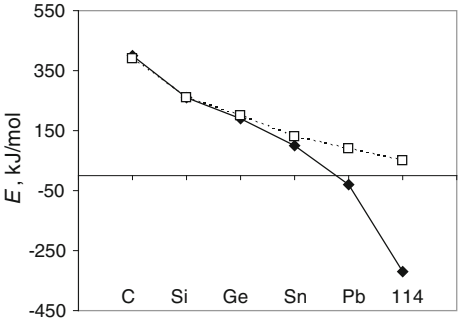

Fig. 45 Relativistic DFC (*solid line*) and nonrelativistic HF (*dashed line*) calculated energies of the decomposition reaction $MH_4 \rightarrow MH_2 + H_2$ (M = C, Si, Ge, Sn, Pb, and Fl) [256]. From [13]

while the molecules are bent at a scalar relativistic level, SO coupling is so strong that only $7p_{3/2}$ AOs of Lv are involved in bonding, which favors linear molecular geometries for MX_2 with heavy terminal halogen atoms.

Electronic structures of IF, AtF and 117F were considered at the DC and RECP levels of theory [74]. D_e(117F) was shown to be the largest among the group-17 fluorides. It was found that D_e(117F) is 0.1 eV increased by SO effects in contrast to the other group 17 fluorides. The SO effects are opposite for all the three spectroscopic constants of 113F and 117F. For $117F_3$, the RECP calculations have shown that the D_{3h} geometry is not the proper one, in difference from AtF_3, thus again indicating that the VSEPR theory is not applicable to the heaviest elements [74, 259]. The SO effect was shown to stabilize this molecule by 1.2 eV, which is unusually large for atoms with open p-shells. A strong ionic character of the bond may be responsible for this huge stabilization.

117Cl is predicted to be bound by a single π bond and have a relativistically (SO) increased bond length [260].

Element 118. The chemistry of element 118 should be interesting due to the very large SO splitting, of 11.8 eV, of the 7p AO [21]. The relativistic destabilization of the four $7p_{3/2}$ electrons suggests that element 118 should be relatively reactive and the most electropositive in the group (see Sect. 5). It was predicted to form a 118-Cl bond [261].

The destabilization of the $np_{3/2}$ AOs should also result in the increasing stability of the 2+ and 4+ oxidation states in group 18. The RECP calculations for the decomposition reactions $MF_2 \rightarrow M + F_2$ and $MF_4 \rightarrow MF_2 + F_2$, where M = Xe, Rn and element 118, confirmed the increasing stability of the fluorides in the group, as a result of the increasing polarizability of the central atom [74, 262]. The SO effects were shown to stabilize $118F_4$ by a significant amount of about 2 eV, though they enlarge R_e by 0.05 Å. Thus, the trends in increasing R_e and D_e in this group are continued with element 118. Also, the following trends in the stability of the fluorides were established: $RnF_2 < HgF_2 < PbF_2$, while $CnF_2 < FlF_2 < 118F_2$.

The influence of the SO interaction on the geometry of group-18 MF_4 was investigated by the RECP SOCI/CCSD calculations [249, 262, 263]. It was shown that a D_{4h} geometrical configuration for XeF_4 (calculated in agreement with experiment) and for RnF_4 (calculated) becomes slightly unstable for $118F_4$. A T_d configuration becomes more stable than the D_{4h} one in $118F_4$ by about 0.2 eV. The reason for this unusual geometry is the availability of only the stereochemically active four $7p_{3/2}$ electrons for bonding. This is another example of the inapplicability of the VSEPR theory for the heaviest elements [263]. It was also predicted that the fluorides of element 118 should most probably be ionic rather than covalent, as in the case of Xe. This prediction might be useful for future gas-phase chromatography experiments.

6.6 Elements with Z > 118

6.6.1 Elements 119 and 120

Chemical properties of elements 119 and 120 predicted on the basis of atomic DF calculations are described in [1, 2]. They are shown to be determined by the valence 8s electrons and are expected to follow those of alkali- and alkali-earth elements in chemical groups 1 and 2, respectively. An increasing relativistic stabilization of the ns AOs of the elements of these groups with increasing Z results in a reversal of trends in such properties as IP, EA, α, and AR, as described in Sect. 5.2. Recently, interest in the chemistry of these elements has been renewed, since these are the next elements that are awaiting discovery after Z = 118. Volatility of atoms of elements 119 and 120 might be studied in the long term using some advanced chromatography (e.g., vacuum) techniques that can cope with extremely short (presumably sub-millisecond) half-lives of their isotopes. In recent theoretical works [143, 144], properties that are of interest for such chromatography studies, i.e., ΔH_{sub} and ΔH_{ads} of elements 119 and 120 on noble metals, were predicted on the basis of 4*c*-DFT calculations of intermetallic compounds.

Homonuclear dimers and sublimation of metals. Calculated binding energies and other spectroscopic properties of the group-1 and 2 M_2 are given in Table 19 [143, 144]. (The calculations are in very good agreement with the measured properties where available. A comparison with other calculations for the lighter homologs of elements 119 and 120 is given in [143, 144]). Plots, demonstrating trends in these properties are shown in Figs. 46, 47.

One can see that in these groups, there is a reversal of trends in $D_e(M_2)$ at Cs and Ba, respectively, though in an opposite way. The reason for the different behavior is a different type of the M–M bonding in these groups: a covalent one in group 1, while a van der Waals one in group 2, even though both are defined by the behavior of the ns AOs.

Table 19 Spectroscopic properties of M_2 (M = K, Rb, Cs, Fr, and element 119) and (M = Ca, Sr, Ba, Ra, and element 120): equilibrium bond lengths, R_e (in Å), dissociation energies, D_e (in eV) and vibrational frequencies, ω_e (in cm^{-1}) [143, 144]

Mol.	Group 1			Mol.	Group 2		
	R_e	D_e	ω_e		R_e	D_e	ω_e
K_2	3.942	0.52	91	Ca_2	4.236	0.14	66
	3.924	*0.52*	*92*		*4.277*	*0.14*	*64*
Rb_2	4.224	0.48	58	Sr_2	4.493	0.13	44
	4.180	*0.48*	*58*		*4.498*	*0.13*	*40*
Cs_2	4.673	0.43	41	Ba_2	4.831	0.23	43
	4.646	*0.45*	*42*		–	–	–
Fr_2	4.610	0.44	33	Ra_2	5.19	0.11	25
$(119)_2$	4.265	0.55	41	$(120)_2$	5.65	0.02	9

[a] Italics are experimental values (see references in [143, 144])

Thus, $(119)_2$ having a σ_g^2 ground state should be most strongly bound by covalent forces and have a shorter bond (about that of Rb_2) caused by the contraction of the 8s AO. On the contrary, $(120)_2$ with a $\sigma_g^2\sigma*_u^2$ ground state should be most weakly, among the homologs, bound by van der Waals forces (the number of bonding and antibonding electrons is the same), and the bond should be the longest. $R_e(M_2)$ of group-1 elements show a reversal of the increasing trend at Cs due to the relativistic contraction of the ns AO. $R_e(M_2)$ of group-2 elements, however, reveal a steady increase in the group which is explained by the participation of the $np_{3/2}$ and (n–1)d AOs in bonding in addition to the ns AOs.

As one can see from Figs. 46, 47, the M–M-bonding correlates with ΔH_{sub} of metals in these groups with the same reversal of trends at Cs and Ba, respectively. Using these correlations and the calculated D_e of $(119)_2$ and $(120)_2$, ΔH_{sub} of element 119 and 120 of 94 kJ/mol and 150 kJ/mol, respectively, were predicted [143, 144]. According to these data, element 119 metal should be as strongly bound as K, while element 120 metal should be most weakly bound in group 2, though stronger than the 119 one.

Intermetallic dimers and adsorption on noble metals. To predict adsorption of elements 119 and 120 on noble metals, e.g., on gold used in chromatography experiments, electronic structures of MAu, where M are group-1 and 2 metals, were calculated using the 4*c*-DFT method [143, 144]. The obtained binding energies and other spectroscopic properties are given in Table 20. (There are no practically experimental data for R_e of the lighter species, expect of that for CaAu. The calculated dissociation energies are somewhat larger, but perfectly follow the experimental trend in group 1. A comparison with other calculations for the lighter

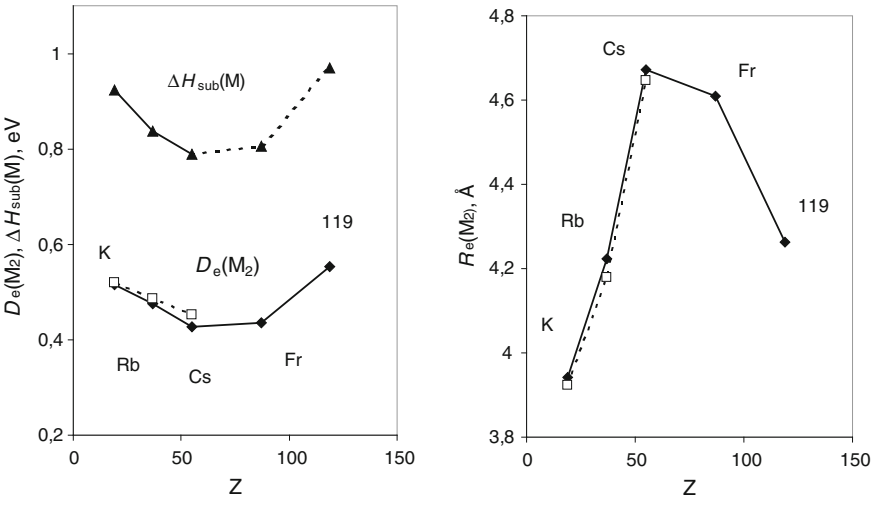

Fig. 46 Dissociation energies, D_e and equilibrium bond lengths, R_e of group-1 M_2 (filled rhomboids are 4*c*-DFT calculations [144], open *squares*—experiment), as well as ΔH_{sub} (filled *triangles* are experiment [142], open ones—estimates). From [144]

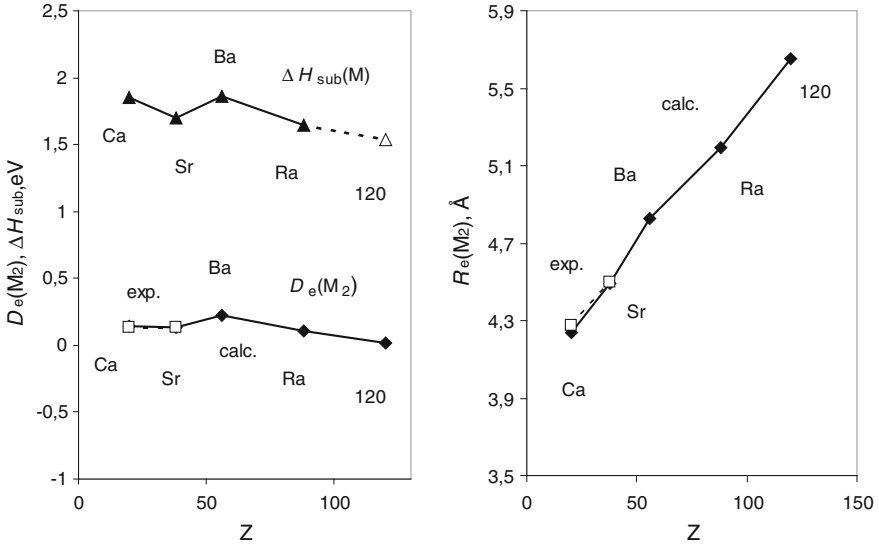

Fig. 47 Dissociation energies, D_e and equilibrium bond lengths, R_e of group-2 M_2 (filled rhomboids are 4*c*-DFT calculations [143], open *squares*—experiment), as well as ΔH_{sub} (filled *triangles* are experiment [142], open ones—estimates). Reprinted with permission from V. Pershina, A. Borschevsky, J. Anton, J. Chem. Phys. **136**, 134317 (2012). Copyright 2012 American Institute of Physics

homologs of elements 119 and 120 are given in [143, 144]). Trends in these properties are shown in Figs. 48, 49.

According to the data of Table 20, elements 119 and 120 should form stable compounds with gold. The D_e(MAu) values show a reversal of the increasing trend at Cs and Ba in group 1 and 2, respectively, so that both 119Au and 120Au should be the weakest among the considered homologs in these group. The trend is defined by the behavior of the ns AOs, whose relativistic stabilization in the groups starts to dominate over the orbital expansion beyond Cs and Ba, respectively. As a result of this stabilization, electronegativities of elements 119 and 120 approach that of Au. This diminishes the electron density transfer from M to Au, and therefore, the bond strength of these dimers. The R_e(MAu) values increase in both groups: since bonding is of preferentially ionic character, the trend is defined by the steadily expanding $(n–1)p_{3/2}$ AOs of the M^+ and M^{2+} ions with Z, respectively. Dipole moments of MAu have also a reversal of the trend in group 1 at Cs and an overall increasing trend in group 2 [143, 144].

The M-Au binding energies in the dimers correlate with the semi-empirical $-\Delta H_{ads}$(M) of K through Cs, and Ca through Ba on gold [238]. Using these correlations in groups 1 and 2, $-\Delta H_{ads}$ of Fr and element 119 on gold of 136 kJ/mol and 106 kJ/mol, respectively, and of Ra and element 120 of 237 kJ/mol and 172 kJ/mol, respectively, were determined. Using correlations with $-\Delta H_{ads}$(M) on other noble metals, ΔH_{ads} of these elements on Ag and Pt were also

Table 20 Spectroscopic properties of MAu (M = K, Rb, Cs, Fr, and element 119) and (M = Ca, Sr, Ba, Ra, and element 120): Equilibrium bond lengths, R_e (in Å), dissociation energies, D_e (in eV), and vibrational frequencies, ω_e (in cm^{-1}) [143, 144]

Mol.	Group 1			Mol.	Group 2		
	R_e	D_e	ω_e		R_e	D_e	ω_e
KAu	2.856	2.76	173	CaAu	2.627	2.71	221
	–	*2.75*	–		*2.67*	*2.55*	*221*
RbAu	2.967	2.75	122	SrAu	2.808	2.63	159
	–	*2.48*	–		–	–	–
CsAu	3.050	2.91	100	BaAu	2.869	3.01	145
	–	*2.53*	–		–	–	–
FrAu	3.097	2.75	89	RaAu	2.995	2.56	105
119Au	3.074	2.44	92	120Au	3.050	1.90	97

[a] Italics are experimental values (see references in [143, 144]

predicted (Figs. 48, 49). The very moderate $-\Delta H_{ads}$ values of elements 119 and 120, the lowest in groups 1 and 2, especially on Ag (63 kJ/mol and 50 kJ/mol, respectively), are indicative of the possibility of adsorption chromatography measurements for these elements.

The ΔH_{sub} and $-\Delta H_{ads}$ values show that there is no proportionality between these quantities in group 1, as they change in the opposite way with Z. In group 2, there is, however, a correlation between ΔH_{sub} and $-\Delta H_{ads}$.

Thermodynamic properties of metals of elements 113 through 120 were predicted in [264] using atomic calculations and mathematical models.

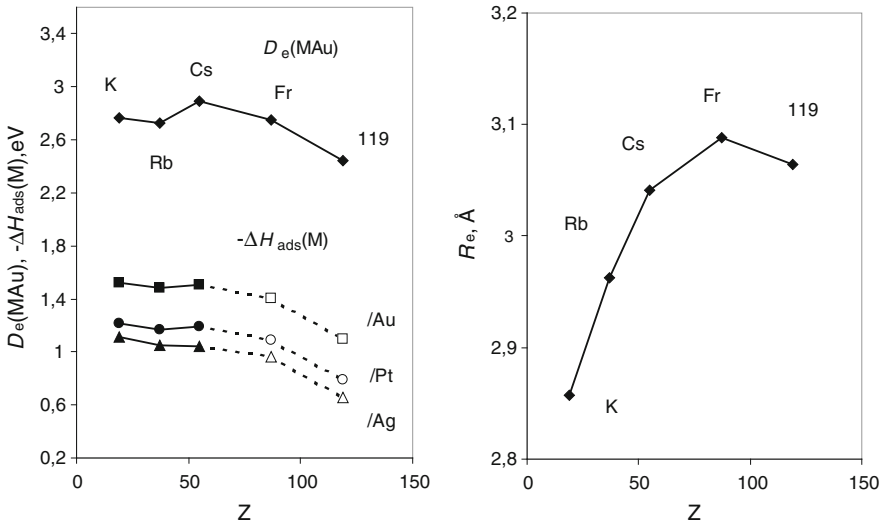

Fig. 48 4*c*-DFT dissociation energies, D_e, and equilibrium bond lengths, R_e, of group-1 MAu, as well as adsorption enthalpies $-\Delta H_{ads}$ (filled symbols are semi-empirical calculations [238], while open ones—obtained via correlations with D_e(MAu) on Au, Pt, and Ag). From [144]

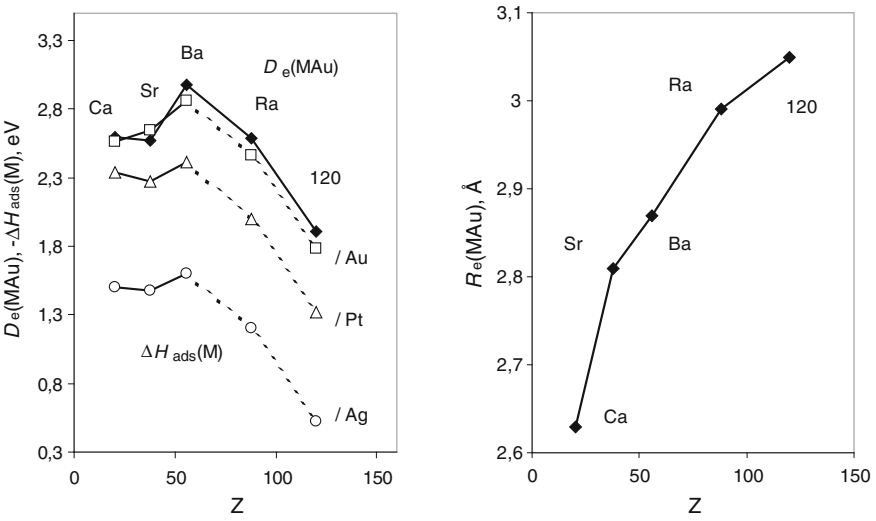

Fig. 49 4*c*-DFT dissociation energies, D_e, and equilibrium bond lengths, R_e, of group-2 MAu, as well as adsorption enthalpies $-\Delta H_{ads}$ (filled symbols are semi-empirical calculations [238], while open ones—obtained via correlations with D_e(MAu) on Au, Pt, and Ag). From [143]

Other compounds. Hydrides and fluorides of elements 119 and 120 were considered within the PP and *ab initio* DF approximations [245, 265, 266]. It was shown that bond distances decrease from the 7th to the 8th period for group-1 and 2 elements due to the relativistic ns AO contraction. The 119F was found to be less ionic than lighter alkaline fluoride homologs in contrast to the expectations based on the periodic trends.

6.6.2 Elements with Z > 120

The chemistry of elements heavier than Z = 120 should be defined by many open shells and their mixing [1, 2]. Due to the very strong relativistic effects, it will be much more different to anything known before. However, without relativistic effects, it would have also been very different due to the very large orbital effects.

Very few molecular calculations exist in this superheavy domain. Properties of elements heavier than 120 predicted on the basis of atomic calculations are discussed in [1–5], as well as at the beginning on this chapter. More recent considerations of their chemistry can be found in [267, 268].

A list of possible molecules of elements in the range Z = 121–164 was suggested in [268], though their verification should be left to future theoretical studies. Interesting examples are those where the elements are in unusual valence states or coordination, like, e.g., $144F_8$ (an analog of PuF_8), or $148O_6$ (an analog of UO_6). Quasi-relativistic multiple-scattering calculations on $125F_6$ have found that

Table 21 Trends in volatility of the group-4 through 8 compounds and the group-12 and 14 atoms

Group	Species	Theoretically predicted	Ref.	Experimentally observed	Ref.
4	MCl_4, MBr_4	Hf < Rf	[9]	Hf < Rf	[272]
5	ML_5 (L = Cl,Br)	Nb < Ta < Db	[162, 164]	(DbO_3Br)	[273]
		$DbCl_5 > DbOCl_3$	[163]	$DbCl_5 > DbOCl_3$	[273]
	$MBr_5 \rightarrow MBr_6^-$	Nb > Ta > Db	[164]	Nb > Ta > Db	[187–189]
				Db > Nb > Ta	[190]
6	MO_2Cl_2	Mo > W > Sg	[167]	Mo > W > Sg	[185, 186]
7	MO_3Cl	Tc > Re > Bh	[168]	Tc > Re > Bh	[184]
8	MO_4	Ru < Os > Hs	[170]	Os > Hs	[182]
12	M	Hg < Cn	[210–213]	Hg < Cn	[202, 203]
14	M	Pb << Fl < Cn	[213, 226]	Fl > Cn	[222]
			[216, 217]	Fl ≤ Cn	[223]

bonding is defined by the $5g^1$ electron, the situation being analogous to NpF_6 with the $5f^1$ electron [269]. There are noncorrelated DF calculations for fluorides of element 126 [270, 271].

Accurate predictions of properties of specific compounds will be quite a challenging task in this area. This may need inclusion of the QED effects to reach the required accuracy.

6.7 Summary of Predictions of Volatility of the Heaviest Elements and their Compounds

Predicted trends in volatility of the heaviest elements and their compounds compared to the experimental observations are summarized in Table 21. One can see that almost all the predictions for group-4 through 8, as well as for group 12 are confirmed by the experiments. In addition, the calculated absolute values of ΔH_{ads} are in very good agreement with the experimental ones, as discussed above. The only open question is volatility of group 4 and 5 pure halides, which might need further experimental or/and theoretical considerations. Predictions for Fl are also awaiting further experimental verifications.

7 Aqueous Chemistry of the Transactinides

7.1 Redox Potentials

Knowledge of the relative stability of oxidation states of elements, i.e., redox potentials, $E°$, is very important for a chemical application. Trends in the stability of various oxidation states of the heaviest elements were predicted earlier on the

basis of atomic DF and DS calculations in combination with models based on a Born-Haber cycle (see [1, 2]). The results, however, depend on the model used and often disagree. Later, oxidation states of Rf, Db, and Sg were estimated [145, 165, 274, 275] using known $E°$ of the lighter homologs [276] and results of atomic MCDF calculations of the IPs [25–28].

For an oxidation–reduction reaction

$$M^{z+n} + ne \leftrightarrow M^{z+}, \tag{20}$$

the redox potential is defined as

$$E° = -\Delta G°/nF, \tag{21}$$

where $\Delta G°$ is the free energy of reaction (20) and F is the Faraday number.

$E°$ could then be estimated using a correlation between $E°$ and IP, since

$$\Delta G° = -(\mathrm{IP} + \Delta G°_{\mathrm{hydr}}), \tag{22}$$

where $\Delta G°_{\mathrm{hydr}}$ is a free energy of hydration, being a smooth function of atomic number, and can therefore easily be evaluated. Thus, using the MCDF calculated IPs and experimentally known $E°$ [276, 277] unknown $E°$ of the transactinides in acidic solutions were determined using a linear correlation between these quantities in the chemical groups (see [145, 165, 274, 275] for the values, also a comparison with the homologs). One of those correlations for group-6 species indicating a decrease in the stability of the 4+ state with respect to the 6+ state in group 6, as a decrease in $E°(MO_3/MO_2)$, is shown in Fig. 50, as an example. The $E°$ of the transactinides are given in Table 22.

The obtained values of the redox potentials show the following trends: The stability of the maximum oxidation state increases within groups 4 through 6, while that of lower oxidation states decreases. Along the 7th period, the stability of the maximum oxidation state decreases, because $E°\left(\mathrm{Lr}^{3+}/\mathrm{Lr}^{2+}\right) < E°\left(\mathrm{Rf}^{\mathrm{IV}}/\mathrm{Rf}^{3+}\right) < E°\left(\mathrm{Db}^{\mathrm{V}}/\mathrm{Db}^{\mathrm{IV}}\right) < E°\left(\mathrm{Sg}^{\mathrm{VI}}/\mathrm{Sg}^{\mathrm{V}}\right)$. A similar trend is observed for

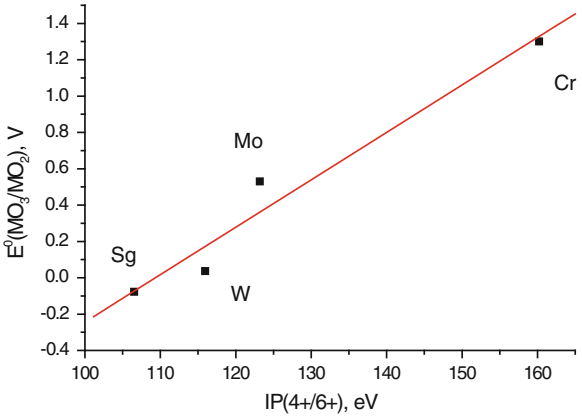

Fig. 50 Correlation between IP(4+/6+) and standard potentials $E°(MO_3/MO_2)$, where M = Cr, Mo, W, and Sg. Reprinted with permission from V. Pershina, E. Johnson, B. Fricke, J. Phys. Chem. A **103**, 8463 (1999). Copyright 1999 American Chemical Society

Table 22 Redox potentials of Lr, Rf, Db, and Sg in aqueous acidic solutions

Potential	Lr[a]	Rf	Db[f]	Sg[g]
$E°(M^{VI}/M^{V})$	–	–	–	−0.046 (MO_3/M_2O_5) −0.05 (M^{VI}, H^+/M)
$E°(M^{V}/M^{IV})$	–	–	−1.0 (M_2O_5/MO_2) −1.13 (MO_2^+/MO^{2+})	−0.11 (M_2O_5/MO_2) −0.35 (M^{V}, H^+/M^{IV},H^+)
$E°(M^{IV}/M^{3+})$	8.1	−1.5 (M^{4+}/M^{3+})[c]	−1.38 (MO_2/M^{3+})	−1.34 (MO_2/M^{3+}) −0.98 ($M(OH)_2^{2+}/M^{3+}$)
$E°(M^{3+}/M^{2+})$	−2.6	−1.7 (M^{3+}/M^{2+})[c]	−1.20	−0.11
$E°(M^{3+}/M)$	−1.96[b]	−1.97 (M^{3+}/M)[d]	−0.56	0.27
$E°(M^{IV}/M)$	–	−1.85 (M^{4+}/M)[e] −1.95 (MO_2/M)[e]	−0.87 (MO_2/M)[d]	−0.134 (MO_2/M) −0.035 ($M(OH)_2^{2+}$/M)
$E°(M^{V}/M)$	–	–	−0.81 (M_2O_5/M)	−0.13 (M_2O_5/M)[d]
$E°(M^{VI}/M)$	–	–	–	−0.12 (MO_3/M) −0.09 (M^{VI}, H^+/M)

[a] [277]; [b] [276]; [c] [275]; [d] roughly estimated from the other $E°$; [e] [165]; [f] [274]; [g] [145]

$E°\left(M^{Zmax}/M\right)$, see Table 22. (The roman numbers denote the valence states in complex compounds). As was shown earlier, the increasing stability of the maximum oxidation state in groups 4, 5 and 6 is a relativistic effect. The estimates of redox potentials confirm that the 3+ and 4+ states for Db and Sg, respectively, will be unstable. Figure 50 shows this for Sg, as an example. One can see that decreasing IPs($M^{4+} \rightarrow M^{6+}$) result in decreasing $E°(M^{VI}/M^{IV})$, so that the 4+ state of Sg with respect to the 6+ state will be even less stable than the 4+ state of the lighter homologs. (See also Sect. 5.2 and "Liquid-Phase Chemistry of Superheavy Elements" for experiments).

7.2 Hydrolysis and Complex Formation

Complex formation of the heaviest elements is studied experimentally by liquid–liquid extractions, or ion exchange separations (see "Liquid-Phase Chemistry of Superheavy Elements"). For a simple complex ML_n, the cumulative complex formation constant

$$\beta_n = [ML_n][M]^{-1}[L]^{-n} \tag{23}$$

is a measure of its stability. For step-wise processes, consecutive constants K_i are used. If various ML_n^{z-n} complexes exist in the aqueous phase, but only one $(ML_i)^{p-}$ complex in the organic phase, the distribution coefficient, K_d, for the anion exchange separations is given by the following equation [278]

$$K_d = \frac{K_{\mathrm{DM}}[RB^+L^-]^p_{\mathrm{org}}\beta_i[L^-]^{i-p}}{\sum_0^N \beta_n[L^-]^n}, \tag{24}$$

where K_{DM} is the association constant with the organic cation. Thus, a sequence in the K_{d} values for a series of species under consideration, e.g., for elements of one group, reflects a sequence in the stability of their complexes.

Complex formation is known to increase in the transition element groups. In aqueous solutions it, however, competes with hydrolysis. This may change trends in the stabilities of complexes and, finally, in their extraction into an organic phase, or sorption by a resin.

One should distinguish between hydrolysis of cations and hydrolysis of complexes [279]. The former is described as a process of a successive loss of protons

$$\mathrm{M(H_2O)}_n^{z+} \leftrightarrow \mathrm{MOH(H_2O)}_{n-1}^{(z-1)+} + \mathrm{H^+}. \tag{25}$$

In acidic solutions, hydrolysis involves either the cation, anion, or both, and is competing with the complex formation described by the following equilibrium

$$x\mathrm{M(H_2O)}_{w^\circ}^{z+} + y\mathrm{OH^-} + i\mathrm{L^-} \leftrightarrow \mathrm{M}_x\mathrm{O}_u\mathrm{(OH)}_{z-2u}\mathrm{(H_2O)}_w\mathrm{L}_i^{(xz-y-i)+} + (xw^\circ + u - w)\mathrm{H_2O}. \tag{26}$$

7.2.1 Theoretical Model for Prediction of Complex Formation

In order to predict a sequence in K_{d} (Eq. 24), one should predict a sequence in the formation constants of a series of species of interest. For a reaction like, e.g., (25) or (26),

$$\log K_i = -\Delta G^{\mathrm{r}}/2.3RT, \tag{27}$$

where ΔG^{r} is the free energy change of the complex formation reaction. To obtain it in a straightforward way, binding or total energies of species in the left and right parts of the reaction should be calculated. Such relativistic calculations, with full geometry optimization for the heaviest elements, are extremely computer time intensive. In addition, the obtained accuracy might be insufficient in predicting stabilities of similar species of homologs. Therefore, the following efficient model was suggested by us.

In a fashion analogous to that of Kassiakoff and Harker [280], the following expression for the free energy of formation of the $\mathrm{M}_x\mathrm{O}_u\mathrm{(OH)}_v\mathrm{(H_2O)}_w^{(xz-2u-v)+}$ species from the elements was adopted

$$-\Delta G^f(u,v,w)/2.3RT = \sum a_i + \sum a_{ij} + \log P - \log(u!v!w!2^w) + (2u+v+1)\log 55.5. \tag{28}$$

The first term on the right hand side of Eq. 28, $\sum a_i$, is the non-electrostatic contribution from M, O, OH, and H_2O, which is related to the overlap population, OP. For a reaction,

$$\Delta \sum a_i = \Delta E^{\mathrm{OP}} = k\Delta \mathrm{OP}, \tag{29}$$

where k is an empirical coefficient. The next term, $\sum a_{ij}$, is a sum of each pairwise electrostatic (Coulomb) interaction:

$$E^C = \sum a_{ij} = -B \sum_{ij} Q_i Q_j / d_{ij}, \tag{30}$$

where d_{ij} is the distance between moieties i and j; Q_i and Q_j are their effective charges and $B = 2.3RTe^2/\varepsilon$, where ε is a dielectric constant. For a reaction, ΔE^{C} is the difference in E^{C} for the species in the left and right parts of the reaction. P in Eq. 28 is the partition function representing the contribution of structural isomers if there are any. The last two terms are statistical: one is a correction for the indistinguishable configurations of the species, and the other is a conversion to the molar scale of concentration for the entropy. Σa_{ij} and Σa_i for each compound are then calculated directly via a Mulliken analysis implemented in most of the quantum chemical methods (e.g., 4c-DFT [87]); see Sect. 4.3.3. To predict $\log K_i$ or $\log \beta_i$ for transactinide complexes, coefficients k and B should then be defined by fitting $\log K_i$ to experimental values for the lighter homologs. Using this model, hydrolysis and complex formation constants were predicted for a large number of aqueous compounds of group-4 through 6 elements [281–289] in very good agreement with experiment; see "Liquid-Phase Chemistry of Superheavy Elements". Results of these calculations and comparison with experimental data reveal that a change in the electrostatic metal–ligand interaction energy (ΔE^{C}) of a complex formation reaction contributes predominantly in the change in ΔG^{f}, i.e., in ΔG^{r}. Thus, only by calculating ΔE^{C} can trends in the complex formation be reliably predicted.

7.2.2 Rf

As other group-4 elements, Rf undergoes hydrolysis and complex formation in acidic solutions. These processes for Zr, Hf, and Rf in HF and HCl solutions were studied theoretically using the model described in the previous section [285]. The following reactions were considered: the first hydrolysis step

$$\mathrm{M(H_2O)_8^{4+}} \leftrightarrow \mathrm{MOH(H_2O)_7^{3+}}, \tag{31}$$

the step-wise fluorination

$$\mathrm{M(H_2O)_8^{4+}} \leftrightarrow \mathrm{MF(H_2O)_7^{3+}} \ldots \leftrightarrow \ldots \mathrm{MF_3(H_2O)_5^{+}} \ldots \leftrightarrow \cdots \tag{32}$$

$$\mathrm{MF_4(H_2O)_2} \leftrightarrow \ldots \mathrm{MF_5(H_2O)^{-}} \leftrightarrow \mathrm{MF_6^{2-}}, \tag{33}$$

Table 23 Calculated Coulomb part, ΔE^{C} (in eV), of the free energy change of some typical hydrolysis and complex formation reactions, Eqs. (31–34), for Zr, Hf, and Rf. From [285]

Reactions	Zr	Hf	Rf
$M(H_2O)_8^{4+} \leftrightarrow MOH(H_2O)_7^{3+}$	−4.69	−4.61	−4.11
$M(H_2O)_8^{4+} \leftrightarrow MF(H_2O)_7^{3+}$	0.002	0.015	0.395
$M(H_2O)_8^{4+} \leftrightarrow MF_4(H_2O)_4$	15.86	15.84	16.52
$M(H_2O)_8^{4+} \leftrightarrow MF_6^{2-}$	50.76	50.91	51.10
$M(H_2O)_8^{4+} \leftrightarrow MCl_6^{2-}$	52.15	52.50	53.06
$M(H_2O)_8^{4+} \leftrightarrow MCl_4$	47.99	47.82	47.85

and the complete chlorination

$$M(H_2O)_8^{4+} + \ 6HCl \leftrightarrow MCl_6^{2-}. \tag{34}$$

Calculated ΔE^{C} for some of the reactions of Eqs. (31–34) are given in Table 23. The data of the first row there suggest the following trend in hydrolysis of the group-4 cations Zr > Hf > Rf. The first hydrolysis constant $\log K_{11}(Rf) \approx -4$ was then determined in good agreement with the experimental value of -2.6 ± 0.7 [290]. The predicted trend is also in agreement with the experimental data for Zr and Hf giving $\log K_{11}(Zr) = 0.3$ and $\log K_{11}(Hf) = -0.25$ [279]. One should note here that a simple model of hydrolysis [279] based on the ratio of a cation charge to its size would give an opposite and, hence, a wrong trend from Zr to Hf, since $IR(Zr^{4+}) > IR(Hf^{4+})$ [148].

The following useful trends were deduced from the calculated ΔE^{C} (Table 23). For the cation exchange separations (CIX) performed at < 0.1 M HF (no hydrolysis), i.e., for extraction of the positively charged complexes, the K_d values will change in the following way in group-4: Zr ≤ Hf < Rf. This is caused by the decreasing trend in the formation of the positively charged complexes according to Eq. 32: Zr ≥ Hf > Rf. (In the case of formation of complexes with a lower positive charge from complexes with a higher positive charge, a sequence in the K_d values is opposite to a sequence in the complex formation. This is because complexes with a higher charge are better sorbed on the CIX resin than those with a lower charge). This trend was, indeed, observed in the experiments on the CIX separations of group-4 elements at low HF concentrations [291, 292]. For the formation of anionic complexes sorbed by anion exchange (AIX) resins, the trend becomes more complicated depending on pH, i.e., depending on whether the fluorination starts from hydrated or hydrolyzed species. Thus, for experiments conducted in 10^{-3}–10^{-1} M HF (where some hydrolyzed or partially fluorinated species are present), the trend for the formation of MF_6^{2-} (Eq. 33) should be reversed in group 4: Rf ≥ Zr > Hf. Such a trend was observed in the experiments on the AIX separations of group-4 elements from 0.02 M HF [293]. The weaker sorption of Rf from HF solutions of > 10^{-3} M (in 0.1 M HNO_3) on the AIX column was, however, found in [291]. This was explained (and also shown by

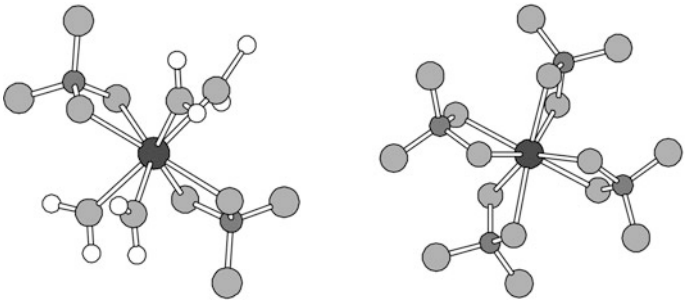

Fig. 51 $M(SO_4)_2(H_2O)_4$ and $M(SO_4)_4^{4-}$ complexes of Zr, Hf, and Rf. Reprinted with permission from V. Pershina, D. Polakova, J.P. Omtvedt, Radiochim. Acta **94**, 407 (2006). Copyright 2006 Oldenbourg Wissenscheftsverlag GmbH

additional experiments) by a strong competition between NO_3^- and Rf complexes for adsorption on the active resin sites. A similar result was obtained in [294], where the formation constant of RfF_6^{2-} was reported at least one order of magnitude smaller than those of ZrF_6^{2-} and HfF_6^{2-}.

For the AIX separations at 4–8 M HCl, where no hydrolysis should occur at such high acidities, the data of Table 23 suggest that the trend in the complex formation and K_d values should be continued with Rf: Zr > Hf > Rf. The AIX separations [294] of group-4 elements from aqueous 4–8 M HCl solutions have, however, shown the following sequence in K_d values: Rf > Zr > Hf. This experimental result cannot find its theoretical explanation.

The TBP extraction of group-4 elements from 8 M HCl showed the K_d of Rf in between those of Zr and Hf: Zr > Rf > Hf [295]. Such an inversion of the trend is consistent with the theoretical trend for the formation of the MCl_4 species, see Table 23. However, the following trend Zr > Hf ≈ Rf was observed in [296]. Some further calculations for the $MCl_4(TBP)_2$ complexes should be performed to study this case in more detail.

Complex formation of group-4 elements in H_2SO_4 solutions was studied theoretically in [288]. In this work, relative values of the free energy change of the $M(SO_4)_2(H_2O)_4$, $M(SO_4)_3(H_2O)_2^{2-}$ and $M(SO_4)_4^{4-}$ (M = Zr, Hf, and Rf) formation reactions from hydrated and partially hydrolyzed cations were calculated using the 4*c*-DFT method. (Figure 51 shows geometrical configurations of two of these complexes). The obtained ΔE^C and trends for one type of the complex formation reaction starting from $M(H_2O)_8^{4+}$ are given in Table 24, as an example.

Table 24 Coulomb part of the free energy change, ΔE^C (in eV), of the complex formation reactions [288]

Reaction	Zr	Hf	Rf	Trend
$M(H_2O)_8^{4+} \leftrightarrow M(SO_4)_2(H_2O)_4$	−35.72	−35.84	−33.60	Hf > Zr > > Rf
$M(H_2O)_8^{4+} \leftrightarrow M(SO_4)_3(H_2O)_2^{2-}$	−42.43	−42.43	−39.37	Zr = Hf > > Rf
$M(H_2O)_8^{4+} \leftrightarrow M(SO_4)_4^{4-}$	−45.14	−45.02	−41.38	Zr > Hf > > Rf
$M(H_2O)_8^{4+} \leftrightarrow RM(SO_4)_4$	−41.04	−40.78	−37.65	Zr > Hf > > Rf

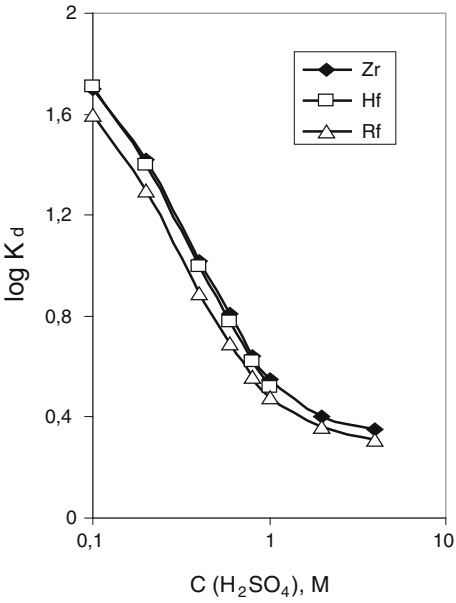

Fig. 52 Predicted logK_d for the extraction of Hf and Rf by amines with respect to the measured one for Zr. Reprinted with permission from V. Pershina, D. Polakova, J.P. Omtvedt, Radiochim. Acta **94**, 407 (2006). Copyright 2006 Oldenbourg Wissenschaftsverlag GmbH

Analogously, ΔE^{C} were obtained for a complex formation reaction starting from the hydrolyzed cations, i.e., $MOH(H_2O)_7^{3+} \leftrightarrow M(SO_4)_n(H_2O)_{8-2n}$. The results have indicated the same trend in the complex formation, Zr > Hf > > Rf, as for the reactions of Table 24. The obtained on their basis logK_d for extraction of Zr, Hf, and Rf by amines are shown in Fig. 52.

Experiments on sorption of Zr, Hf, and Rf from H_2SO_4 solutions by amines confirmed the predicted trend in the complex formation, Zr > Hf > > Rf, and have given the K_d(Rf) values closed to the predicted ones [280, 281].

7.2.3 Db

Like group-4 cations, group-5 ones undergo hydrolysis according to the reaction

$$M(H_2O)_6^{5+} \leftrightarrow M(OH)_6^{-} + 6H^{+}. \quad (35)$$

In [281], hydrolysis of the cations of Nb, Ta, Db, and Pa, for a comparison, was studied theoretically using the model described in Sect. 7.2.1. The calculated relative ΔE^{C} of reaction (35) are given in Table 25. The ΔE^{C} data are indicative of the following trend in hydrolysis of group-5 cations: Nb > Ta > Db > > Pa. This sequence is in agreement with experiments on hydrolysis of Nb, Ta, and Pa [279]. A simple model of hydrolysis does not again reproduce the difference between Nb and Ta having equal IR. The present model based on the real (relativistic) distribution of the electronic density describes correctly the experimental observations.

Table 25 E^C and ΔE^C (in eV) for reaction $M(H_2O)_6^{5+} \leftrightarrow M(OH)_6^-$, where M = Nb, Ta, Db, and Pa. From [281]

Complex	Nb	Ta	Db	Pa
$M(OH)_6^-$	−21.74	−23.33	−21.48	−19.53
$M(H_2O)_6^{5+}$	−21.92	−25.38	−25.37	−29.71
ΔE^C	0.18	2.05	3.89	9.18

Further on, complex formation of group-5 elements in HF, HCl, and HBr solutions was studied theoretically using the same approach [282, 283]. (A motivation for this study was the unexpected behavior of Db (Ha at that time) in the experiments on extraction into triisooctyl amine (TIOA) from mixed HCl/HF solutions [298]: Db was extracted similarly to Pa and not to Ta).

In HCl solutions, a large variety of complexes, such as $M(OH)_2Cl_4^-$, $MOCl_4^-$, $MOCl_5^{2-}$ and MCl_6^- (M = Nb, Ta, Db, and Pa) can be formed with different degrees of hydrolysis according to the following equilibrium

$$M(OH)_6^- + iL^- \leftrightarrow MO_u(OH)_{z-2u}L_i^{(6-i)-}. \quad (36)$$

To predict their stability, 4*c*-DFT calculations for this species were performed in [282, 283]. Obtained ΔE^C for reaction (36) are given in Table 26.

The data of Table 26 suggest the following trend in the complex formation of these elements: Pa > > Nb > Db > Ta. Taking into account the association with the organic cation, the following trend was predicted for sorption of the group-5 complexes by an anion exchanger

$$Pa \gg Nb \geq Db > Ta. \quad (37)$$

Thus, complexes of Pa should be formed in much more dilute HCl solutions, while a much higher acid concentration is needed to form those of Ta. The calculations also predicted the following sequence in the formation of various types of complexes as a function of the acid concentration: $M(OH)_2Cl_4^- > MOCl_4^- > MCl_6^-$ in agreement with experimental data for Nb, Ta, and Pa. The calculations also reproduced the $MF_6^- > MCl_6^- > MBr_6^-$ sequence as a function of the type of ligand (see Table 27).

The theoretical investigations have shown that the trend in the complex formation and extraction (sequence 37) known for Nb, Ta, and Pa turned out to be *reversed* in going to Db. This could not be predicted by any extrapolation of this

Table 26 ΔE^C (in eV) for reaction $M(OH)_6^- \leftrightarrow M(OH)_nCl_m^-$, where M = Nb, Ta, Db, and Pa. From [282, 283]

Metal	$M(OH)_2Cl_4^-$	$MOCl_4^-$	MCl_6^-
Nb	13.56	18.40	19.57
Ta	14.32	19.80	20.78
Db	14.29	19.67	20.46
Pa	11.68	16.29	17.67

Table 27 ΔE^C (in eV) for reaction $M(OH)_6^- \leftrightarrow ML_6^-$, where M = Nb, Ta, Db, and Pa, and L = F, Cl, and Br. From [283]

Complex	F	Cl	Br
NbL_6^-	12.20	19.57	21.40
TaL_6^-	12.69	20.78	22.63
DbL_6^-	12.38	20.46	22.11
PaL_6^-	12.19	17.67	19.91

property within the group, which would have given a continuous, and hence, wrong trend, but came as a result of the relativistic electronic structure calculations for real chemical equilibrium. According to these results, a recommendation was made to repeat the AIX separations in pure HCl or HF solutions. Accordingly, amine separations of the group-5 elements were systematically redone by Paulus et al. [299]. A reversed extraction sequence Pa > Nb ≥ Db > Ta, as that predicted theoretically (sequence 37), was then observed.

7.2.4 Sg

Hydrolysis. Experiments on the CIX separations of Sg from 0.1 M HNO_3 solutions showed that Sg did not elute from the CIX column, in contrast to Mo and W [300]. This non-tungsten-like behavior of Sg was tentatively attributed to its lower tendency to hydrolyze (deprotonate) compared to that of W. To interpret the behavior of Sg in these experiments and to predict its hydrolysis at various pH values, free energies of the following protonation reactions for Mo, W, and Sg

$$\begin{aligned} MO_4^{2-} \leftrightarrow MO_3(OH)^- \leftrightarrow\ & MO_2(OH)_2(H_2O)_2 \leftrightarrow \\ MO(OH)_3(H_2O)_2^+ \leftrightarrow\ & M(OH)_4(H_2O)_2^{2+} \leftrightarrow \ldots \leftrightarrow M(H_2O)_6^{6+} \end{aligned} \quad (38)$$

were considered theoretically [284]. The ΔE^C for these consecutive protonation steps were calculated using the 4*c*-DFT method. The results shown in Table 28 indicate that for the first two protonation steps, the trend in group-6 is reversed: Mo < Sg < W. For the further protonation process, the trend is continued with Sg: Mo < W < Sg.

Table 28 ΔE^C (in eV) for the stepwise protonation of MO_4^{2-} (M = Mo, W, and Sg). From [284]

Reaction	ΔE^C		
	Mo	W	Sg
$MO_4^{2-} + H^+ \leftrightarrow MO_3(OH)^-$	−12.28	−13.13	−12.96
$MO_3(OH)^- + H^+ + 2H_2O \leftrightarrow MO_2(OH)_2(H_2O)_2$	−21.43	−22.08	−21.61
$MO_2(OH)_2(H_2O)_2 + H^+ \leftrightarrow MO(OH)_3(H_2O)_2^+$	−5.84	−6.35	−6.65
$MO(OH)_3(H_2O)_2^+ + H^+ \leftrightarrow M(OH)_4(H_2O)_2^{2+}$	−0.43	−0.76	−1.23
$M(OH)_4(H_2O)_2^{2+} + 4H^+ \leftrightarrow \ldots M(H_2O)_6^{6+}$	41.97	38.71	37.11

Table 29 log$K$ for the step-wise protonation of MO_4^{2-} (M = Mo, W, and Sg). From [284]

Reaction	logK_n		
	Mo	W	Sg
$MO_4^{2-} + H^+ \leftrightarrow MO_3(OH)^-$	3.7	3.8	3.74
$MO_3(OH)^- + H^+ + 2H_2O \leftrightarrow MO_2(OH)_2(H_2O)_2$	3.8	4.3	4.1 ± 0.2
$MO_4^{2-} + 2H^+ + 2H_2O \leftrightarrow MO_2(OH)_2(H_2O)_2$	7.50	8.1	8.9 ± 0.1
$MO_2(OH)_2(H_2O)_2 + H^+ \leftrightarrow MO(OH)_3(H_2O)_2^+$	0.93	0.98	1.02

Thus, the same reversal of the trend is predicted for the protonation of oxyanions of the group-6 elements as that for the complex formation of the group-4 and 5 elements. The predicted trends in the complex formation are in agreement with experiments for Mo and W at various pHs [279]. For the protonation of positively charged complexes, the predicted trend Mo < W < Sg is in line with the experimental observations for Sg [300]. Using the procedure described in Sect. 7.2.1, log$K$ were determined for Sg, as given in Table 29 [284].

Complex formation. Complex formation of Mo, W, and Sg in HF solutions was studied theoretically on the basis of the 4*c*-DFT calculations [286] of the following step-wise fluorination process

$$\begin{aligned} MO_4^{2-}[\text{or } MO_3(OH)^-] + HF \leftrightarrow MO_3F^- \leftrightarrow \\ MO_2F_2(H_2O)_2 \leftrightarrow MO_2F_3(H_2O)^- \leftrightarrow MOF_5^-. \end{aligned} \quad (39)$$

The calculated ΔE^C indicate a very complicated dependence of the complex formation of these elements and trends on the pH and HF concentration. A plot of predicted log$K$ of W and Sg with respect to log$K$(Mo) in AIX separations from HF solutions at all the range of acid concentrations is shown in Fig. 53. There, below 10^{-2} M HF, negatively charged and neutral hydrolyzed complexes are in the aqueous phase, but negatively charged and neutral fluoride complexes are in the organic phase. At higher HF concentrations both neutral and positively charged

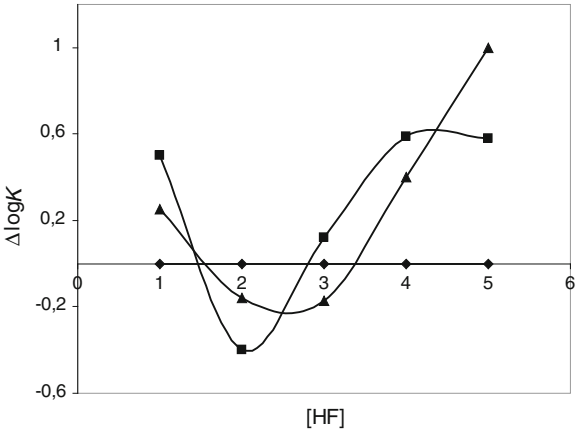

Fig. 53 Predicted relative values of logK_d of W (*squares*) and Sg (*triangles*) with respect to those of Mo (*rhomboids*) by AIX separations from HF solutions as a function of the acid concentration. Points 1 through 5 correspond to the following extracted complexes: MO_3F^-, $MO_2F_2(H_2O)_2$, $MO_2F_3(H_2O)^-$, $MO_2F_4^{2-}$ and MOF_5^-. From [286]

hydrolyzed species occur in the aqueous phase, but negatively charged fluoride complexes are extracted into the organic phase. One can see from Fig. 53 that at the lowest HF concentrations ($< \sim 0.1$ M HF), a reversal of the trends in K_d occurs in the group, while at higher HF molarities ($> \sim 0.1$ M HF), the trend is continued with Sg: Mo < W < Sg. At the range of these HF concentrations, separation between the homologs is the best.

The obtained sequences are in agreement with experiment on Mo and W [301]. Future experiments on the AIX separations of group-6 elements from HF solutions should clarify the extraction position of Sg in the group.

7.2.5 Hs

Experiments [303, 304] with volatile tetroxides of group-8 elements have shown that HsO_4 reacts with the moisturized NaOH surface forming obviously the sodium hassate (VIII), $Na_2[HsO_4(OH)_2]$, by analogy with $Na_2[OsO_4(OH)_2]$ according to the reaction

$$2NaOH + HsO_4 \rightarrow Na_2\left[HsO_4(OH)_2\right]. \quad (40)$$

In [287], the reactivity of RuO_4, OsO_4, and HsO_4 with NaOH was studied on the basis of the 4*c*-DFT calculations of the components of the reaction of Eq. 40 and the model described in Sect. 7.2.1. The ΔE^C values for the $MO_4 \rightarrow Na_2[MO_4(OH)_2]$ reaction of 8.04 eV, 5.09 eV and 5.63 eV for Ru, Os, and Hs, respectively, are indicative of the following trend in the complex formation: Os > Hs > > Ru, in agreement with experiment for Os and Ru. The predicted lower reactivity of HsO_4 with NaOH as compared to that of OsO_4 has so far not clearly been revealed experimentally [305].

7.3 Summary of the Aqueous Chemistry Studies

A summary of the predicted trends in hydrolysis, complex formation and extraction of the heaviest element complexes and their homologs as compared to the experimental results is given in Table 30. As one can see, most of the predictions were confirmed by experiments for the heaviest elements and their homologs, while some of them are still awaiting verification, as in the case of Sg in HF solutions.

The calculations have shown that the theory of hydrolysis [279] based on the relation between the cation size and charge does not explain all the experimental behavior, like, e.g., the difference between Nb and Ta, or Mo and W. Only by performing relativistic calculations for real chemical equilibrium in solutions can complex formation and hydrolysis constants, as well as distribution coefficients between an aqueous and organic phases (or sorption coefficients) and their order in

Table 30 Trends in hydrolysis and complex formation of the group-4 through 8 elements

Group	Extracted complex	Theoretically predicted	Ref.	Experiment. observed	Ref.
4	Hydrolysis of M^{4+}	Zr > Hf > Rf	[285]	Zr > Hf > Rf	[290]
	$MF_x(H_2O)_{8-x}^{z-x}(x \leq 4)$	Zr > Hf > Rf	[285]	Zr > Hf > Rf	[291, 292]
	MF_6^{2-}	Rf ≥ Zr > Hf	[285]	Rf ≥ Zr > Hf	[293]
				Zr > Hf > > Rf	[291, 294]
	MCl_6^{2-}	Zr > Hf > Rf	[285]	Rf > Zr > Hf	[295]
	MCl_4	Rf > Hf > Zr	[285]	Zr > Rf > Hf	[296]
				Zr > Hf ≈ Rf	[297]
	$M(SO_4)_4^{4-}$	Zr > Hf > > Rf	[288]	Zr > Hf > > Rf	[298, 299]
5	Hydrolysis of M^{5+}	Nb > Ta > Db	[281]	Nb > Ta	[270]
	$MOCl_4^-$, MCl_6^-	Nb ≥ Db > Ta	[282]	Nb ≥ Db > Ta	[301]
	MF_6^-, MBr_6^-	Nb > Db > Ta	[283]	Nb > Db > Ta	[301]
6	Hydrolysis of M^{6+}	Mo > W > Sg	[284]	Mo > W > Sg	[302]
	Hydrolysis of $MO_2(OH)_2$	Mo > Sg > W	[284]	Mo > W	[302]
	$MO_2F_2(H_2O)_2$	Mo > Sg > W	[286]	Mo > W	[303, 304, 306, 307]
	MOF_5^-	Mo < W < Sg	[286]	Mo < W	[303]
8	$MO_4(OH)_2^{2-}$	Os > Hs > > Ru	[287]	Os ≥ Hs	[305]

the chemical groups be correctly predicted. Results of such calculations have also shown the predominant contribution in ΔG^r to be a change in the electrostatic metal–ligand interaction energy, ΔE^C. Thus, by calculating only this term can trends in the complex formation be reliably predicted.

7.4 Prospects for Aqueous Chemistry Studies

Experimental aqueous studies of chemical properties of elements heavier than Sg will depend on the development of experimental techniques that can cope with production rates of less than one atom per hour and short half-lives.

From element 107 on, the maximum oxidation state is expected to be relatively unstable in solutions. It would, therefore, be interesting to conduct experiments probing the stability of lower oxidation states. The stability of Bh^{VII} relative to Bh^{IV} could be established by AIX separations of group-7 elements in acidic solutions. In HCl solutions Tc and Re undergo the complexation reaction $MO_4^- + HCl \leftrightarrow MCl_6^{2-}$ simultaneously with reduction. The K_d curves for Tc and Re show peaks at about 7–8 M HCl associated with the reduction [306, 307]. The peak for Tc is at lower HCl concentrations than that of Re indicating an earlier reduction of Tc, which means that Tc is less stable in the 7+ oxidation state (or more stable in the 4+ state) than Re. The position of the peak on the K_d curve

Table 31 Formation enthalpies (in kcal/mol) for some compounds of Hg [303, 304]

Compound	Phase	F	Cl	Br	J
HgX_2	Gas	−70.2	−35.0	−20.4	−3.84
HgX_2	Aqueous	–	−6.9	−10.7	−15.0
HgX_3^-	Aqueous	–	−2.2	−3.0	−3.6
HgX_4^{2-}	Aqueous	–	0.1	−4.1	−4.0

for Bh would, therefore, be indicative of the relative stability of its 7+ oxidation state. It would also be interesting to conduct similar reduction experiments with Hs. Its homologs are known to have the following reduction potentials: $RuO_4 + nHCl \rightarrow RuCl_5OH^{2-} + Cl_2 + nH_2O$ of $E^\circ = 0.14$ V and $OsO_4 + 8HCl \rightarrow H_2OsCl_6 + Cl_2 + 4H_2O$ of $E^\circ = -0.36$ V.

Cn should have a complex ion chemistry, like other elements at the second half of the 6d transition series. A tendency to form stronger bonding with "soft" ligands is foreseen in [1, 2] by analogy with Hg showing the increasing stability of the aqueous complexes from F to Cl to Br and to I (Table 31). The increasing stability constants in this row has, however, another reason, namely the decreasing hydrolysis $HgX_2 + H_2O \leftrightarrow Hg(OH)X$: 1.4% (Cl), 0.08% (Br), 0% (I) [303, 304]. The stability of the gas and crystal phase compounds of Hg, on the contrary, decreases from F to Cl to Br and to I (Table 31).

The formation enthalpy of CnF_2 was calculated at the PP level as −75.33 kcal/mol as compared to the calculated −88.4 kcal/mol for HgF_2 [153]. Thus, taking into account the decreasing stability of the 2+ oxidation state in group 12, experiments could be conducted with probably only CnI^+ and CnI_2. The possibility of formation of CnF_5^- and CnF_3^- was also considered in [153] (by analogy with Hg where the addition of an F^- to HgF_2 or HgF_4 was found energetically favorable), though these compounds will undergo strong hydrolysis in aqueous solutions and will not be stable. Thus, the only possibility would be the formation of $CnBr_5^-$ or CnI_5^-.

Fl should also have a greater tendency to form complexes in solutions than Pb. Since the stability of the 2+ state increases within group 14, Fl would probably form $M^{2+} + X_2 \leftrightarrow MX^+$ (X = Cl, Br, and I) and $M^{2+} + X_2 \leftrightarrow MX_2$ or $MX_2 + X_2 \leftrightarrow MX_3^-$ or MX_4^{2-} by analogy with Pb. (In 11 M HCl, $PbCl_6^{4-}$ is known). As in group 12, the stability of the gas-phase compounds of Pb decreases from F to Cl to Br and to I, while in aqueous solutions it is the other way around. The reason for that is a decreasing hydrolysis from F to Cl to Br and to I (fluoride complexes are not known) according to the reaction $MX_2 \leftrightarrow M(OH)X$, $M(OH)_2$ or $M(OH)_3^-$ [305]. Since the 2+ oxidation state of Fl should be more stable than Pb^{2+}, Fl can be extracted as MBr_3^- or MI_3^-. In [140], the existence of FlF_6^- was suggested, though in solutions this compound will undergo strong hydrolysis. The stability of various complexes of Fl versus stability of the hydrolysis products could be a subject of further theoretical investigations.

8 Conclusions and Outlook

Spectacular developments in the relativistic quantum theory, computational algorithms and computer techniques allowed for accurate calculations of properties of the heaviest elements and their compounds. Nowadays, atomic DC(B) correlated calculations including QED effects reaching an accuracy of few meV for electronic transitions and ionization potentials are available for these elements. These calculations allowed for reliable predictions of electronic configurations of the heaviest elements up to $Z = 122$. For heavier elements, as well as for the midst of the 6d-element series, MCDF calculations are still the source of useful information. On their basis, the end of the Periodic Table from the electronic structure point of view is predicted for $Z = 173$. Treatment of QED effects permitted also relative accurate predictions of inner-shell ionization potentials.

Most of molecular calculations were performed with the use of relativistic DFT and RECP methods that turned out to be complimentary both conceptionally and quantitatively. Their combination is presently the best way to study properties of complex systems of the heaviest elements. DC *ab initio* molecular methods are in the phase of development and their routine application to the heaviest systems is still a matter of future.

Using all those methods, reliable predictions of properties of the heaviest element and their compounds became available. Theoretical calculations permitted establishment of important trends in spectroscopic properties, chemical bonding, stabilities of oxidation states, ligand-field effects, complexing ability and other of the heaviest elements, as well as the role and magnitude of relativistic effects. Detailed studies are offered for elements Rf through 120, as well as for some species of even heavier elements. A high accuracy of total energy calculations allowed for predictions of stability of species, their geometry and energies of chemical reactions in the gas and aqueous phases, as well on surfaces of metals. However, fully relativistic description of adsorption processes on complicated or inert surfaces is still problematic. Therefore, some models were used in practical applications. Also, physico-chemical models were helpful in predicting some other properties that are difficult to handle in a straightforward way, such as, e.g., extraction from aqueous solutions or ion exchange separations. Such studies were performed for elements Rf through Hs, Cn, Fl, and element 113. Some estimates of adsorption enthalpies of even heavier elements, up to $Z = 120$, on noble metals are also available.

Being often conducted in a close link to the experiment, those theoretical works were indispensable for designing chemical experiment and interpreting its outcome. An experimental input was also helpful in improving theoretical models and encouraging a higher accuracy of the calculations. The synergism between the theoretical and experimental research in this field have resulted in better understanding of the chemistry of these exotic species and the role of relativistic effects.

It was shown that the heaviest elements are basically homologs of their lighter congeners in the chemical groups, though their properties may be rather different

due to very large relativistic effects on their electron shells. Relativistic effects were found to be predominant over the orbital one in the electronic structures of the elements of the 7th period and heavier. They are responsible for trends in the chemical groups (a continuation, or a reversal) with increasing Z from the elements of the 6th period. Thus, for elements of the 7th period and heavier, the use of relativistic methods is mandatory. Straightforward extrapolations of properties from lighter congeners may, therefore, result in erroneous predictions.

Although rich information has been collected, a number of open questions still remain. For elements which were chemically identified, a more detailed study, both theoretical and experimental, should follow. New compounds of chemically identified elements, e.g., carbonyls of Sg, or organometallic ones of Hs, should be synthesized and chemically investigated. For the not yet studied elements, like Mt, Ds, Rg, or elements 115 through 118, isotopes suitable for chemical studies should be first found, as well as their nuclear decay properties should be known, so that they can be positively identified. Their separation will also need new technological developments to cope with the very low production rates and short half-lives. In this area, theoretical chemistry will have a number of exciting tasks to predict the experimental behavior in the chemical separation experiments. Even though some basic properties of these elements have been theoretically outlined, more detailed studied should follow taking into account experimental details.

Whether it will ever be possible to experimentally investigate chemical properties of elements heavier than $Z = 118$ remains an open question. The chemistry of these superheavy elements, therefore, rests at the time being on a purely theoretical basis. A number of interesting chemical species for investigations is suggested. Properties of these elements and their compounds will be even more exciting than of those elements which have already been studied, since resemblance with their lighter homologs will be even less pronounced. Some further methodical developments in the relativistic quantum theory resulting in the creation of fully relativistic *ab initio* molecular, cluster, and solid-state codes, also with inclusion of the QED effects on an SCF basis, are needed to achieve a required accuracy of the predicted quantities for those very high Z numbers. The future calculations will also need powerful supercomputers.

References

1. Fricke, B., Waber, J.T.: Theoretical predictions of the chemistry of superheavy elements. Actinide Rev. **1**, 433–485 (1971)
2. Fricke, B.: Superheavy elements. A prediction of their chemical and physical properties. Struct. Bond. **21**, 89–144 (1975)
3. Keller Jr, O.L., Seaborg, G.T.: Chemistry of the transactinide elements. Ann. Rev. Nucl. Sci. **27**, 139–166 (1977)
4. Seaborg, G.T., Keller, O.L., Jr: Future elements. In: Katz, J.J., Seaborg, G.T., Morss, L.R. (eds.) The Chemistry of the Actinide Elements, 2nd edn, vol. 2, pp. 1629–1646. Chapman and Hall, London (1986)

5. Seaborg, G.T.: Evolution of the modern periodic table. J. Chem. Soc. Dalton Trans. 3899–3907 (1996)
6. Pershina, V.: Electronic structure and properties of the transactinides and their compounds. Chem. Rev. **96**, 1977–2010 (1996)
7. Pershina, V., Kratz, J.V.: Experimental and theoretical studies of the chemistry of the heaviest elements. In: Hess, B.A. (ed.) Relativistic Effects in Heavy-Element Chemistry and Physics, pp. 219–244. Wiley, New York (1997)
8. Schwerdtfeger, P., Seth, M.: Relativistic effects on the superheavy elements. In: von Rague Schleyer, P (ed.) Encyclopedia on Calculational Chemistry, vol. 1, pp. 2480–2499. Wiley, New York (1998)
9. Pershina, V., Fricke, B.: Electronic structure and chemistry of the heaviest elements. In: Greiner, W., Gupta, R.K. (eds.) Heavy Elements and Related New Phenomena, pp. 194–162. World Scientific, Singapore (1999)
10. Pershina, V.: The Chemistry of the superheavy elements and relativistic effects. In: Schwerdtfeger, P. (ed.) Relativistic Electronic Structure Theory, Part II, pp. 1–80. Elsevier, Amsterdam (2002)
11. Pershina, V.: Theoretical chemistry of the heaviest elements. In: Schädel, M. (ed.) The Chemistry of Superheavy Elements, pp. 31–94. Kluwer, Dordrecht (2003)
12. Hoffman, D.C., Lee, D.M., Pershina, V.: Transactinide elements and future elements. In: Morss, L.R., Edelstein, N.M., Fuger, J., Katz, J.J. (eds.) The Chemistry of the Actinide and Transactinide Elements, vol. 3, 3d edn, pp. 1652–1752. Springer, Dordrecht (2006)
13. Pershina, V.: Electronic structure and chemistry of the heaviest elements. In: Barysz, M., Ishikawa, Y. (eds.) Relativistic Methods for Chemists, pp. 452–520. Springer, Dordrecht (2010)
14. Pershina, V.: Relativistic electronic structure studies on the heaviest elements. Radiochim. Acta **99**, 459–476 (2011)
15. Cotton, S.A.: After the actinides, then what? Chem. Soc. Rev. **25**, 219–227 (1996)
16. Seaborg, G.T., Metallurgical Laboratory Memorandum MUC-GTS-858, 17 July 1944
17. Seaborg, G.T.: The chemical and radioactive properties of the heavy elements. Chem. Eng. News **23**, 2190–2193 (1945)
18. Mann, J.B.: Stability of 8p electrons in superheavy elements. J. Chem. Phys. **51**, 841–842 (1969)
19. Mann, J.B., Waber, J.T.: SCF relativistic Hartree-Fock calculations on the superheavy elements 118–131. J. Chem. Phys. **53**, 2397–2406 (1970)
20. Fricke, B., Greiner, W., Waber, J.T.: The continuation of the periodic table up to $Z = 172$. The chemistry of superheavy elements. Theoret. Chim. Acta **21**, 235–260 (1971)
21. Desclaux, J.P.: Relativistic Dirac-Fock expectation values for atoms with $Z = 1$ to $Z = 120$. At. Data Nucl. Data Tables **12**, 311–386 (1973)
22. Nefedov, V.I., Yarzhemcky, V.G., Trzhaskovskaya, M.B.: Periodic low as applied to superheavy elements: Specific features arising from relativistic effects. Russ. J. Inorg. Chem. **49**, 1871–1874 (2004)
23. Desclaux, J.P., Fricke, B.: Relativistic prediction of the ground state of atomic lawrencium. J. Phys. **41**, 943–946 (1980)
24. Glebov, V.A., Kasztura, L., Nefedov, V.S., Zhuikov, B.L.: Is element 104 (kurchatovium) a p-element? II. Relativistic calculations of the electronic atomic structure. Radiochim. Acta **46**, 117–121 (1989)
25. Johnson, E., Fricke, B., Keller Jr, O.L., Nestor Jr, C.W., Tucker, T.C.: Ionization potentials and radii of atoms and ions of element 104 (unnilquadium) and of hafnium (2+) derived form multiconfiguration Dirac-Fock calculations. J. Chem. Phys. **93**, 8041–8050 (1990)
26. Fricke, B., Johnson, E., Rivera, G.M.: Ionization potentials and radii of atoms and ions of element 105 (unnilpentium) and ions of tantalum derived from multiconfiguration Dirac-Fock calculations. Radiochim. Acta **62**, 17–25 (1993)
27. Johnson, E., Pershina, V., Fricke, B.: Ionization potentials of seaborgium. J. Phys. Chem. **103**, 8458–8462 (1999)

28. Johnson, E., Fricke, B., Jacob, T., Dong, C.Z., Fritzsche, S., Pershina, V.: Ionization potentials and radii of neutral and ionized species of elements 107 (bohrium) and 108 (hassium) from extended multiconfiguration Dirac-Fock calculations. J. Phys. Chem. **116**, 1862–1868 (2002)
29. Pyper, N.C., Grant, I.P.: Theoretical chemistry of the 7p series of superheavy elements. I. Atomic structure studies by multi-configuration Dirac-Fock theory. Proc. R. Soc. Lond. A **376**, 483–492 (1981)
30. Nefedov, V.I., Trzhaskovskaya, M.B., Yarzhemcky, V.G.: Electronic configurations and the Periodic Table for superheavy elements. Doklady Phys. Chim. **408**, 149–151 (2006)
31. Pyykkö, P.: A suggested periodic table up to $Z \leq 172$, based on Dirac-Fock calculations on atoms and ions. Phys. Chem. Chem. Phys. **13**, 161–168 (2011)
32. Kaldor, U., Eliav, E.: Energies and other properties of heavy atoms and molecules. In: Hernandes-Laguna, A., Maruani, J., Mcweeny, R., Wilson, S. (eds.) Quantum Systems in Chemistry and Physics, vol. I, pp. 161–176. Kluwer, Dordrecht (2000)
33. Eliav, E., Kaldor, U.: Four-component electronic structure methods. In: Barysz, M., Ishikawa, Y. (eds.) Relativistic Methods for Chemists, pp. 279–350. Springer, Dordrecht (2010)
34. Eliav, E., Shmulyian, S., Kaldor, U., Ishikawa, Y.: Transition energies of lanthanum, actinium, and eka-actinium (element 121). J. Chem. Phys. **109**, 3954 (1998)
35. Eliav, E., Landau, A., Ishikawa, Y., Kaldor, U.: Electronic structure of eka-thorium (element 122) compared with thorium. J. Phys. B. **35**, 1693 (2002)
36. Indelicato, P., Bieron, J., Jönnson, P.: Are MCDF calculations 101% correct in the superheavy element range? Theor. Chem. Acc. **129**, 495–505 (2011)
37. Pyykkö, P.: Relativistic effects in structural chemistry. Chem. Rev. **88**, 563–594 (1988)
38. Schwarz, W.H.E., van Wezenbeck, E., Snijders, J.G., Baerends, E.J.: The origin of relativistic effects of atomic orbitals. J. Phys. B. **22**, 1515–1530 (1989)
39. Baerends, E.J., Schwarz, W.H.E., Schwerdtfeger, P., Snijders, J.G.: Relativistic atomic orbital contractions and expansions: magnitude and explanations. J. Phys. B. **23**, 3225–3240 (1990)
40. Onoe, J.: Atomic-number dependence of relativistic effects on chemical bonding. Adv. Quant. Chem. **37**, 311–323 (2000)
41. Autschbach, J., Siekierski, S., Schwerdtfeger, P., Seth, M., Schwarz, W.H.E.: Dependence of relativistic effects on electronic configuration in the neutral atoms of d- and f-block elements. J. Comput. Chem. **23**, 804–813 (2002)
42. Labzowsky, L.N., Goidenko, I.: QED theory of atoms. In: Schwerdtfeger, P. (ed.) Relativistic Electronic Structure Theory, Part I, pp. 401–467. Elsevier, Amsterdam (2002)
43. Lindgren, I.: Relativistic many-body and QED calculations on atomic systems. Int. J. Quant. Chem. **57**, 683–695 (1996)
44. Gaston, N., Schwerdtfeger, P., Nazarewicz, W.: Ionization potential of internal conversion electrons for the superheavy elements 112, 114 116, and 118. Phys. Rev. A **66**, 062505(10) (2002)
45. Thierfelder, C., Schwerdtfeger, P., Hessberger, F.P., Hofmann, S.: Dirac-Hartree-Fock studies of X-ray transitions in meitnerium. Eur. Phys. J. A **36**, 227–231 (2008)
46. Pyykkö, P., Tokman, M., Labzowsky, L.N.: Estimated valence-level Lamb shifts for group 1 and group 11 metal atoms. Phys. Rev. A **57**, R689–R692 (1998)
47. Thierfelder, C., Schwerdtfeger, P.: Quantum electrodynamic corrections for the valence shell in heavy many-electron atoms. Phys. Rev. A **82**, 062503(10) (2010)
48. Goidenko, I., Labsowsky, L., Eliav, E., Kaldor, U., Pyykkö, P.: QED effects to the binding energy of the eka-radon ($Z = 118$) negative ion. Phys. Rev. A **67**, 020102R(1–3) (2003)
49. Sucher, J.: Foundation of the relativistic theory of many-electron atoms. Phys. Rev. A **22**, 348–362 (1980)
50. DIRAC package. Dirac, a relativistic *ab initio* electronic structure program, written by Aa, H.J., Jensen, T.S., Visscher, L. with contributions from Bakken, V., Eliav, E., Enevoldsen, T., Fleig, T., Fossgaard, O., Helgaker, T., Laerdahl, J., Larsen, C.V., Norman, P., Olsen, J.,

Pernpointner, M., Pedersen, J.K., Ruud, K., Salek, P., van Stralen, J.N.P., Thyssen, J., Visser, O., Winther, T. (http://dirac.chem.sdu.dk)
51. Malli, G., da Silva, A.B.F., Ishikawa, Y.: Highly accurate relativistic universal Gaussian basis set: Dirac-Fock-Coulomb calculations for atomic systems up to nobelium. J. Chem. Phys. **101**, 6829–6834 (1994)
52. Visscher, L., Aerts, P.J.C., Visser, O., Nieuwpoort, W.C.: Kinetic balance in contracted basis sets for relativistic calculations. Int. J. Quant. Chem. **40**, 131–139 (1991)
53. Faegri, K.: Relativistic Gaussian basis sets for the elements K-Uuo. Theor. Chem. Acc. **105**, 252–258 (2001)
54. Faegri, K., Dyall, K.G.: Basis sets for relativistic calculations. In: Schwerdtfeger, P. (ed.) Relativistic Electronic Structure Theory, Part I, pp. 259–290. Elsevier, Amsterdam (2002)
55. Dyall, K.: Relativistic double-zeta, triple-zeta, and quadruple-zeta basis sets for the 7p elements, with atomic and molecular applications. Theor. Chem. Acc. **131**, 1172–1174 (2012)
56. Guilherme, L., de Macedo, M., Borin, A.C., da Silva, A.B.F.: Prolapse-free relativistic Gaussian basis sets for the superheavy elements up to Uuo (Z = 118) and Lr (Z = 103). At. Data Nucl. Data Tables **93**, 931–961 (2007)
57. Desclaux, J.P.: A multiconfiguration relativistic Dirac-Fock program. Comp. Phys. Comm. **9**, 31–45 (1975)
58. Grant, I.P.: Variational methods for Dirac wave equations. J. Phys. B **19**, 3187–3206 (1986)
59. Parpia, F.A., Froese-Fisher, S., Grant, I.P.: GRASP92: A package for large-scale relativistic atomic structure calculations. Comp. Phys. Comm. **175**, 745–747 (2006)
60. Balasubramanian, K.: Relativistic computations of the electronic states of the superheavy element 114 and 114^{+}. Chem. Phys. Lett. **341**, 601–607 (2001); *ibid*, Erratum. **351**, 161–162 (2002)
61. Schwerdtfeger, P. (ed.): Relativistic Electronic Structure Theory. Parts I and II. Elsevier, Amsterdam (2002)
62. Dyall, K.G., Faegri, K., Jr.: Relativistic Quantum Chemistry, Oxford University Press, New York (2007)
63. Barysz, M., Ishikawa, Y. (eds.): Relativistic Methods for Chemists, Springer, Dordrecht (2010)
64. Visscher, L.: Post-Dirac-Fock methods. In: Schwerdtfeger, P. (ed.) Relativistic Electronic Structure Theory, Part I, pp. 291–331. Elsevier, Amsterdam (2002)
65. Saue, T.: Post Dirac-Fock-methods-properties. In: Schwerdtfeger, P. (ed.) Relativistic Electronic Structure Theory, Part I, pp. 332–397. Elsevier, Amsterdam (2002)
66. Wolf, A., Reiher, M., Hess, B.A.: Two-component methods and the generalized Douglas-Kroll-Transformation. In: Schwerdtfeger, P. (ed.) Relativistic Electronic Structure Theory, Part I, pp. 622–663. Elsevier, Amsterdam (2002)
67. Barysz, M.: Two-component relativistic theories. In: Barysz, M., Ishikawa, Y. (eds.) Relativistic Methods for Chemists, pp. 165–190. Springer, Dordrecht (2010)
68. Douglas, M., Kroll, N.M.: Quantum electrodynamical corrections to the fine structure of helium. Ann. Phys. **82**, 89–155 (1974)
69. Kutzelnigg, W.: The relativistic many-body problem in molecular theory. Phys. Scr. **36**, 416–431 (1987)
70. Dolg, M.: Relativistic effective core potentials. In: Schwerdtfeger, P. (ed.) Relativistic Electronic Structure Theory, Part I, pp. 793–862. Elsevier, Amsterdam (2002)
71. Schwerdfeger, P.: The pseudopotential approximation in electronic structure theory. Chem. Phys. Chem. **12**, 3143–3155 (2011)
72. Huzinaga, S., Cantu, A.A.: Theory of separability of many-electron systems. J. Chem. Phys. **55**, 5543–5549 (1971)
73. Seijo, L., Barandiaran, Z.: Relativistic *ab initio* model potentials calculations for molecules and embedded clusters. In: Schwerdtfeger, P. (ed.) Relativistic Electronic Structure Theory, Part I, pp. 417–475. Elsevier, Amsterdam (2002)

74. Lee, Y.S.: Two-component relativistic effective core potential calculations for molecules. In: Schwerdtfeger, P. (ed.) Relativistic Electronic Structure Theory, Part II, pp. 352–416. Elsevier, Amsterdam (2002)
75. Cao, X., Dolg, M.: Relativistic pseudopotentials. In: Barysz, M., Ishikawa, Y. (eds.) Relativistic Methods for Chemists, pp. 215–270. Springer, Dordrecht (2010)
76. Lee, Y.L., Ermler, W.C., Pitzer, R.M.: *Ab initio* effective core potentials including relativistic effects. I. Formalism and applications to the Xe and Au atoms. J. Chem. Phys. **67**, 5861–5876 (1977)
77. Nash, C.S., Bursten, B.E., Ermler, W.C.: *Ab initio* relativistic effective potentials with spin-orbit operators. VII. Am through element 118. J. Chem. Phys. **106**, 5153–5142 (1997)
78. Schwerdtfeger, P., Seth, M.: Private communication (2011)
79. Hangle, T., Dolg, M., Hanrath, M., Cao, X., Stoll, H., Schwerdtfeger, P.: Accurate relativistic energy-consistent pseudopotentials for the superheavy elements 111 to 118 including quantum electrodynamic effects. J. Chem. Phys. **136**, 214105 (1–10) (2012)
80. Kahn, L.R., Hay, P.J., Cowan, R.D.: Relativistic effects in *ab initio* effective core potentials for molecular calculations. Applications to the uranium atom. J. Chem. Phys. **68**, 2386–2398 (1978)
81. Hay, P.J.: *Ab initio* studies of exited states of polyatomic molecules including spin-orbit and multiplet effects: The electronic states of UF_6. J. Chem. Phys. **79**, 5469–5483 (1983)
82. Titov, A.V., Mosyagin, N.S.: Generalized relativistic effective core potentials: Theoretical grounds. Int. J. Quant. Chem. **71**, 359–401 (1999)
83. Kohn, W., Becke, A.D., Parr, R.G.: Density functional theory of electronic structure. J. Phys. Chem. **100**, 12974–12980 (1996)
84. Rosen, A.: Twenty to thirty years of DV-Xα calculations: A survey of accuracy and applications. Adv. Quant. Chem. **29**, 1–47 (1997)
85. Engel, E.: Relativistic density functional theory: Foundations and basic formalism. In: Schwerdtfeger, P. (ed.) Relativistic Electronic Structure Theory, Part I, pp. 523–621. Elsevier, Amsterdam (2002)
86. van Wüllen, C.: Relativistic density functional theory. In: Barysz, M., Ishikawa, Y. (eds.) Relativistic Methods for Chemists, pp. 191–214. Springer, Dordrecht (2010)
87. Anton, J., Fricke, B., Engel, E.: Noncollinear and collinear relativistic density-functional program for electric and magnetic properties of molecules. Phys. Rev. A **69**, 012505(10) (2004)
88. Jacob, T., Geschke, D., Fritzsche, S., Sepp, W.-D., Fricke, B., Anton, J., Varga, S.: Adsorption on surfaces simulated by an embedded cluster approach within the relativistic density functional theory. Surf. Sci. **486**, 194–202 (2001)
89. Liu, W., Hong, G., Dai, D., Li, L., Dolg, M.: The Beijing four-component density functional program package (BDF) and its application to EuO, EuS, YbO, and YbS. Theor. Chem. Acc. **96**, 75–83 (1997)
90. Rosen, A., Ellis, D.E.: Relativistic molecular calculations in the Dirac-Slater model. J. Chem. Phys. **62**, 3039–3049 (1975)
91. Mitin, A.V., van Wüllen, C.: Two-component relativistic density-functional calculations of the dimers of the halogens from bromide through element 117 using effective core potential and all-electron methods. J. Chem. Phys. **124**, 064305(7) (2006)
92. ADF, Theoretical Chemistry, Vrije Universiteit Amsterdam, The Netherlands (www.scm.com)
93. Ziegler, T., Tschinke, V., Baerends, E.J., Snijders, J.G., Ravenek, W.: Calculations of bond energies in compounds of heavy elements by a quasi-relativistic approach. J. Phys. Chem. **93**, 3050–3056 (1989)
94. van Lenthe, E., Baerends, E.J., Snijders, J.G.: Relativistic total energy using regular approximation. J. Chem. Phys. **101**, 9783–9792 (1994)
95. Sundholm, D.: Perturbation theory based on quasi-relativistic hamiltonians. In: Schwerdtfeger, P. (ed.) Relativistic Electronic Structure Theory, Part I, pp. 758–792. Elsevier, Amsterdam (2002)

96. Faas, S., van Lenthe, J.H., Hennum, A.C., Snijders, J.G.: An *ab initio* two-component relativistic methods including spin-orbit coupling using the regular approximation. Chem. Phys. **113**, 4052–4059 (2000)
97. Hess, B.A.: Relativistic electronic structure calculations employing a two-component no-pair formalism with external-field projection operators. Phys. Rev. A **33**, 3742–3748 (1986)
98. van Wüllen, C.: Relation between different variants of the generalized Douglas-Kroll transformation through sixth order. J. Chem. Phys. **120**, 7307–7313 (2004)
99. Nasluzov, V.A., Rösch, N.: Density functional based structure optimization for molecules containing heavy elements: Analytical energy gradients for the Douglas-Kroll-Hess scalar relativistic approach to the LCGTO-DF method. Chem. Phys. **210**, 413–425 (1996)
100. Häberlen, O.D., Chung, S.-C., Stener, M., Rösch, N.: From clusters to bulk: A relativistic density functional investigation on a series of gold clusters Au_n, $n = 6,\ldots, 147$. J. Chem. Phys. **106**, 5189–5201 (1997)
101. Ziegler, T., Snijders, J.G., Baerends, E.J.: On the origin of relativistic bond contraction. Chem. Phys. Lett. **75**, 1–4 (1980)
102. Case, D.A., Yang, C.Y.: Relativistic scattered wave calculations on UF_6. J. Chem. Phys. **72**, 3443–3448 (1980)
103. Eschrig, H., Richter, M., Opahle, I.: Relativistic solid state calculations. In: Schwerdtfeger, P. (ed.) Relativistic Electronic Structure Theory, Part I, pp. 723–776. Elsevier, Amsterdam (2002)
104. Collins, C.L., Dyall, K.G., Schaeffer, H.F., III: Relativistic and correlation effects in CuH, AgH, and AuH: Comparison of various relativistic methods. J. Chem. Phys. **102**, 2024–2031 (1995)
105. Dyall, K.G.: Second-order Möller-Plesset perturbation theory for molecular Dirac-Hartree-Foch wavefunctions. Theory for up to two open-shell electrons. Chem. Phys. Lett. **224**, 186–194 (1994)
106. Kaldor, U., Hess, B.A.: Relativistic all-electron coupled-cluster calculations on the gold atom and gold hydride in the framework of the Douglas-Kroll transformation. Chem. Phys. Lett. **230**, 1–7 (1994)
107. Schwerdtfeger, P., Brown, J.R., Laerdahl, J.K., Stoll, H.: The accuracy of the pseudopotential approximation. III. A comparison between pseudopotential and all-electron methods for Au and AuH. J. Chem. Phys. **113**, 7110–7118 (2000)
108. Lee, H.-S., Han, Y.-K., Kim, M.C., Bae, C., Lee, Y.S.: Spin-orbit effects calculated by two-component coupled-cluster methods: Test calculations on AuH, Au_2, TiH and Tl_2. Chem. Phys. Lett. **293**, 97–102 (1998)
109. Liu, W., van Wüllen, C.: Spectroscopic constants of gold and eka-gold (element 111) diatomic compounds: the importance of spin-orbit coupling. J. Chem. Phys. **110**, 3730–3735 (1999)
110. Huber, K.P., Herzberg, G.: Constants of Diatomic Molecules. Van Nostrand Reinhold, New York (1979)
111. Pyykkö, P.: Theoretical chemistry of gold. Angew. Chem. Int. Ed. **43**, 3312–4456 (2004)
112. Eliav, E., Kaldor, U., Ishikawa, Y.: Ground state electron configuration of rutherfordium: Role of dynamic correlation. Phys. Rev. Lett. **74**, 1079–1082 (1995)
113. Eliav, E., Kaldor, U., Schwerdtfeger, P., Hess, B.A., Ishikawa, Y.: Ground state electron configuration of element 111. Phys. Rev. Lett. **73**, 3203–3206 (1994)
114. Eliav, E., Kaldor, U., Ishikawa, Y.: Transition energies in mercury and eka-mercury (element 112) by the relativistic coupled-cluster method. Phys. Rev. A **52**, 2765–2769 (1995)
115. Eliav, E., Kaldor, U., Ishikawa, Y., Seth, M., Pyykkö, P.: Calculated energy levels of thallium and eka-thallium (element 113). Phys. Rev. A **53**, 3926–3933 (1996)
116. Landau, A., Eliav, E., Ishikawa, Y., Kaldor, U.: Electronic structure of eka-lead (element 114) compared with lead. J. Chem. Phys. **114**, 2977–2980 (2001)
117. Eliav, E., Kaldor, U., Ishikawa, Y.: The relativistic coupled-cluster method: transition energies of bismuth and eka-bismuth. Mol. Phys. **94**, 181–187 (1998)

118. Eliav, E., Kaldor, U., Ishikawa, Y., Pyykkö, P.: Element 118: The first rare gas with an electron affinity. Phys. Rev. Lett. **77**, 5350–5352 (1996)
119. Pershina, V., Borschevsky, A., Eliav, E., Kaldor, U.: Adsorption of inert gases including element 118 on noble metal and inert surfaces from *ab initio* Dirac–Coulomb atomic calculations. J. Chem. Phys. **129**, 144106(9) (2008)
120. Eliav, E., Vilkas, M.J., Ishikawa, Y., Kaldor, U.: Ionization potentials of alkali atoms: towards meV accuracy. Chem. Phys. **311**, 163–168 (2005)
121. Landau, A., Eliav, E., Ishikava, Y., Kaldor, U.: Benchmark calculations of electron affinities of the alkali atoms sodium to eka-francium (element 119). J. Chem. Phys. **115**, 2389–2392 (2001)
122. Eliav, E., Kaldor, U., Ishikawa, Y.: Transition energies of ytterbium, lutetium, lawrencium by relativistic coupled-cluster method. Phys. Rev. A **52**, 291–291 (1995)
123. Borschevsky, A., Pershina, V., Eliav, E., Kaldor, U.: Prediction of atomic properties of element 115 and its adsorption on inert surfaces. GSI Annual Report 2010, GSI Report 2011, p. 207
124. Borschevsky, A., Pershina, V., Eliav, E., Kaldor, U.: Benchmark calculations of atomic properties of elements 113–122. Presentation at the TAN2011 Conference, Sochi, 5–11 Sept 2011. (http://tan11.jinr.ru/Final_Programme-TAN11.htm)
125. Borschevsky, A., Pershina, V., Eliav, E., Kaldor, U.: *Ab initio* predictions of atomic properties of element 120, with comparison to lighter homologs, Phys. Rev. A, **87**, 022502-1-8 (2013)
126. Pershina, V., Borschevsky, A., Eliav, E., Kaldor, U.: Atomic properties of element 113 and its adsorption on inert surfaces from *ab initio* Dirac-Coulomb calculations. J. Phys. Chem. A **112**, 13712–13716 (2008)
127. Pershina, V., Borschevsky, A., Eliav, E., Kaldor, U.: Prediction of the adsorption behavior of elements 112 and 114 on inert surfaces from *ab initio* Dirac-Coulomb atomic calculations. J. Chem. Phys. **128**, 024707(9) (2008)
128. Borschevsky, A., Pershina, V., Eliav, E., Kaldor, U.: Electron affinity of element 114, with comparison to Sn and Pb. Chem. Phys. Lett. **480**, 49–51 (2009)
129. Eliav, E.: Private communication (2011)
130. Pershina, V.: Unpublished
131. Lim, I.S., Pernpointer, M., Laerdahl, J.K., Schwerdtfeger, P., Neogrady, P., Urban, M.: Relativistic coupled-cluster static dipole polarizabilities of the alkali metals from Li to element 119. Phys. Rev. A. **60**, 2822–2828 (1999)
132. Lim, I.S., Schwerdtfeger, P., Metz, B., Stol, H.: All-electron and relativistic pseudopotential studies for the group 1 element polarizabilities from K to element 119. J. Chem. Phys. **122**, 104103(12) (2005)
133. Thierfelder, C., Assadollahzadeh, B., Schwerdtfeger, P., Schäfer, S.: Relativistic and electron correlation effects in static dipole polarizabilities for the group-14 elements from carbon to element $Z = 114$: theory and experiment. Phys. Rev. A. **78**, 052506(7) (2008)
134. Umemoto, K., Saito, S.: Electronic configuration of superheavy elements. J. Phys. Soc. Jap. **65**, 3175–3179 (1996)
135. Yu, Y.J., Li, J.G., Dong, C.Z., Ding, X.B., Fritsche, S., Fricke, B.: The excitation energies, ionization potentials and oscillator strengths of neutral and ionized species of Uub ($Z = 112$) and the homologue elements Zn, Cd and Hg. Eur. Phys. J. D **44**, 51–56 (2007)
136. Yu, Y.J., Dong, C.Z., Li, J.G., Fricke, B.: The excitation energies, ionization potentials, and oscillator strengths of neutral and ionized species of Uuq ($Z = 114$) and the homolog elements Ge, Sn, and Pb. J. Chem. Phys. **128**, 124316(7) (2008)
137. Chang, Z., Li., J., Dong, C.: Ionization potentials, electron affinities, resonance excitation energies, oscillator strengths, and ionic radii of element Uus ($Z = 117$) and astatine. J. Phys. Chem. A **114**, 13388–13394 (2010)
138. Dzuba, V.A., Flambaum, V.V., Silvestrov, P.G., Sushkov, O.P.: Many-body perturbation-theory calculations in atoms with open shells. Phys. Rev. A **44**, 2828–2831 (1991)

139. Nash, C.S.: Atomic and molecular properties of elements 112, 114 and 118. J. Phys. Chem. A **109**, 3493–3500 (2005)
140. Schwedtfeger, P., Seth, M.: Relativistic quantum chemistry of the superheavy elements. Closed-shell element 114 as a case study. J. Nucl. Radiochem. Sci. **3**, 133–136 (2002)
141. Moore, C.E.: Atomic energy levels. Natl. Stand. Ref. Data Ser., Natl. Bur. Stand.: Washington, 1971
142. Haynes, W.M. (ed.): CRC Handbook of Chemistry and Physics, 93rd edn. CRC Press, Boca Raton (2012)
143. Pershina, V., Borschevsky, A., Anton, J.: Theoretical predictions of properties of group-2 elements including element 120 and their adsorption on noble metal surfaces. J. Chem. Phys., **136**, 134317 (1–10) (2012)
144. Pershina, V., Borschevsky, A., Anton, J.: Fully relativistic study of intermetallic dimers of group-1 elements K through element 119 and prediction of their adsorption on noble metal surfaces. Chem. Phys. **395**, 87–94 (2012)
145. Pershina, V., Johnson, E., Fricke, B.: Theoretical estimates of redox potentials for group 6 elements, including element 106, seaborgium, in acid solutions. J. Phys. Chem. A **103**, 8463–8470 (1999)
146. Slater, J.C.: Atomic radii in crystals. J. Chem. Phys. **41**, 3199–3204 (1964)
147. Bondi, A.: Van der Walls volumes and radii. J. Phys. Chem. **68**, 441–451 (1964)
148. Shannon, R.D.: Revised effective ionic radii and systematic studies of interatomic distances in halides and chalcogenides. Acta Crystallogr. Sect. A **32**, 751–767 (1976)
149. Pyykkö, P., Atsumi, M.: Molecular single-bond covalent radii for elements 1–118. Chem. Eur. J. **15**, 186–197 (2009)
150. Pyykkö, P., Riedel, S., Patzsche, M.: Triple-bond covalent radii. Chem. Eur. J. **11**, 3511–3620 (2005)
151. Seth, M., Dolg, M., Fulde, P., Schwerdtfeger, P.: Lanthanide and actinide contractions: relativistic and shell structure effects. J. Am. Chem. Soc. **117**, 6597–6598 (1995)
152. Bilewicz, A.: The ionic radii of Rf^{4+}, Db^{5+} and Sg^{6+}. Radiochim. Acta **88**, 833–836 (2000)
153. Seth, M., Schwerdtfeger, P., Dolg, M.: The Chemistry of the superheavy elements. I. Pseudopotentials for 111 and 112 and relativistic coupled cluster calculations for $(112)H^+$ $(112)F_2$, and $(112)F_4$. J. Chem. Phys. **106**, 3623–3632 (1997)
154. Goeben, D., Hohm, U.: Dipole polarizability, Cauchy moments, and related properties of Hg. J. Phys. Chem. **100**, 7710–7712 (1996)
155. Pershina, V., Bastug, T.: Relativistic effects on experimentally studied gas-phase properties of the heaviest elements. Chem. Phys. **311**, 139–150 (2000)
156. Pyykkö, P., Desclaux, J.P.: Dirac-Fock one-center calculations. The model systems TiH_4, ZrH_4, HfH_4, and $(104)H_4$. Chem. Phys. Lett. **50**, 503–507 (1977)
157. Pyykkö, P., Desclaux, J.P.: Dirac-Fock one-center calculations show $(114)H_4$ to resemble PbH_4. Nature **226**, 336–337 (1977)
158. Pyykkö, P., Desclaux, J.P.: Dirac-Fock one-center calculations. VI. The tetrahedral and octahedral model systems CeH_4, ThH_4, CrH_6, MoH_6, WH_6, UH_6 and $(106)H_6$. Chem. Phys. **34**, 261–280 (1978)
159. Varga, S., Fricke, B., Hirata, M., Bastug, T., Pershina, V., Fritzsche, S.: Total energy calculations of $RfCl_4$ and homologues in the framework of relativistic Density Functional Theory. J. Phys. Chem. A **104**, 6495–6498 (2000)
160. Pershina, V., Sepp, W.-D., Fricke, B., Rosen, A.: Relativistic effects in physics and chemistry of element 105. I. Periodicities in properties of group 5 elements. Electronic structure of the pentachlorides. J. Chem. Phys. **96**, 8367–8378 (1992)
161. Pershina, V., Fricke, B.: Relativistic effects in physics and chemistry of element 105. IV. Their influence on the electronic structure and related properties. J. Chem. Phys. **99**, 9720–9729 (1993)
162. Pershina, V., Sepp, W.-D., Fricke, B., Kolb, D., Schädel, M., Ionova, G.V.: Relativistic effects in physics and chemistry of element 105. II. Electronic structure and properties of group 5 elements bromides. J. Chem. Phys. **97**, 1116–1122 (1992)

163. Pershina, V., Sepp, W.-D., Bastug, T., Fricke, B., Ionova, G.V.: Relativistic effects in physics and chemistry of element 105. III. Electronic structure of hahnium oxyhalides as analogs of group 5 elements oxyhalides. J. Chem. Phys. **97**, 1123–1131 (1992)
164. Pershina, V., Anton, J.: Theoretical predictions of properties and gas-phase chromatography behaviour of bromides of group-5 elements Nb, Ta and element 105, Db. J. Chem. Phys. **136**, 034308(7) (2012)
165. Pershina, V., Fricke, B.: Electronic structure and properties of the group 4, 5, and 6 highest chlorides including elements 104, 105, and 106. J. Phys. Chem. **98**, 6468–6473 (1994)
166. Pershina, V., Fricke, B.: Group 6 oxychlorides $MOCl_4$, where M = Mo, W, and element 106 (Sg): electronic structure and thermochemical stability. J. Phys. Chem. **99**, 144–150 (1995)
167. Pershina, V., Fricke, B.: Group 6 dioxydichlorides MO_2Cl_2 (M = Cr, Mo, W, and element 106, Sg): The electronic structure and thermochemical stability. J. Phys. Chem. **100**, 8748–8751 (1996)
168. Pershina, V., Bastug, T.: The electronic structure and properties of group 7 oxychlorides, MO_3Cl, where M = Tc, Re, and element 107. Bh. J. Chem. Phys. **113**, 1441–1446 (2000)
169. Pershina, V., Bastug, T., Fricke, B.: Relativistic effects on the electronic structure and volatility of group-8 tetroxides MO_4, where M = Ru, Os and element 108, Hs. J. Chem. Phys. **122**, 124301(9) (2005)
170. Pershina, V., Anton, J., Jacob, T.: Fully-relativistic DFT calculations of the electronic structures of MO_4 (M = Ru, Os, and element 108, Hs) and prediction of physisorption. Phys. Rev. A **78**, 032518(5) (2008)
171. Han, Y.-K., Son, S.-K., Choi, Y.J., Lee, Y.S.: Structures and stabilities for halides and oxides of transactinide elements Rf, Db, and Sg calculated by relativistic effective core potential methods. J. Phys. Chem. **103**, 9109–9115 (1999)
172. Malli, G.L., Styszynski, J.: *Ab initio* all-electron fully relativistic Dirac-Fock-Breit calculations for molecules of the superheavy transactinide elements: rutherfordium tetrachloride. J. Chem. Phys. **109**, 4448–4455 (1998)
173. Malli, G.: Dramatic relativistic effects in atomization energy and volatility of the superheavy hassium tetroxide and OsO_4. J. Chem. Phys. **117**, 10441–10443 (2002)
174. Filatov, M., Cremer, D.: Calculation of electronic properties using regular approximation to relativistic effects: the polarizabilities of RuO_4, OsO_4, and HsO_4 (Z = 108). J. Chem. Phys. **119**, 1412–2012 (2003)
175. Dolg, M., Wedig, U., Stoll, H., Preuss, H.: Energy adjusted *ab initio* pseudopotentials for the first row transition elements. J. Chem. Phys. **86**, 866–872 (1987)
176. Andrae, D., Häussermann, U., Dolg, M., Stoll, H., Preuss, H.: Energy-adjusted *ab initio* pseudopotentials for the second and third row transition elements. Theor. Chem. Acc. **77**, 123–141 (1990)
177. Nash, C.S., Bursten, B.E.: Comparisons among transition metal, actinide and transactinide complexes: the relativistic electronic structures of $Cr(CO)_6$, $W(CO)_6$, $U(CO)_6$ and $Sg(CO)_6$. New J. Chem. **19**, 669–675 (1995)
178. Zvara, I.: The Inorganic Radiochemistry of Heavy Elements. Springer, Dordrecht (2008)
179. Eichler, B., Zvara, I.: Evaluation of the enthalpy of adsorption from thermodynamic data. Radiochim. Acta **30**, 233–238 (1982)
180. Zvara, I.: Simulation of thermochromatography process by the Monte Carlo method. Radiochim. Acta **38**, 95–101 (1985)
181. Zvara, I.: Problems in thermochromatographic separations of radioelements. J. Radioanal. Nucl. Chem. **204**, 123–134 (1996)
182. Düllmann, Ch., Brüchle, W., Dressler, R., Eberhardt, K., Eichler, B., Eichler, R., Gäggeler, H.W., Ginter, T.N., Glaus, F., Gregorich, K.E., Hoffman, D.C., Jäger, E., Jost, D.T., Kirbach, U.W., Lee, D.E., Nitsche, H., Patin, J.B., Pershina, V., Piguet, D., Qin, Z., Schädel, M., Schausten, B., Schimpf, E., Schött, H.-J., Soverna, S., Sudowe, R., Thörle, P., Timokhin, S.N., Trautmann, N., Türler, A., Vahle, A., Wirth, G., Yakushev, A.B., Zielinski, P.M.: Chemical investigation of hassium (element 108). Nature **418**, 859–862 (2002)

183. Pershina, V.: Predictions of adsorption behaviour of the heaviest elements in a comparative study from the electronic structure calculations. Radiochim. Acta **93**, 125–131 (2005)
184. Eichler, R., Brüchle, W., Dressler, R., Düllman, Ch.E., Eichler, B., Gäggeler, H.W., Gregorich, K.E., Hoffman, D.C., Hübener, S., Jost, D.T., Kirbach, U.W., Laue, C.A., Lavanchy, V.M., Nitsche, H., Patin, J.B., Piguet, D., Schädel, M., Shaughnessy, D.A., Strellis, D.A., Taut, S., Tobler, L., Tsyganov, Y.S., Türler, A., Vahle, A., Wilk, P.A., Yakushev, A.B.: Chemical characterization of bohrium (element 107). Nature **407**, 63–65 (2000)
185. Schädel, M., Brüchle, W., Dressler, R., Eichler, B., Gäggeler, H.W., Günther, R., Gregorich, K.E., Hoffman, D.C., Hübener, S., Jost, D.T., Kratz, J.V., Paulus, W., Schumann, D., Timokhin, S., Trautmann, N., Türler, A., Wirth, G., Yakushev, A.B.: Chemical properties of element 106 (seaborgium). Nature, **388**, 55–57 (1997)
186. Türler, A., Brüchle, W., Dressler, R., Eichler, B., Eichler, R., Gäggeler, H.W., Gärtner, M., Glatz, J.-P., Gregorich, K.E., Hübener, S., Jost, D.T., Lebedev, V.Y., Pershina, V., Schädel, M., Taut, S., Timokhin, N., Trautmann, N., Vahle, A., Yakushev, A.B.: First measurements of a thermochemical property of a seaborgium compound. Angew. Chem. Int. Ed. **38**, 2212–2213 (1999)
187. Zvara, I., Belov, V., Domanov, V.P., Shalaevski, M.R.: Sov. Radiochem. **18**, 371 (1976)
188. Gäggeler, H.W., Jost, D.T., Kovacs, J., Scherer, U.W., Weber, A., Vermeulen, D., Türler, A., Gregorich, K.E., Czerwinski, R.A., Kadkhodayan, B., Lee, D.M., Nurmia, M., Hoffman, D.C., Kratz, J.V., Gober, M.K., Zimmermann, H.P., Schädel, M., Brüchle, W., Schimpf, E., Zvara, I.: Gas phase chromatography experiments with bromides of tantalum and element 105. Radiochim. Acta **57**, 93–100 (1992)
189. Türler, A., Eichler, B., Jost, D.T., Piguet, D., Gäggeler, H.W., Gregorich, K.E., Kadkhodayan, B., Kreek, S.A., Lee, D.M., Mohar, M., Sylwester, E., Hoffman, D.C., Hübener, S.: On-line gas phase chromatography with chlorides of niobium and hahnium (element 105). Radiochim. Acta **73**, 55–66 (1996)
190. Qin, Z., Lin, M.S., Fan, F.L., Huang, W.X., Yan, X.L., Bai, J., Wu, X.L., Lei, F.A., Ding, H.J., Ma, F., Li, G.S., Zhou, H.B., Guo, J.S.: On-line gas chromatographic studies of Nb, Ta, and Db bromides. Radiochim. Acta **100**, 285–290 (2012)
191. Gyanchandani, J., Sikka, S.K.: Structural properties of rutherfordium. An *ab initio* study. Phys. Lett. A **376**, 620–625 (2012)
192. Rosen, A., Fricke, B., Morovic, T., Ellis, D.E.: J. Phys. C-4, Suppl. 4, **40**, C-4/218 (1979)
193. Patzschke, M., Pyykkö, P.: Darmstadtium carbonyl and carbide resemble platinum carbonyl and carbide. The Royal. Soc. Chem., Chem. Commun. 1982–1983 (2004)
194. Seth, M., Schwerdtfeger, P., Dolg, M., Faegri, K., Hess, B.A., Kaldor, U.: Large relativistic effects in molecular properties of the hydride of superheavy element 111. Chem. Phys. Lett. **250**, 461–465 (1996)
195. Dolg, M., Stoll, H., Seth, M., Schwerdtfeger, P.: On the performance of energy-consistent spin-orbit pseudopotentials: (111)H revised. Chem. Phys. Lett. **345**, 490–496 (2001)
196. Han, Y.-K., Hirao, K.: Two-component coupled-cluster calculations for the hydride of element 111: on the performance of relativistic effective core potentials. Chem. Phys. Lett. **328**, 453–458 (2000)
197. Seth, M., Schwerdtfeger, P.: A comparison of relativistic and electron correlation effects for (111)F, (111)H and (111)Li. Chem. Phys. Lett. **318**, 314–318 (2000)
198. Anton, J., Fricke, B., Schwerdtfeger, P.: Non-collinear and collinear four-component relativistic molecular density functional calculations. Chem. Phys. **311**, 97–103 (2005)
199. Seth, M., Cooke, F., Schwerdtfeger, P., Heully, J.-L., Pelissier, M.: The chemistry of the superheavy elements. II. The stability of high oxidation states in group 11 elements: Relativistic coupled cluster calculations for the di-, tetra- and hexafluoro metallates of Cu, Ag, Au, and element 111. J. Chem. Phys. **109**, 3935–3943 (1998)
200. Pitzer, K.S.: Are elements 112, 114, and 118 relatively inert gases? J. Chem. Phys. **63**, 1032–1033 (1975)

201. Yakushev, A.B., Zvara, I., Oganessian, Y.T., Belozerov, A.V., Dmitriev, S.N., Eichler, B., Hübener, S., Sokol, E.A., Türler, A., Yeremin, A.V., Buklanov, G.V., Chelnokov, M.L., Chepigin, V.I., Gorshkov, V.A., Gulyaev, A.V., Lebedev, V.Y., Malyshev, O.N., Popeko, A.G., Soverna, S., Szeglowski, Z., Timokhin, S.N., Tretyakova, S.P., Vasko V.M., Itkis, M.G.: Chemical identification and properties of element 112. Radiochim. Acta **91**, 433–439 (2003)
202. Eichler, R., Aksenov, N.V., Belozerov, A.V., Bozhikov, G. A., Chepigin, V.I., Dmitriev, S.N., Dressler, R., Gäggeler, H.W., Gorshkov, V.A., Haenssler, F., Itkis, M.G., Laube, A., Lebedev, V.Y., Malyshev, O.N., Oganessian, Y.T., Petrushkin, O.V., Piguet, D., Rasmussen, P., Shishkin, S.V., Shutov, S.V., Svirikhin, A.I., Tereshatov, E.E., Vostokin, G.K., Wegrzecki, M., Yeremin, A.V.: Chemical characterization of element 112. Nature **447**, 72–75 (2007)
203. Eichler, R., Aksenov, N.V., Belozerov, A.V., Bozhikov, G.A., Chepigin, V.I., Dmitriev, S.N., Dressler, R., Gäggeler, H.W., Gorshkov, A.V., Itkis, M.G., Haenssler, F., Laube, A., Lebedev, V.Y., Malyshev, O.N., Oganessian, Y.T., Petrushkin, O.V., Piguet, D., Popeko, A.G., Rasmussen, P., Shishkin, S.V., Serov, A.A., Shutov, A.V., Svirikhin, A.I., Tereshatov, E.E., Vostokin, G.K., Wegrzecki, M., Yeremin, A.V.: Thermochemical and physical properties of element 112. Angew. Chem. Int Ed. **47**, 3262–3266 (2008)
204. Liu, W., Dolg, M., Schwerdtfeger, P.: Benchmark relativistic all-electron density functional and *ab initio* pseudopotential study of group12 dimers M_2 (M = Zn, Cd, Hg and eka-Hg). Unpublished
205. Zee, R.D., Blankespoor, S.C., Zweier, T.S.: Direct spectroscopic determination of the Hg_2 bond length and an analysis of the 2540 Å band. J. Chem. Phys. **88**, 4650–4654 (1988)
206. Gaston, N., Opahle, I., Gäggeler, H.W., Schwerdtfeger, P.: Is Eka-Mercury (element 112) a group 12 metal? Angew. Chem. Int. Ed. **46**, 1663–1666 (2007)
207. Eichler, B.: Das Flüchtigkeitsverhalten von Transactiniden im Bereich um Z = 114 (Voraussage). Kernenergie **19**, 307–311 (1976)
208. Soverna, S.: Doctoral Thesis, Universität Bern (2004)
209. Soverna, S., Dressler, R., Düllmann, C.E., Eichler, B., Eichler, R., Gäggeler, H.W., Haenssler, F., Niklaus, J.P., Piguet, D., Qin, Z., Türler, A., Yakushev, A.: Thermochromatographic studies of mercury and radon on transition metal surfaces. Radiochim. Acta **93**, 1–8 (2005)
210. Pershina, V., Bastug, T., Fricke, B., Jacob, T., Varga, S.: Intermetallic compounds of the heaviest elements: the electronic structure and bonding of dimers of element 112 and its homolog Hg. Chem. Phys. Lett. **365**, 176–183 (2002)
211. Pershina, V., Bastug, T., Sarpe-Tudoran, C., Anton, J., Fricke, B.: Predictions of adsorption behaviour of the superheavy element 112. Nucl. Phys. A **734**, 200–213 (2004)
212. Sarpe-Tudoran, C., Fricke, B., Anton, J., Pershina, V.: Adsorption of superheavy elements on metal surfaces. J. Chem. Phys. **126**, 174702(5) (2007)
213. Pershina, V., Anton, J., Jacob, T.: Theoretical predictions of adsorption behavior of elements 112 and 114 and their homologs Hg and Pb. J. Chem. Phys. **131**, 084713(8) (2009)
214. Rykova, E.A., Zeitsevskii, A., Mosyagin, N.S., Isaev, T.A., Titov, A.V.: Relativistic effective core potential calculations of Hg and eka-Hg (E112) interactions with gold: spin-orbit density functional theory modelling of Hg-Au_n and E112-Au_n systems. J. Chem. Phys. **125**, 241102(3) (2006)
215. Zaitsevskii, A., Rykova, E.A., Mosyagin, N.S., Titov, A.V.: Towards relativistic ECP/DFT description of chemical bonding in E112 compounds: spin-orbit and correlation effects in E112X versus HgX (X = H, Au). Cent. Eur. J. Phys. **4**, 448–460 (2006)
216. Zaitsevkii, A., Titov, A.: Relativistic pseudopotential model for superheavy elements: applications to chemistry of eka-Hg and eka-Pb. Russ. Chem. Rev. **78**, 1173–1181 (2009)
217. Zaitsevski, A., van Wüllen, C., Rykova, E.A.: Two-component relativistic density functional modeling of the adsorption of element 114 (eka-led) on gold. Phys. Chem. Chem. Phys. **12**, 4152–4156 (2010)

218. Mosyagin, N.S., Isaev, T.A., Titov, A.V.: Is E112 a relatively inert element? Benchmark relativistic correlation study of spectroscopic constants in E112H and its cation. J. Chem. Phys. **124**, 224302–(1–5) (2006)
219. Nakajima, T., Hirao, K.: Numerical illustration of third-order Douglas-Kroll method: Atomic and molecular properties of superheavy element 112. Chem. Phys. Lett. **329**, 511–516 (2000)
220. Kaupp, M., von Schering, H.G.: Gaseous mercury(IV) fluoride, HgF_4: An *ab initio* study. Angew. Chem., Int. Ed. Engl., **32**, 861–863 (1993)
221. Kaupp, M., Dolg, M., Stoll, H., von Schnering, H.G.: Oxidation state +IV in group 12 chemistry: *ab initio* study of zinc(IV), cadmium(IV), and mercury(IV) fluorides. Inorg. Chem., **33**, 2122–2131 (1994)
222. Eichler, R., Aksenov, N.V., Albin, Y.V., Belozerov, A.V., Bozhikov, G.A., Chepigin, V.I., Dmitriev, S.N., Dressler, R., Gäggeler, H.W., Gorshkov, V.A., Henderson, R.A., Johnsen, A.M., Kenneally, J.M., Lebedev, V.Y., Malyshev, O.N., Moody, K.J., Oganessian, Y.T., Petrushkin, O.V., Piguet, D., Popeko, A.G., Rasmussen, P., Serov, A., Shaughnessy, D.A., Shishkin, S.V., Shutov, A.V., Stoyer, M.A., Stoyer, N.J., Svirikhin, A.I., Tereshatov, E.E., Vostokin, G.K., Wegrzecki, M., Wilk, P.A., Wittwer, D., Yeremin, A.V.: Indication for a volatile element 114. Radiochim. Acta, **88**, 133–139 (2010)
223. Yakushev, A.: Private communication 2011
224. König, S., Gäggeler, H.W., Eichler, R., Haenssler, F., Soverna, S., Dressler, R., Friedrich, S., Piguet, D., Tobler, L.: The production of long-lived Thallium-isotopes and their thermochromatography studies on quartz and gold. PSI Annual report, 2006, Jan 2005, p. 5
225. Pershina, V., Borschevsky, A., Anton, J., Jacob, T.: Theoretical predictions of trends in spectroscopic properties of homonuclear dimers and volatility of the 7p elements. J. Chem. Phys. **132**, 194341(11) (2010)
226. Pershina, V., Anton, J., Fricke, B.: Intermetallic compounds of the heaviest elements and their homologs: The electronic structure and bonding of MḾ, where M = Ge, Sn, Pb, and element 114, and Ḿ = Ni, Pd, Pt, Cu, Ag, Au, Sn, Pb, and element 114. J. Chem. Phys. **127**, 134310(9) (2007)
227. Wood, C.P., Pyper, N.C.: An *ab initio* relativistic calculation for $(E113)_2$. Chem. Phys. Lett. **84**, 614–621 (1981)
228. Liu, W., van Wüllen, Ch., Han, Y.K., Choi, Y.J., Lee, Y.S.: Spectroscopic constants of Pb and eka-lead compounds: comparsion of different approaches. Adv. Quant. Chem. **39**, 325–355 (2001)
229. van Wüllen, C.: Relativistic density functional calculations on small molecules. In: Schwerdtfeger, P. (ed.) Relativistic Electronic Structure Theory, Part II, pp. 598–655. Elsevier, Amsterdam (2002)
230. Liu, W., van Wüllen, C., Wang, F., Li, L.: Spectroscopic constants of MH and M_2 (M = Tl, E113, Bi, E115): Direct comparisons of four- and two-component approaches in the framework of relativistic density functional theory. J. Chem. Phys. **116**, 3626–3634 (2002)
231. Liu, W., Peng, D.: Infinite-order quasirelativistic density functional method based on the exact matrix quasirelativistic theory. J. Chem. Phys. **125**, 044102(1–10) (2006)
232. Peng, D., Liu, W., Xiao, Y., Cheng, L.: Making four- and two-component relativistic density functional methods fully equivalent based on the idea of "from atoms to molecule". J. Chem. Phys. **127**, 104106(15) (2007)
233. Kullie, O., Saue, T.: Range-separated density-functional theory: a 4-component relativistic study of the rare gas dimers He_2, Ne_2, Ar_2, Kr_2, Xe_2, Rn_2 and Uuo_2. Chem. Phys. **395**, 54–62 (2012)
234. Pitzer, K.S., Balasubramanian, K.: Properties of ten electronic states of diatomic lead from relativistic quantum calculations. J. Phys. Chem. **86**, 3068–3070 (1982)
235. Heaven, M.C., Miller, T.A., Bondybey, V.E.: Laser spectroscopy of lead molecules produced by laser vaporization. J. Phys. Chem. **87**, 2071–2075 (1983)

236. Hermann, A., Furthmüller, J., Gäggeler, H.W., Schwerdtfeger, P.: Spin-orbit effects in structural and electronic properties for the solid state of the group-14 elements from carbon to superheavy element 114. Phys. Rev. B **82**, 155116(8) (2010)
237. Pershina, V., Borschevsky, A., Anton, J., Jacob, T.: Theoretical predictions of trends in spectroscopic properties of gold containing dimers of the 6p and 7p elements and their adsorption on gold. J. Chem. Phys. **133**, 104304(10) (2010)
238. Rossbach, H., Eichler, B.: Adsorption von Metallen auf metallische Oberflächen und Möglichkeiten ihrer Nutzung in der Kernchemie, B, pp. 1–20. Akademie der Wissenschaft der DDR, Report No. ZFK-527 (1984)
239. Eichler, B., Kratz, J.V.: Electrochemical deposition of carrier-free radionuclides. Radiochim. Acta **88**, 475–482 (2000)
240. Pershina, V., Anton, J., Jacob, T.: Electronic structures and properties of MAu and MOH, where M = Tl and element 113. Chem. Phys. Lett. **480**, 157–160 (2009)
241. Fox-Beyer, B.S., van Wüllen, C.: Theoretical modelling of the adsorption of thallium and element 113 atoms on gold using two-component density functional methods with effective core potentials. Chem. Phys. **395**, 95–103 (2012)
242. Haenssler, F., Eichler, R., Gäggeler, H.W., Soverna, S., Dressler, R., Piguet, D., Schippering, M.: Thermochromatographic studies of ^{212}Pb on metal surfaces. PSI Annual Report 2005 (2006), p. 3; Eichler, R.: private communication
243. Saue, T., Faegri, K., Gropen, O.: Relativistic effects on the bonding of heavy and superheavy hydrogen halides. Chem. Phys. Lett. **263**, 360–366 (1996)
244. Seth, M., Schwerdtfeger, P., Faegri, K.: The chemistry of superheavy elements. III. Theoretical studies on element 113 compounds. J. Chem. Phys. **111**, 6422–6433 (1999)
245. Thierfelder, C., Schwerdtfeger, P., Kroes, A., Borschevsky, A., Fricke, B. Scalar relativistic and spin-orbit effects in closed-shell superheavy-element monohydrides. Phys. Rev. A **80**, 022501-1-10 (2009)
246. Han, Y.-K., Bae, C., Lee, Y.S.: Two-component calculations for the molecules containing superheavy elements: spin-orbit effects for (117)H, (113)H, and (113)F. J. Chem. Phys. **110**, 8969–8975 (1999)
247. Han, Y.-K., Bae, C., Son, S.-K., Lee, Y.S.: Spin–orbit effects on the transactinide p-block element monohydrides MH (M = element 113–118). J. Chem. Phys. **112**, 2684–2691 (2000)
248. Choi, Y.J., Han, Y.K., Lee, Y.S.: The convergence of spin–orbit configuration interaction calculations for TlH and 113H. J. Chem. Phys. **115**, 3448–3453 (2001)
249. Nash, C.S., Bursten, B.E.: Spin-orbit, VSEPR theory, and the electronic structure of heavy and superheavy group IVA hydrides and group VIIIA tetrafluorides. A partial role reversal for elements 114 and 118. J. Phys. Chem. A **103**, 402–410 (1999)
250. Balasubramanian, K.: Electronic states of the superheavy element 113 and (113)H. Chem. Phys. Lett. **361**, 397–404 (2002)
251. Vest, B., Klinkhammer, K., Thierfelder, C., Lein, M., Schwerdtfeger, P.: Kinetic and thermodynamic stability of the group 13 trihydrides. Inorg. Chem. **48**, 7953–7961 (2009)
252. Balasubramanian, K.: Breakdown of the singlet and triplet nature of electronic states of the superheavy element 114 dihydride ($114H_2$). J. Chem. Phys. **117**, 7426–7432 (2002)
253. Nash, C.S., Crockett, W.W.: An anomalous bond angle in $(116)H_2$. Theoretical evidence for supervalent hybridization. J. Phys. Chem. A **110**, 4619–4621 (2006)
254. Faegri, K., Saue, T.: Diatomic molecules between very heavy elements of group 13 and group 17: a study of relativistic effects on bonding. J. Chem. Phys. **115**, 2456–2464 (2001)
255. Schwerdtfeger, P.: Second-order Jahn—Teller distortions in group 17 fluorides EF_3 (E = Cl, Br, I, and At). Large relativistic bond angle changes in AtF_3. J. Phys. Chem. **100**, 2968–2973 (1996)
256. Seth, M., Faegri, K., Schwerdtfeger, P.: The stability of the oxidation state +4 in group 14 compounds from carbon to element 114. Angew. Chem. Int. Ed. Engl. **37**, 2493–2496 (1998)

257. Grant, I.P., Pyper, N.C.: Theoretical chemistry of superheavy elements E116 and E114. Nature **265**, 715–717 (1977)
258. van Wüllen, C., Langermann, N.: Gradients for two-component quasirelativistic methods. Application to dihalogenides of element 116. J. Chem. Phys. **126**, 114106(9) (2007)
259. Bae, C., Han, Y.-K., Lee, Y.S.: Spin–orbit and relativistic effects on structures and stabilities of group 17 fluorides EF_3 (E = I, At, and element 117): relativity induced stability for the D_{3h} structure of $(117)F_3$. J. Phys. Chem. A **107**, 852–858 (2003)
260. Malli, G.L.: Relativistic and electron correlation effects in molecules of heavy elements. In: Malli, G. (ed.) Relativistic and Electron Correlation Effects in Molecules and Solids, NATO ASI Series, vol. 318, pp. 1–15. Plenum, New York (1994)
261. Pitzer, K.S.: Fluorides of radon and element 118. J. Chem. Soc., Chem. Commun. 760–761 (1975)
262. Han, Y.K., Lee, Y.S.: Structure of RgF_4 (Rg = Xe, Rn, and element 118. $n = 2,4$) calculated by two-component spin-orbit methods. A spin-orbit inducted isomer of $(118)F_4$. J. Phys. Chem. A **103**, 1104–1108 (1999)
263. Nash, C.S., Bursten, B.E.: Spin-orbit coupling versus the VSEPR method: On the possibility of a nonplanar structure for the super-heavy noble gas tetrafluoride $(118)F_4$. Angew. Chem. Int. Ed. **38**, 151–153 (1999)
264. Bonchev, D., Kamenska, V.: Predicting the properties of the 113–120 transactinide elements. J. Phys. Chem. **85**, 1177–1186 (1981)
265. Schwerdtfeger, P.: Relativistic effects in molecular structure of s- and p-block elements. In: Domenicano, A., Hargittai, I. (eds.) Strength from Weakness: Structural Consequences of Weak Interactions in Molecules, Supermolecules, and Crystals, NATO Science Series, pp. 169–190. Kluwer, Dordrecht (2002)
266. Miranda, P.S., Mendes, A.P.S., Gomes, J.S., Alves, C. N., de Souza, A.R., Sambrano, J.R., Gargano, R., de Macedo, L.G.M.: *Ab initio* correlated all electron Dirac-Fock calculations for eka-francium fluoride (E119F). J. Braz. Chem. Soc., **23**, 1104–1113 (2012)
267. Pyykkö, P.: The physics behind chemistry and the periodic table. Chem. Rev. **112**, 371–284 (2012)
268. Pyykkö, P.: Predicting new, simple inorganic species by quantum-chemical calculations: some successes. Phys. Chem. Chem. Phys. **14**, 14734–14742 (2012)
269. Makhyoun, M.A.: On the electronic structure of $5g^1$ complexes of element 125: A quasi-relativistic MS-Xα study. J. Chim. Phys. **85**, 917–924 (1988)
270. Malli, G.L.: Dissociation energy of ekaplutonium fluoride E126F: The first diatomic with molecular spinors consisting of g atomic spinors. J. Chem. Phys. **124**, 071102(2) (2006)
271. Malli, G.L.: Thirty years of relativistic self-consistent field theory for molecules: Relativistic and electron correlation effects for atomic and molecular systems of transactinide superheavy elements up to ekaplutonium E126 with g-atomic spinors in the ground state configuration. Theor. Chem. Acc. **118**, 473–482 (2007)
272. Kadkhodayan, B., Türler, A., Gregorich, K.E., Baisden, P.A., Czerwinski, K.R., Eichler, B., Gäggeler, H.W., Hamilton, T.M., Jost, T.M., Kacher, C.D., Kovacs, A., Kreek, S.A., Lane, M.R., Mohar, M.F., Neu, M.P., Stoyer, N.J., Sylwester, E.R., Lee, D.M., Nurmia, M.J., Seaborg, G.T., Hoffman, D.C.: On-line chromatographic studies of chlorides of Rutherfordium and homologs Zr and Hf. Radiochim. Acta **72**, 169–178 (1996)
273. Türler, A.: Gas phase chemistrty experiments with transactinide elements. Radiochim. Acta **72**, 7–17 (1996)
274. Ionova, G.V., Pershina, V., Johnson, E., Fricke, B., Schädel, M.: Redox reactions for group 5 elements, including element 105, in aqueous solutions. J. Phys. Chem. **96**, 11096–11101 (1992)
275. Johnson, E., Fricke, B.: Prediction of some thermodynamic properties of selected compounds of element 104. J. Phys. Chem. **95**, 7082–7084 (1991)
276. Bratsch, S.G.: Standard electrode potentials and temperature coefficients in water at 298.15 K. J. Phys. Chem. Ref. Data **18**, 1–21 (1989)

277. Bratsch, S.G., Lagowski, J.J.: Actinide thermodynamic predictions. 3. Thermodynamics of compounds and aqua-ions of the 2+, 3+, and 4+ oxidation states and standard electrode potentials at 298.15 K. J. Phys. Chem. **90**, 307–312 (1986)
278. Ahrland, S., Liljenzin, J.O., Rydberg, J.: Solution chemistry. In: Bailar, J. (ed.) Comprehensive Inorganic Chemistry, vol. 5, pp. 519–542. Pergamon Press, Oxford (1973)
279. Baes Jr, C.F., Mesmer, R.E.: The Hydrolysis of Cations. John Wiley, New York (1976)
280. Kassiakoff, A., Harker, D.: The calculations of the ionization constants of inorganic oxygen acids from their structures. J. Am. Chem. Soc. **60**, 2047–2055 (1938)
281. Pershina, V.: Solution chemistry of element 105. Part I: Hydrolysis of group 5 cations: Nb, Ta, Ha and Pa. Radiochim. Acta **80**, 65–74 (1998)
282. Pershina, V.: Solution chemistry of element 105. Part II: Hydrolysis and complex formation of Nb, Ta, Ha and Pa in HCl solutions. Radiochim. Acta **80**, 75–84 (1998)
283. Pershina, V., Bastug, T.: Solution chemistry of element 105. Part III: Hydrolysis and complex formation of Nb, Ta, Db and Pa in HF and HBr solutions. Radiochim. Acta **84**, 79–84 (1999)
284. Pershina, V., Kratz, J.V.: Solution chemistry of element 106: theoretical predictions of hydrolysis of group 6 cations Mo, W, and Sg. Inorg. Chem. **40**, 776–780 (2001)
285. Pershina, V., Trubert, D., Le Naour, C., Kratz, J.V.: Theoretical predictions of hydrolysis and complex formation of group-4 elements Zr, Hf and Rf in HF and HCl solutions. Radiochim. Acta **90**, 869–877 (2002)
286. Pershina, V.: Theoretical treatment of the complexation of element 106, Sg in HF solutions. Radiochim. Acta **92**, 455–462 (2004)
287. Pershina, V.: Theoretical investigations of the reactivity of MO_4 and the electronic structure of $Na_2[MO_4(OH)_2]$, where M = Ru, Os, and Hs (element 108). Radiochim. Acta **93**, 373–376 (2005)
288. Pershina, V., Polakova, D., Omtvedt, J.P.: Theoretical predictions of complex formation of group-4 elements Zr, Hf, and Rf in H_2SO_4 solutions. Radiochim. Acta **94**, 407–414 (2006)
289. Kratz, J.V., Pershina, V.: Experimental and theoretical study of the chemistry of the heaviest elements. In: Hess, B.A. (ed.) Relativistic Effects in Heavy-Element Chemistry and Physics, pp. 219–244. Wiley, West Sussex (2003)
290. Czerwinski, K.R.: Studies of fundamental properties of rutherfordium (element 104) using organic complexing agents. Doctoral Thesis, LBL Berkeley (1992)
291. Strub, E., Kratz, J.V., Kronenberg, A., Nähler, A., Thörle, P., Zauner, S., Brüchle, W., Jäger, E., Schädel, M., Schausten. B., Schimpf, E., Zongwei, Li, Kirbach, U., Schumann, D., Jost, D., Türler, A., Asai, M., Nagame, Y., Sakara, M., Tsukada, K., Gäggeler, H.W., Glanz, J.P.: Fluoride complexation of rutherfordium (Rf, element 104). Radiochim. Acta **88**, 265–271 (2000)
292. Ishii, A., Toyoshima, A., Tsukada, K., Asai, M., Toume, H., Nishinaka, I., Nagame, Y., Miyashita, S., Mori, T., Suganuma, H., Haba, H., Sakamaki, M., Goto, M., Kudo, H., Akiyama, K., Oura, Y., Nakahara, H., Tashiro, Y., Shinohara, A., Schädel, M., Brüchle, W., Pershina, V., Kratz, J.V.: Fluoride complexation of element 104, rutherfordium (Rf), investigated by cation-exchange chromatography. Chem. Lett. **37**, 288–289 (2008)
293. Trubert, D., Le Naour, C., Hussonois, M., Brillard, L., Montroy Gutman, F., Le Du, J.F., Constantinescu, O., Barci, V., Weiss, B., Gasparro, J., Ardisson, G.: In: Abstracts of the 1st Intern. Conf. on Chemistry and Physics of the Transactinides, Seeheim, 26–30 Sept (1999)
294. Toyoshima, A., Haba, H., Tsukada, K., Asai, M., Akiyama, K., Goto, S., Ishii, Y., Nishinaka, I., Sato, T.K., Nagame, Y., Sato, W., Tani, Y., Hasegawa, H., Matsuo, K., Saika, D., Kitamoto, Y., Shinohara, A., Ito, M., Saito, J., Kudo, H., Yokoyama, A., Sakama, M., Sueki, K., Oura, Y., Nakahara, H., Schädel, M., Brüchle, W., Kratz, J.V.: Hexafluoro complex of rutherfordium in mixed HF/HNO_3 solutions. Radiochim. Acta **96**, 125–134 (2008)
295. Haba, H., Tsukada, K., Asai, M., Goto, S., Toyoshima, A., Nishinaka, I., Akiyama, K., Hirata, M., Ichikawa, S., Nagame, Y., Shoji, Y., Shigekawa, M., Koike, T., Iwasaki, M., Shinohara, A., Kaneko, T., Maruyama, T., Ono, S., Kudo, H., Oura, Y., Sueki, K.,

Nakahara, H., Sakama, M., Yokoyama, A., Kratz, J.V., Schädel, M., Brüchle, W.: Anion-exchange behavior of Rf in HCl and HNO_3 solutions. J. Nucl. Radiochem. Sci. **3**, 143–146 (2002)
296. Günther, R., Paulus, W., Kratz, J.V., Seibert, A., Thörle, P., Zauner, S., Brüchle, W., Jäger, E., Pershina, V., Schädel, M., Schausten, B., Schumann, D., Eichler, B., Gäggeler, H.W., Jost, D.T., Türler, A.: Chromatographic study of rutherfordium (element 104) in the system HCl/Tributylphosphate (TBP). Radiochim. Acta **80**, 121–128 (1998)
297. Haba, H., Tsukada, K., Asai, M., Toyoshima, A., Ishii, Y., Toume, H., Sato, T., Nishinaka, I., Ichikawa, T., Ichikawa, S., Nagame, Y., Sato, W., Matsuo, K., Kitamoto, Y., Tashiro, Y., Shinohara, A., Saito, J., Ito, M., Ikezawa, T., Sakamaki, M., Goto, S., Kudo, H., Kikunaga, H., Arai, M., Kamataki, S., Yokoyama, A., Akiyama, K., Sueki, K., Oura, Y., Schädel, M., Brüchle, W., Kratz, J.V.: Extraction behavior of rutherfordium into tributylphosphate from hydrochloric acid. Radiochim. Acta **95**, 1–6 (2007)
298. Omtvedt, J.P., Polyakova, D., Alstad, J., Bjornstad, T., Düllmann, C.E., Folden III, C.M., Garcia, M.A., Gates, J., Gregorich, K.E., Hoffman, D.C., Nelson, S.L., Nitsche, H., Omtwedt, L., Pershina, V., Samadani, F., Skarnemark, G., Stavsetra, L., Sudove, R., Wilson, R.E., Zheng, L., Zielinski, P.M. Radiochim. Acta, to be submitted
299. Li, Z.J., Toyoshima, A., Tsukada, K., Nagame, Y.: Ion-exchange behavior of Zr and Hf as homologues of element 104, Rf, in H_2SO_4 and $H_2SO_4/HClO_4$ mixed solutions. Radiochim. Acta **98**, 7–12 (2010)
300. Kratz, J.V., Zimmermann, H.P., Scherer, U.W., Schädel, M., Brüchle, W., Gregorich, K.E., Gannett, C.M., Hall, H.L., Henderson, R.A., Lee, D.M., Leyba, J.D., Nurmia, M., Hoffman, D.C., Gäggeler, H.W., Jost, D., Baltensperger, U., Ya Nai-Qi, Türler, A., Lienert, C.: Chemical properties of element 105 in aqueous solution: Halide complex formation and anion exchange into Triisoctyl amine. Radiochim. Acta **48**, 121–133 (1989)
301. Paulus, W., Kratz, J.V., Strub, E., Zauner, S., Brüchle, W., Pershina, V., Schädel, M., Schausten, B., Adams, J.L., Gregorich, K.E., Hoffman, D.C., Lane, M.R., Laue, C., Lee, D.M., McGrath, C.A., Shaughnessy, D.K., Strellis, D.A., Sylwester, E.R.: Chemical properties of element 105 in aqueous solution: extraction of the fluoride-, chloride-, and bromide complexes of the group-5 elements into an aliphatic amine. Radiochim. Acta **84**, 69–77 (1999)
302. Schädel, M., Brüchle, W., Jäger, E., Schausten, B., Wirth, G., Paulus, W., Günther, R., Eberhardt, K., Kratz, J.V., Seibert, A., Strub, E., Thörle, P., Trautmann, N., Waldek, W., Zauner, S., Schumann, D., Kirbach, U., Kubica, B., Misiak, R., Nagame, Y., Gregorich, K.E.: Aqueous chemistry of seaborgium ($Z = 106$). Radiochim. Acta **83**, 163–165 (1998)
303. Kronenberg, A.: Entwicklung einer online-Chromatographie für Element 106 (Seaborgium), Doctoral Thesis, University of Mainz (2001)
304. Pfrepper, G., Pfrepper, R., Kronenberg, A., Kratz, J.V., Nähler, A., Brüchle, W., Schädel, M.: Continuous on-line chromatography of short lived isotopes of tungsten as homolog of seaborgium (element 106). Radiochim. Acta **88**, 273–278 (2000)
305. von Zweidorf, A., Angert, R., Brüchle, W., Bürger, S., Eberhartdt, K., Eichler, R., Hummrich, H., Jäger, E., Kling, H.-O., Kratz, J.V., Kuczewski, B., Langrock, G., Mendel, M., Rieth, U., Schädel, M., Schausten, B., Schimpf, E., Thörle, P., Trautmann, N., Tsukada, K., Wiehl, N., Wirth, G.: Evidence for the formation of sodium hassate(VIII). Radiochim. Acta **92**, 855–861 (2004)
306. Caletka, R., Krivan, V.: Anion-exchage behaviour of some elements in HF-HCl medium. J. Radioanal. Nucl. Chem. **142**, 373–382 (1990)
307. Caletka, R., Krivan, V.: Behaviour of 18 elements in HF and HF-NH_4F media on anion exchanger in various ionic forms. J. Radioanal. Nucl. Chem. **142**, 359–371 (1990)
308. Markus, Y. (ed.): Solvent Extraction Reviews, vol. 5. Marcel Dekker, New York (1971)
309. Aylett, B.J.: Group IIB. In: Baylar; J.C. (ed.) Comprehensive Inorganic Chemistry, Vol. 3, pp. 187–328. Pergamon Press, Oxford (1973)
310. Abel, E.W.: Lead. In: Baylar, J.C. (ed.) Comprehensive Inorganic Chemistry, vol. 2, pp. 105–146. Pergamon Press, Oxford (1973)